

ÉCOLE DE TECHNOLOGIE SUPÉRIEURE  
UNIVERSITÉ DU QUÉBEC

MASTER THESIS PRESENTED TO  
ÉCOLE DE TECHNOLOGIE SUPÉRIEURE

IN PARTIAL FULFILLMENT OF THE REQUIREMENTS FOR  
A MASTER'S DEGREE IN MECHANICAL ENGINEERING  
M. Eng.

BY  
Mohammadreza MAJLESI

ICE MEASUREMENT ON THE WIND TURBINES' BLADES  
BY CLOSE-RANGE PHOTOGRAMMETRY METHODS

MONTREAL, 27 JULY 2015 TO BUREAU DES CYCLES SUPÉRIEURS

© Copyright 2015 reserved by Mohammadreza MAJLESI



This Creative Commons licence allows readers to download this work and share it with others as long as the author is credited. The content of this work can't be modified in any way or used commercially.

**BOARD OF EXAMINERS**

THIS THESIS HAS BEEN EVALUATED  
BY THE FOLLOWING BOARD OF EXAMINERS

Mr. CHRISTIAN MASSON, Thesis Supervisor  
Mechanical Engineering Department at École de technologie supérieure

Mr. SOUHEIL-ANTOINE TAHAN, Thesis Co-supervisor  
Mechanical Engineering Department at École de technologie supérieure

Mr. MICHEL RIOUX, President of the Board of Examiners  
GPA Department at École de technologie supérieure

Mr. HUSSEIN IBRAHIM, Member of the jury  
Wind Energy Techno Center (TCE)

THIS THESIS WAS PRESENTED AND DEFENDED  
IN THE PRESENCE OF A BOARD OF EXAMINERS AND PUBLIC

2 JUNE 2015

AT ÉCOLE DE TECHNOLOGIE SUPÉRIEURE



## ACKNOWLEDGMENT

I would like to express my special appreciation and thanks to my advisor Professor Dr. **Christian Masson**, you have been a tremendous mentor for me. I would like to thank you for selecting me as your student and encouraging my research and for the useful comments, remarks and engagement through the learning process of this master thesis. Your advice on both research as well as on my career have been priceless. I would also like to thank my Co-supervisor, Professor Dr. **Souheil-Antoine Tahan** for introducing me to the topic as well for the support on all the way. I also want to thank you for your brilliant comments and suggestions in all steps of my study, thanks to you.

A special thanks to my family. Words cannot express how grateful I am to, my mother and father for all of the sacrifices that you have made on my behalf. Your prayer for me was what sustained me thus far. I would also like to thank all of my friends who supported me in writing, and incited me to strive towards my goal. At the end I would like express appreciation to my beloved wife **SAEED** who spent sleepless nights and was always my support in the moments when there was no one to answer my queries and finally my son **DANESH** providing me unlimited happiness and pleasure.



# MESURE DE LA GLACE SUR LES PALES DES ÉOLIENNES PAR DES MÉTHODES DE PHOTOGRAMMÉTRIE À COURTE PORTÉE

Mohammadreza MAJLESI

## RESUME

La numérisation photogrammétrique pour mesurer l'épaisseur de glace est tout à fait nouvelle dans le domaine de l'énergie éolien. Lorsque les pales du rotor ont été montées sur la tour de l'éolienne, effectuer les inspections de l'épaisseur de la glace était presque impossible dans le passé, mais par les méthodes de modélisation à base de l'image, l'extraction de la géométrie des pales givrées sous la forme de modèles en maille est possible.

Dans ce mémoire de recherche, une maquette 3D des pales d'éoliennes sans glace est conçue dans le logiciel CATIA et considéré comme les données de référence de CAO. Un prototype de ce modèle CAO est construit par une machine d'impression 3D. Après la peinture, nous avons ajouté 3 modèles des cibles (retro targets) sur les surfaces des pales. Un appareil photo reflex numérique est utilisé pour capter plusieurs images des objets avec différents modes d'éclairages et d'illuminations. Une série de nuages de points est produite en utilisant la méthode de structure de mouvement (SfM) et le logiciel VisualSfM. Chaque nuage de points a un système arbitraire de coordonnées qui est mis à l'échelle et transféré au système de coordonnées global par transformation à l'aide du logiciel CATIA en se basant sur les caractéristiques similaires entre le nuage de points 3D et les données de référence de CAO. Lorsque la glace a une texture suffisante, comme du givre blanc, cette texture peut être captée dans les images et un nuage de points correspondant à la région captée sera également détecté. La position de la glace sur les pales est détectée par cibles (retro targets) codé sur la surface de la pale et à l'ordre d'acquisition des images. Le nuage de points générés et son maillage sont comparés avec les données de référence de CAO et le résultat est montré en format 3D, qui détermine la forme, l'épaisseur et la masse approximative de glace sur les pales.

Cette étude a porté sur la faisabilité de la reconstruction de modèles de maillage polygonal 3D par l'image captée d'une pale d'éolienne avec un ensemble d'appareils photo reflex numériques. L'objectif principal de cette modélisation est identifié le volume et la forme des zones de glace accumulée sur les pales de l'éolienne dans les régions arctiques. Une comparaison géométrique de ces modèles de maillage triangulaires avec les données CAO de pale non-glacé pourrait révéler la géométrie de la glace accumulée.

**Mots-clés:** Photogrammétrique à courte portée, Photogrammétrique rapprochée, Méthode de détection de glace, Modélisation 3D à base d'images, Structure du mouvement, Transformation de similarité en 3D.



# ICE MEASUREMENT ON THE WIND TURBINES' BLADES BY CLOSE-RANGE PHOTOGRAMMETRY METHODS

Mohammadreza MAJLESI

## ABSTRACT

Photogrammetric scanning for measuring the thickness of ice is quite new in the wind energy field. When the rotor blades were mounted on the wind turbine tower, ice thickness inspections became nearly impossible to be performed in the past but by image base modeling methods, geometry extraction of ice of frosted blades are possible in the form of mesh models.

In this research thesis, 3D model of wind turbine blades without ice is designed as reference Master CAD data. A prototype of this CAD model is made by a 3D printer machine which after painting, a pattern of retro targets is added to blades surfaces. Digital Single-Lens Reflex (SLR) camera is used to capture several images of objects with different modes of lighting and illumination. A series of point clouds is produced by using the Structure from Motion (SfM) method and VisualSfM software. Each point cloud has an arbitrary coordinate system that is scaled and transferred to Global Coordinate System by 3D transform on CATIA software based on similar features between 3D point cloud and master CAD data. When the ice has sufficient texture, such as rime ice and the texture is captured in the images, a point cloud corresponding to the captured region will also be detected. The position of ice on the blades is detected by coded retro targets on blade's surface and the order of image acquisition. The generated point cloud and its mesh are compared with the Master CAD or reference geometric model and finally shows in 3D format, the shape, thickness and approximate mass of ice on the blades.

This study focused on the feasibility of reconstruction of 3D polygonal mesh models by images captured from a wind turbine blade with a configuration of digital SLR cameras. The main objective of this reconstruction is to identify the volume and shape of ice-accumulated areas on the wind turbine blades in arctic regions. Geometrical comparison of these triangular mesh models with the non-iced blade CAD data could reveal the geometry of accumulated ice.

**Keywords:** Close-Range Photogrammetry, Ice detection method, Image-based Modeling, Three dimensional modeling, Structure from motion, 3D Similarity transform.



## TABLE OF CONTENTS

	Page
INTRODUCTION .....	1
CHAPTER 1      ATMOSPHERIC ICING OF WIND TURBINES & ICE DETECTION SYSTEMS.....	6
1.1            Introduction.....	6
1.2            Main type of atmospheric ice accumulation .....	8
1.2.1      In-cloud icing .....	8
1.2.2      Precipitation icing.....	9
1.3            Ice detection methods .....	11
1.3.1      Direct detection .....	12
1.3.1.1    Direct detection by reflective light sensor, HoloOptics.....	12
1.3.1.2    Stereo imaging from web cameras.....	14
1.3.1.3    Reflection of polarized infrared light, IceHawk® .....	16
1.3.1.4    Infrared spectroscopy.....	17
1.3.1.5    Reflected light from inside.....	19
1.3.1.6    Fiber optic cable with special clad.....	19
1.4            Limitations or disadvantages of current ice detection systems.....	20
CHAPTER 2      INTRODUCTION TO CLOSE RANGE PHOTOGRAMMETRY & IMAGE BASE MODELING .....	23
2.1            The photogrammetric process.....	24
2.1.1      Photogrammetry, recording and analysis procedures.....	25
2.1.2      Technical components of photogrammetric process .....	27
2.2            Introduction of image base modeling .....	29
2.3            Structure from Motion .....	30
2.4            Poisson surface reconstruction.....	31
2.6            Image base modeling by DSLR camera comparison with laser scanners .....	33
2.7            Structure from Motion & the accuracy of image base modeling.....	36
CHAPTER 3      METHODOLOGY .....	39
3.1            Introduction.....	39
3.2            Image-based modeling & 3D object reconstruction procedures.....	41
3.3            Photogrammetric object recording.....	44

3.3.1	Targeting object.....	44
3.3.2	Light and illumination.....	45
3.3.3	Digital photography.....	49
3.3.4	Camera position & movement for 3D object.....	51
3.3.5	Camera movement for a large 3D object.....	52
3.3.6	Image orientation & camera calibration.....	53
3.4	Orientation & 3D mesh modeling.....	57
3.5	Applied software.....	57
3.5.1	VisualSfM.....	58
3.6	Process simulation of ice measurement on the wind turbines' blades by close-range photogrammetry methods.....	61
3.6.1	Digital-mock-up of master CAD data.....	61
3.6.2	Rapid prototyping of scaled wind turbine blade by 3D printing.....	63
3.6.3	Targeting & determination of control points.....	63
3.6.4	Prototype & photogrammetric object recording.....	64
3.7	Brief history of project case study and Wind Energy Technocentre.....	68
3.8	About Wind Energy TechnoCentre:.....	68
3.9	The methods & equipment for blades access and photography.....	69
3.9.1	Using of the crane for accessing to the blade surfaces and marking the blade.....	69
3.9.2	Using of the blade access suspended platforms.....	70
3.9.3	Using of the maintenance access man hole in the wind turbine hub.....	71
3.9.4	The photography of the objects by remote controlled drone.....	71
3.10	Recommended procedure for photogrammetric object recording via remote control drone.....	72
3.11	The equipment for marking the measuring surfaces.....	74
3.12	The economic challenges in ice measurement on the wind turbines' blades.....	74
CHAPTER 4	RESULT AND CONCLUSION.....	76
4.1	Points cloud reconstruction.....	77
4.2	Mesh generation.....	78
4.3	Scaling and alignment of the model.....	82
4.4	Measurement system analysis.....	87
4.4.1	Prototype process simulation, limitation and consideration.....	93
	CONCLUSION.....	95
	RECOMENDATION.....	97
ANNEX I	PHOTOGRAMMETRY, RECORDING AND ANALYSIS PROCEDURES.....	101
ANNEX II	LASER LIGHT SECTIONING CAMERA.....	103

ANNEX III	CAMERA CALIBRATION PARAMETERS.....	109
ANNEX IV	RETRO TARGETS .....	112
ANNEX V	SIFT/BUNDLER/PMVS2 INPUT OUTPUT.....	118
	LIST OF BIBLIOGRAPHICAL REFRENCES.....	129



## LIST OF TABLES

	Page
Table 1.1	Optical ice detection system in market .....21
Table 3.1	EXIF table tags information in the jpegs images .....50
Table 4.1	Illumination effect on ice feature detection.....82
Table 4.2	Comparison of manual measuring and digital mesh results.....89



## LIST OF FIGURES

		Page
Figure 1.1	Prevailing strong winds. The map indicate regions of wind attractive for wind power development, with average wind speed $> 5\text{ms}^{-1}$ and average generation 33% of rated power. Note the importance of marine situations and upland sites.....	7
Figure 1.2	Problematic ice vanes on the windward side of the blade.....	7
Figure 1.3	Aircraft Propellers with accumulation of precipitation ice on leading edge, image taken between 1969-73, in Sea-king, Wessex. Ontario Canada. (source: <a href="http://www.eacott.com.au/gallery/d/3366-1/icing+4">www.eacott.com.au/gallery/d/3366-1/icing+4</a> ).....	9
Figure 1.4	Frosted ice accumulated on the WT Blade`s shoulder.....	10
Figure 1.5	(Left) T23 & T26 Icing Rate Sensor, (Right) T41 shown on the nacelle at the wind power plant in Hårnösand, northern Sweden. Source: HoloOptic.net ....	13
Figure 1.6	The IR-emitter & photo detector installed on the hub and reflector as retro targets stick on the blades.....	14
Figure 1.7	(Top left) Installed camera on the Nacelle, the lamp on the right is for heating purpose. (Top right) rime ice observed on the blade. (Bottom left) rime ice after 45min heating system on, (bottom right) de-iced blade, some little trace of glazed ice remained on the leading edge. Source : (Cattin, 2015) .....	15
Figure 1.8	(Left) Infralytic Sensor tip with sender/receiver, (Right top) Sketch of rotor hub, (Right down) Sensor location in the blade. Source Brochure: IcesensorInfralytic_EN.pdf.....	18

Figure 2.1	The photogrammetric process: from object to model ((Luhmann, Robson et al. 2006), page 3).....	25
Figure 2.2	Typical photogrammetric products ((Luhmann et al., 2006), page 12) .....	26
Figure 2.3	Recording and analysis procedures (red: can be automated in a digital system) ((Luhmann et al., 2006), page 3) .....	27
Figure 2.4	Three-dimensional reconstructions by image base modeling and Structure from Motion (SfM). Left: overlapped sequential images, Middle: Camera position and Camera path & direction in image recoding, Right: Textured mesh of object. (Horning, 2012) .....	29
Figure 2.5	Right: Schematic of epipolar geometry (Musialski et al., 2013), left: Generated sparse point cloud from unordered images (Furukawa et al., 2009) .....	33
Figure 2.6	Birefringent (double refraction) optical property. when a single light ray strikes a calcite crystal at a right angle to one face, showing two rays emerging. (Britannica, 2015) .....	34
Figure 2.7	Customize laser scanner equipped by laser beam at wavelength 405-460 nm .....	35
Figure 3.1	"Site Nordique Experimental en Éolien CORUS" (SNEEC), Gaspé, near Rivière-au-Renard, Quebec, Photo from the top of the second wind turbine. (eolien.qc.ca, 2015) .....	40
Figure 3.2	Image base modeling and comparison for extraction of ICE on Blade as CAD data .....	41
Figure 3.3	Workflow for Image-Based Modeling & 3D object reconstruction procedures .....	43

Figure 3.4 Curved surface with rows of circular dot targets .....45

Figure 3.5 Ring flash on DSLR camera helps to illuminate from viewing direction of camera, source: www.capture3d.com .....46

Figure 3.6 Spectrum of Blue Violet light,  $\lambda$  between 405 nm to 460 nm .....47

Figure 3.7 Spectra software for light color extraction from wavelength  $\lambda$ .....48

Figure 3.8 Color block with wavelength 432 nm- Code RGB (51, 0, 255).....48

Figure 3.9 Left: Nikon D5200, Center & Right Canon PowerShot Digital Camera .....49

Figure 3.10 Camera position for large Object images recording.....51

Figure 3.11 Tiling procedure for large object.....52

Figure 3.12 3DF Lapyx automatic camera calibration software that extracts the typical intrinsic camera parameters used in Computer Vision.....54

Figure 3.13 Top: Image distortion by simple lens, Down: Different type of Lens Distortion order from left to right; Barrel. Pincushion & Moustache Distortion (<http://www.photocritic.org/articles/everything-about-camera-lenses>).....55

Figure 3.14 PTlens interface.....55

Figure 3.15 Left: Original Photo, Right: Rectified Photo from Same photograph, distortion corrected.....56

Figure 3.16	3D Reconstruction - Using the VisualSfM GUI .....	60
Figure 3.17	VisualSfM with rectified images from PTLens software .....	60
Figure 3.18	Rendered view of Master CAD data of Prototype blade.....	62
Figure 3.19	Digital Mock-Up of the Prototype of Wind Turbine blades on hub .....	62
Figure 3.20	Up: Render view of Master CAD data, Down: Prototype blades with different surface patterns and targeting layout, From top Pattern 1 to 3.....	64
Figure 3.21	Blades with different target pattern.....	65
Figure 3.22	Prototype blade illuminated by color light with $\lambda=432$ .....	66
Figure 3.23	Camera calibration parameter in VisualSfM.....	67
Figure 3.24	RE POWER MM 92 & Crane Withdraws (source: <a href="http://myrenaultzoe.com/index.php/2013/02/17/">http://myrenaultzoe.com/index.php/2013/02/17/</a> : image: T. Larkum).....	69
Figure 3.25	Suspended access equipment for Wind Turbine ( <a href="http://www.spiderstaging.com">www.spiderstaging.com</a> )..	70
Figure 3.26	Access to the blades' surfaces by access man hole in the wind turbine hub (source : <a href="http://www.frontierpro.com">http://www.frontierpro.com</a> ) .....	71
Figure 3.27	Remote controlled Helicopter for WT image acquisition (Source: <a href="http://www.airfoilsycam.com">http://www.airfoilsycam.com</a> ) .....	72
Figure 3.28	Proposed camera movement around the blade by Remote controlled drone .	73

Figure 3.29	Self-inking stamp for coded and non-coded retro target.....	74
Figure 4.1	Generated point cloud of the iced blade-regular light.....	77
Figure 4.2	Point cloud view from pitch angle axis.....	78
Figure 4.3	Generated mesh of 1 <sup>st</sup> blade (recto view). Extracted point cloud from normal lighting .....	79
Figure 4.4	Generated mesh of 1st blade (verso view). Extracted point cloud from normal lighting .....	79
Figure 4.5	Generated mesh of 1 <sup>st</sup> blade (recto view). Extracted point cloud from light with $\lambda=432 \text{ nm}$ .....	80
Figure 4.6	Generated mesh of first blade (Verso view). Extracted point cloud from light with $\lambda=432 \text{ nm}$ .....	80
Figure 4.7	Generated mesh of second blade (Verso view). Extracted point cloud from light with $\lambda=432 \text{ nm}$ .....	81
Figure 4.8	Generated mesh of second blade (Verso view). Extracted point cloud from light with $\lambda=432 \text{ nm}$ .....	81
Figure 4.9	Steel ruler as Ground Control Points (GCP). .....	83
Figure 4.10	Scale Bar in the point cloud .....	84
Figure 4.11	Generated mesh in Digitized Shape Editor Environment of CATIA.....	85

Figure 4.12 3D Similarity transform feature is positioned on the blade ..... 86

Figure 4.13 CAD model aligned with the generated cloud point ..... 87

Figure 4.14 Ice thickness contour of first blade (recto view). Extracted point cloud from regular light ..... 88

Figure 4.15 Ice thickness contour of first blade (verso view). Extracted point cloud from regular light ..... 88

Figure 4.16 Manual measurement of iced region. Filler gauge shows  $\approx 2.9$  mm in area.... 89

Figure 4.17 Composition of used feeler gauges in measurement ..... 90

Figure 4.18 Ice thickness contour of first blade (recto view). Extracted point cloud from light with  $\lambda=432$  nm ..... 90

Figure 4.19 Ice thickness contour of first blade (verso view). Extracted point cloud from light with  $\lambda=432$  nm ..... 91

Figure 4.20 2D ice profile shape on the blade in different span wise of object. The hatched profile is the blade real cross section. Brown show the margin of the ice volume on the blade ..... 92

Figure 4.21 Wind turbine blade as with coded retro targets on surface ..... 94

## LIST OF ABBREVIATIONS

AM	Additive Manufacturing
ANN	Approximate Nearest Neighbors
BA	Bundle Adjustment
BITE	Built In Test Equipment
CAD	Computer Aided Design (Drafting)
CAE	Computer Aided Engineering
CAM	Computer Aided Manufacturing
CAO	Conception Assistée par Ordinateur
CCV	Cold Climat Version
CMOS	Complementary Metal–Oxide–Semiconductor Sensor
CRP	Close Range Photogrammetry
DEM	Digital Elevation Model
DSLR	Digital Single-Lens Reflex <i>camera</i>
EMI	Electro Magnetic Interference
EXIF	Exchangeable Image File Format
FOS	Fiber Optic Sensor
GCP	Ground Control Points
GRP	Glass-fiber-Reinforced Plastic
GUI	Graphic User Interface
IR	Infra Red
JPEG	Joint Photographic Experts Group

## XXIV

LED	Light Emitting Diodes
MP	Mega Pixel
PMVS	Patch-based Multi-View Stereo Algorithm
RANSAC	Random Sample Consensus
RC	Remote Control
RGB	Red Green Blue <i>color code</i>
RT	Retro Target
SBA	Sparse Bundle Adjustment
SfM	Structure from Motion
SIFT	Scale Invariant Feature Transform
SLR	Single-Lens Reflex <i>camera</i>
SNEEC	Site Nordique Expérimental en Éolien CORUS
SO	Small Object
SURF	Speeded Up Robust Features
UI	User Interface
UV	UltraViolet
WESNet	Wind Energy Strategic Network
WT	Wind Turbine

## LIST OF SYMBOLS

$A$	Cross sectional area [ $m^2$ ]
$\omega$	Mass concentration of the particles [kg]
$\vartheta$	Relative velocity [ $\frac{m}{s}$ ]
$\alpha$	Terms of correction factors
$\alpha 1$	Collection efficiency (or collision efficiency)
$\alpha 2$	Sticking efficiency
$\alpha 3$	Ice builds up rate on the surface (blade)
$nm$	Nanometer
$\lambda$	Wavelength [ $nm$ ]



## INTRODUCTION

Globally, fossil fuels are the primary source of electricity with hydropower and nuclear power plants being in use to meet the demands in certain regions of the world. In recent times, concerns about the harmful effects of global warming and emissions of carbon dioxide have created new demands for an alternative and suitable energy source such as wind energy. The benefits of wind energy include an abundant source, pollution free, local power generation at site that reduces long distances transmission losses (Patel, 2012) and economic gains such as investments in rural development as well as creation of new jobs.

Wind energy in Quebec has been developed as part of the Quebec government's 2006–2015 energy strategy, the goal of which is to install 4,000 MW of wind energy capacity in the province by 2015. This objective should be reached in 2018 with the finalization of the projects totaling 800 MW announced in May 2013.

The Quebec government must develop a new energy policy for after 2015. CanWEA recommends that the Quebec government define clear and specific objectives in its next energy policy for the installation of new wind projects totaling 500 MW of capacity per year between 2018 and 2025. This objective is in keeping with the vision of developing the sector, creating wealth and attracting investment to Gaspé, Montréal and elsewhere in the province (canwea.ca, 2013)

However, there are problems associated with wind power generation in cold climates such as Canada, most notably icing.

### **Background**

Atmospheric icing on structures has been a known problem to industries such as aviation and operation and maintenance of power lines for a long time. It is though a fairly new problem for the wind power industry as it has expanded into more arctic and alpine regions where the wind resource is rich but the climatic conditions are more challenging. A large-scale

expansion in this type of terrain demands improved knowledge of how wind turbines perform during icing conditions and what happens to it in extremely low temperatures. Difficulties such as low temperature of gearbox oil, iced-up yaw systems and changed aerodynamics of turbine blades due to icing have to be solved if wind power in cold climates is to be profitable. Some manufacturers have already developed arctic packages for wind turbines, but the icing of the blades still requires further work. There are only a few different de-icing and anti-icing solutions available on the market. There are also some problems to identify the onset of the icing event, which results in increased downtime of power production.

A clear negative aspect from ice accretion is the impact the ice load has on the different components of the wind turbines. Icing can cause problems ranging from decrease of power due to modifications in the aerodynamics of the blades' profile (Jasinski et al., 1998), which results in increased blade vibration and fatigue of wind turbine components (Ganander et Ronsten, 2003) and to additional safety concerns to people and wildlife due to detachment of accumulated ice. Even small amounts of ice on the blades deteriorate their aerodynamic performance. For security reasons related to ice-throw and to prevent the increased wear and the consequent shortening of component lifetime, wind turbines are generally shut down during severe icing events, which in turn lead to further loss of production and therefore economic losses.

The detection of icing poses another problem. There are several ice detection instruments on the market, but none of them seem to be performing satisfactorily. However, improvements are continuously made to enhance the measurement sensitivity and accuracy. The causes and effects of icing on wind turbines are not completely understood and neither are there well-proven solutions readily available to hinder icing. Therefore, this is an area of active research.

## 1) Objective

In many research on the icing of the blades, the ice shapes were defined to approximate the shapes obtained from analysis of the photographs from in-site full-scale wind turbines with icing and from the results of numerical simulations using an ice accretion code (Canice, 2015). The profile shape of icing are modeled based on the numerical simulation from the atmospheric conditions data during one year (Antikainen et Peuranen, 2000) & (Botta, Cavaliere et Holttinen, 1998). This combined use of in-site photographs and ice accretion code take an estimated 3D ice shapes from the blade that is far from the real shape of the ice. This method could not show the mass exact of the ice on the blades that cause unbalancing and resonance in the wind turbine.

The aim of this study is to implement a new approach for measuring ice thickness by photogrammetry and computer vision system. Photogrammetric scanning for measuring the thickness of ice is quit new in this field. In principle, photogrammetric methods can be applied in any situation where the object to be measured can be photographically recorded. When the rotor blades were mounted on the wind turbine tower, ice thickness inspections became nearly impossible to be performed in the past, now by image base modeling of iced blades, geometry extraction are possible. If we focus on the case of Image-based modeling, reconstructed outputs are largely in the form of mesh models. New methodology for measurement by photogrammetric scanning of an installed wind turbines' blades will be proposed. By this methodology the real distribution of ice's mass on the blades surfaces measured by verifying of the shape and dimension of icing rotor blades against CAD or master data of rotor blades . CAD data of master model of wind turbine blade generate by 3D reverse engineering base on the Photogrammetry measurement of clean installed blades with appropriate level of details.

The case study of this thesis is a RePOWER MM92 wind turbine “2-MegaWatt power plant with 92 meter rotor diameter” that installed in the wind farm field in Gaspésie peninsula. In this study, the different methods of access to the blades' surfaces reviewed and suitable economical and practical photography method will be proposed.

## 2) Research Identification

- **Research Objective**

My research topic focuses on reconstruction of three dimensional polygonal mesh models by images captured from wind turbine blade with a configuration of digital SLR cameras. The main objective of this study is to identify the volume and shapes of iced accumulated areas on the wind turbine blades in arctic regions. Comparison of these polygonal mesh models with the master CAD data of clean blade without ice, could be extracted the geometry of iced regions.

The specific aims of this study are as following:

- Inspection and extraction of real air foil section in wind turbine blades (CAD data of the rotors blades in normal and icing condition);
- To find out the distribution of icing mass on the blades surfaces;
- To understand the modified airfoil of the icing blades.

## 3) Research questions

1. What is the 2D ice profile shapes on the blades at different span-wise locations?
2. What is the ice thickness (Glaze ice & Rime ice) on the surface of the rotor blades?

## 4) Innovation Aimed at

Innovation of this research is to develop a new approach for measuring the ice thickness by Photogrammetry and computer vision system. This new approach can be finished to new ice detection systems, which has more advantage than existing commercial ice detection sensor.

This approach can develop a new ice detection system who detects:

- Real distribution and volume of ice on the blade's surface;
- Shape & Geometry of ice on the blade;
- The real shape of Ice in time of measurement (Geometry of modified airfoil);
- Estimated *Mass* and *Thickness* of Ice in measuring time.

## **Thesis Structure**

The research work is organized as follows:

Chapter 1: Introduction, this section presents general overview about the case study, Atmospheric Icing of wind turbines & Ice detection systems available in market. It describes the basic idea of topic, motivation, problem statement, research objectives, and research questions.

Chapter 2: Introduction to Close Range Photogrammetry & image base modeling, deals with theoretical background of the study and literature review. It also explains various components of computer vision and digital photogrammetry & Technical components of photogrammetric process.

Chapter 3 Methodology, this chapter describes the complete workflow of the study and description in details, about data used, hardware and software tools used.

Chapter 4: Results and Conclusion, this chapter describe the experiments on the selected data, achieved results, its discussion and analysis and finally the answer of the research questions in concluded form and recommendations for further study.

Recommendation: This section proposed the important notice & details recommendation in Photogrammetric measuring of Ice for the real case study base on the author knowledge and the experiences from this study.

## **CHAPTER 1**

### **ATMOSPHERIC ICING OF WIND TURBINES & ICE DETECTION SYSTEMS**

This chapter is a brief presentation for atmospheric icing of wind turbines and the existing ice detection methods in the market. The objectives of this chapter were to review the ice detection methods of and propose an alternative system that overcomes the shortcomings of previously tested icing sensors.

#### **1.1 Introduction**

Wind energy is and will increasingly be used at cold climate sites as one of the best locations for wind turbines where are subjected to icing of blades. According to Figure 1.1 the cold climate areas are one of the major attractive areas for wind power development. Resulting out of the external conditions at these sites several effects occur that change the wind turbine behavior and in consequence the efficiency of a wind farm. The calculations show that a wind turbine can lose up to 20% of its annual production output through ice formation (Krogh-Jeppesen, 2014).

Icing of blades in wind turbine blades (Figure 1.2) be able to cause a range of problems, such as complete loss of production, reduction of power reduction by disrupt the aerodynamics airflow, overloading due to delayed stall, increased fatigue of components due to imbalance in the ice load, and damage or harm caused by uncontrolled shedding of large ice chunks.

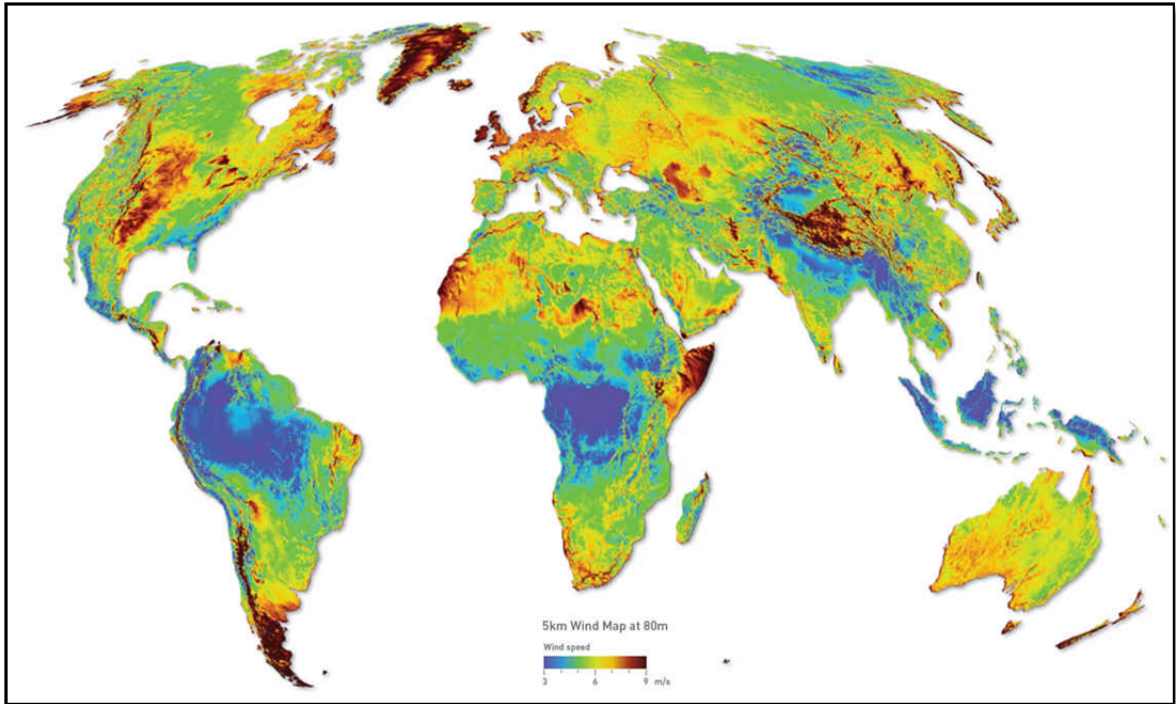


Figure 1.1: Prevailing strong winds. The map indicate regions of wind attractive for wind power development, with average wind speed  $> 5\text{ms}^{-1}$  and average generation 33% of rated power. Note the importance of marine situations and upland sites (Burton et al., 2011).



Figure 1.2: Problematic ice vanes on the windward side of the blade

## 1.2 Main type of atmospheric ice accumulation

Atmospheric icing is the term used to describe the accretion of ice on structures or objects due to either freezing precipitation or freezing fog. According to ISO 12494, two main types of atmospheric ice accumulation are traditionally defined, precipitation icing and in-cloud icing (ISO 12494, 2001).

The main icing mechanisms in wind turbine application are as follows:

- In-cloud icing;
- Precipitation icing.

### 1.2.1 In-cloud icing

In-cloud icing occurs when small, super cooled, airborne water droplets, which make up clouds and fog, freeze upon impacting a surface, which allows formation of ice. These water droplets can remain liquid in the air at temperatures down to  $-35\text{ }^{\circ}\text{C}$  due to their small size but will freeze upon striking a surface which provides a crystallization site (Mason, 2010).

Rime ice is the most common type of in-cloud icing and has the three following forms:

- Hard rime;
- Soft rime;
- Glaze.

The different types of rime and glaze are formed depending on the droplet sizes and the energy balance of the surface in question. For small droplets with almost instantaneous freezing, **Soft rime** forms. With medium sized droplets and slightly slower freezing, **Hard rime** forms. If the buildup of rime is such that a layer of liquid water is present on the surface during freezing, **Glaze** forms.

Rime ice forms ice vanes on the windward side of the blade especially on the leading edge and tip of blades. This leads to eccentric loading by ice. In-cloud icing also depends on

the dimensions of the object exposed, the wind speed and the air temperature (Frohboese, Steiniger et Anders, 2007). In general Rime ice grows as droplets rapidly freeze and forms brittle, opaque, and milky-textured ice.

### 1.2.2 Precipitation icing

Precipitation icing is due to rain or snow freezing on contact with a surface. Precipitation icing can have much higher rates of mass accumulation than in-cloud icing, with possibly greater resulting damage. Relative frequency for the two types of icing is dependent on geographic location and climate. Wet snow can stick to surfaces when in the temperature range of 0–3 °C, while freezing rain requires surface temperatures below 0 °C. Glaze icing can occur throughout most of North America, but is most prevalent along Canada's east and west coastal regions.

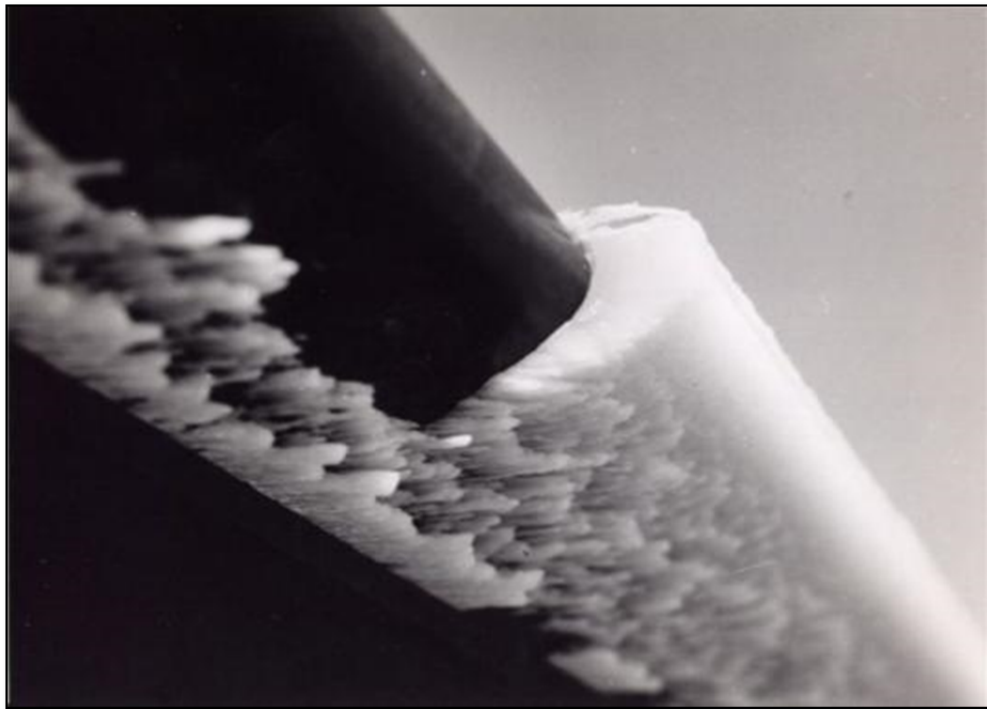


Figure 1.3: Aircraft Propellers with accumulation of precipitation ice on leading edge, image taken between 1969-73, in Sea-king, Wessex. Ontario Canada. (source: [www.eacott.com.au/gallery/d/3366-1/icing+4](http://www.eacott.com.au/gallery/d/3366-1/icing+4))

A physical model for icing is described by Eq. (1.1), as detailed by (Makkonen, 1994) and (Frohboese, Steiniger et Anders, 2007). The variation of mass ( $M$ ) is:

$$\frac{dM}{dt} = \alpha_1 \times \alpha_2 \times \alpha_3 \times \omega \times \vartheta \times A \quad (1.1)$$

Where  $A$  is the cross sectional area of the object with respect to the direction of the particle velocity vector,  $\omega$  is the mass concentration of the particles,  $\vartheta$  is the relative velocity of the particles and the  $\alpha_i$  terms are correction factors with values in the range 0.0–1.0. The collection efficiency (or collision efficiency),  $\alpha_1$ , represents the flux density of particles striking the surface in relation to the maximum possible. The sticking efficiency,  $\alpha_2$ , represents the ratio of the flux density of particles sticking to the surface. The accretion efficiency,  $\alpha_3$ , represents the rate at which ice builds up on the surface in relation to the flux density of particles sticking to the surface



Figure 1.4: Frosted ice accumulated on the WT Blade's shoulder  
(photo by LM Wind Power Group) (kaupunki, 2011)

As described in Eq. (1.1) at area as close to the tip of blades, the highest velocity occurs, sweep a larger volume and collects water or ice from the entire environment. This area has the significant rate of ice accretion.

Glaze ice is *transparent*, hard and *attaches well to surfaces*. Rime ice has *Greater thickness* and *attached more loosely to surface*. The mixture of two type of icing could be occurred due to variation in  $\omega$ , the mass concentration of the particles, the relative velocity of the particles,  $\vartheta$  and change the correction factors of  $\alpha$  during the time of ice accumulation. The attachment of ice to the surface causes the arbitrary change in shape and the mass of ice on the wind turbine in operation.

### 1.3 Ice detection methods

Icing detection of wind turbines has different requirements than detection of icing on aircraft or for meteorological equipment purposes. This is evident when sensors considered for other purposes do not perform adequately when mounted on the wind turbines. As described in Eq. (1.1) the best position for the detection of icing on the blades on the blade itself, in area as close to the tip of blades which has the significant rate of ice accretion. The outer ends of the blades sweep a larger volume and collect water or ice from the entire volume which it is at the blade tip that the highest velocity occurs who is directly related to the relative velocity of the super-cooled water droplets. Another reason is that the blade tips can experience icing due to low clouds even though the nacelle is ice-free.

(Homola, Nicklasson et Sundsbø, 2006) reviewed 29 ice detection methods for use in the wind industry. These methods were discussed based on a set of requirements for a sensor/probe under broad operating conditions. They separated these methods into two groups: Direct method and indirect method.

The **indirect methods** are based upon detecting the weather conditions that lead to icing, such as humidity and temperature, or detecting the effects of icing, such as a reduction in

power production. They then use a model, either empirical or deterministic, to determine when icing is occurring (Homola, Nicklasson et Sundsbø, 2006). The indirect methods are out of scope of this research.

### **1.3.1 Direct detection**

The direct methods detect some property change caused by the accretion of ice. These include mass, reflective properties, electrical or thermal conductivity, dielectric coefficient and inductance. The inductance change probe of (Seegmiller, 1996), the impedance change probe of (Wallace et al., 2002) and the microwave ice detector of (Magenheim, 1977) are examples of direct methods. (Homola, Nicklasson et Sundsbø, 2006) evaluated twenty-four direct methods of ice detection and all the majors of these methods are based on the change in an electrical property with ice accretion appear suitable for use in the wind industry. In the work of (Homola, Nicklasson et Sundsbø, 2006), most of the 29 methods presented were found not to be reliable for ice detection base on the study's set of requirements. These requirements include high sensitivity and wide area detection capabilities. This research evaluates the proposed optical methods from their list separately and compares them to our proposed solution for ice detection in end of Chapter 2.

#### **1.3.1.1 Direct detection by reflective light sensor, HoloOptics**

The HoloOptics (Westerlund, 2004) detects ice by means of optical sensors. An IR-emitter sends out light that is reflected by a probe and registered by a photo detector. It makes use of the fact that the probe's optical properties change with an ice coating. Ice is indicated when 95% of the probe is covered with a 50 $\mu$ m thick layer of clear ice or a 90 $\mu$ m thick layer of any other type of ice. (Heimo et al., 2006)

When the photo detector detects ice, the internal heating is turned on without time delay to de-ice the surface. The time it takes to de-ice the probe depends on several factors, such as icing rate, air and surface temperature and ice type (Montgomerie, 2014). As soon as the ice

is melted, the heating is turned off and ice can accrete on the probe again. Thus, the frequency of ice detections gives the intensity of the ice accretion since build-up and melting of ice on the probe continues for the duration of the icing event.(Persson, 2009) & (Fikke et al., 2006)

The HoloOptics T26 measures ice independently of wind direction by using the four sensors, one for each cardinal direction (north, south, east and west) while the T23 only has one sensor and therefore only detects ice accretion in one direction. This is useful when wind direction is known, as for example when mounted on a nacelle. (Andersen et al., 2011)



Figure 1.5: (Left) T23 & T26 Icing Rate Sensor, (Right) T41 shown on the nacelle at the wind power plant in Härnösand, northern Sweden. Source: HoloOptic.net

The HoloOptic sensors should be mounted on the nacelle of the turbine, and have therefore limited applicability. If the Ice detected on the sensor there is a great probability that ice is accumulated on the blade.

The principal of detection by infrared light could be applicable on the blade, in the event that they are modified such that an IR-emitter & photo detector can be mounted on hub of wind turbine and reflector retro targets sticks on the blades. Figure 1.6 shows IR-emitter & photo detector installed on the hub and reflector retro targets stick on the blades. Accumulated ice shown on the blade surfaces. The field of view of optical instruments (IR-emitter & photo detector) shown in red.

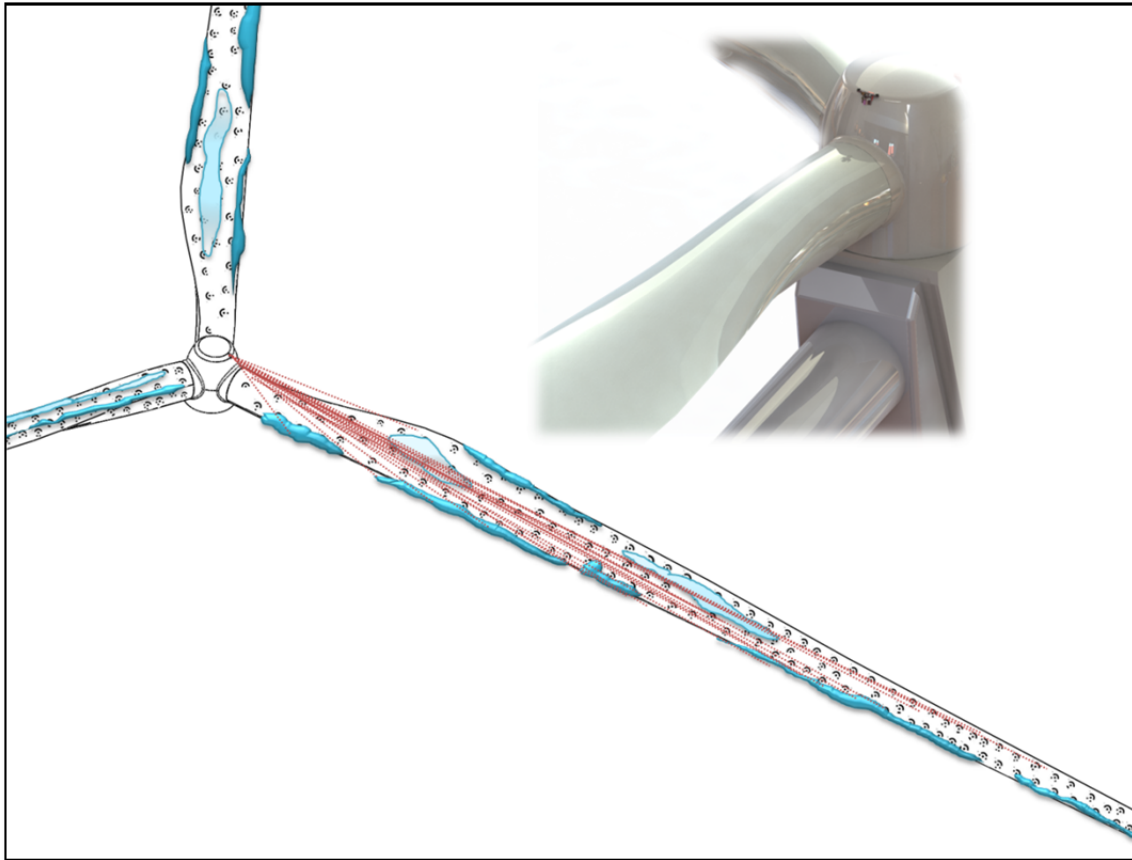


Figure 1.6 : The IR-emitter & photo detector installed on the hub and reflector as retro targets stick on the blades.

### 1.3.1.2 Stereo imaging from web cameras

For observation of wind turbine blades, two Webcams were installed on the nacelle of the wind turbine. One camera is taking a picture of the blade every 15 minutes (blade detection by video motion detection). The second camera is taking regular pictures of the Ultrasonic anemometer mounted on the nacelle of the wind turbine. With these cameras images, ice accretion on the blades of the wind turbine can be observed and analyzed. (Seifert, Westerhellweg et Kröning, 2003)



Figure 1.7 : (Top left) Installed camera on the Nacelle, the lamp on the right is for heating purpose. (Top right) rime ice observed on the blade. (Bottom left) rime ice after 45min heating system on, (bottom right) de-iced blade, some little trace of glazed ice remained on the leading edge. Source : (Cattin, 2015)

Web cameras can be useful during testing of various sensors, and to record the conditions at the wind turbine, but have not yet been demonstrated to be suitable for ice detection for several reasons. In arctic regions there is little light during much of the winter, which requires artificial lighting. This artificial lighting, if in the visible spectrum, can be negative for the visual environmental impact of the wind turbine installation. The second, and perhaps more important reason is the lack of suitable automated image analysis tools, but image analysis is an area in rapid change, which may make this system viable in the near future. The images of web cameras on the nacelle could be used as input for image base modeling which is the subject of this research.

### 1.3.1.3 Reflection of polarized infrared light, IceHawk®

The IceHawk® system (Jamieson et Ray, 2004) scans a surface by sending a beam of polarized infrared light. It detects ice by analyzing the polarization of the reflected signal. When ice is present, the returned infrared signal is un-polarized. A picture of the scanned surface is computed and shown on the IceHawk display with patches of contamination highlighted in red. The system has the ability to "see through" materials such as de/anti-icing fluid, hydraulic fluid and fuel to detect frozen contaminant build-up underneath. The system can detect any frozen contaminant including snow, frost, slush or ice.

A presence of a polarization altering substance on a specular surface is detected by transmitting light from a single strobe light source to the surface over a transmitting path and receiving the transmitted light from the surface. An intensity of the light is measured in both an optical non-isolator state and an isolator state by a same detector by delaying the non-isolated return light for a definite period of time before measuring it with the detector. The measured isolated and non-isolated intensities are converted to logarithmic form, range corrected, and compared to reference data established for the specific specular surface being investigated to detect the presence or absence of the polarization altering substance. Attenuation and backscattering effects of scattering and/or absorbing interference in the transmitted light are compensated so that the reference table is entered at the correct point. Using different intensities of transmitted light increases the dynamic range of the system. (Stern, Schaefer et Maali, 2000)

The proposed system designed for aerospace application & could be interesting as wind turbine icing sensor since it could perhaps examine the blades from a distance. The mounting of the sensor such that the pressure side of the blade is seen requires more study, as current systems using polarized light ice detection have a range limitation of less than 30 m that are less than the regular blade length in wind turbine size in cold climate area.

#### **1.3.1.4 Infrared spectroscopy**

Ice detection is performed current less at the end of a fiber optic cable, which points out of the blade near the tip, where icing starts. The signals are transferred to the sender/receiver, which is located in the hub. From there, the results may be sent to the installation control and used as ice-warnings. Measurement principle is infrared signals, produced by LEDs (Light Emitting Diodes) (Figure 1.8). The signals are sent through the fiber to the tip, where they are partially reflected, and in the case of icing, characteristically absorbed. Lab results with 50m sensor fibers show a clear recognition of ice and indicate that dirt on the fiber tips leads only to weaker signals but seems to be no problem for ice detection so far. The measurement range is between a few micrometers and a few centimeters (depending on the type of ice). Due to varying signal scattering in different types of ice, the result is always an estimate of a layer thickness mean. Measurements can be made every few seconds and hence provide real-time information of the actual icing status of the blade and allow a fast reaction after initial icing or a completed de-icing procedure. Every sensor unit can be equipped with up to three fibers, monitoring three blades or different spots in one blade (Homola, Nicklasson et Sundsbø, 2006)

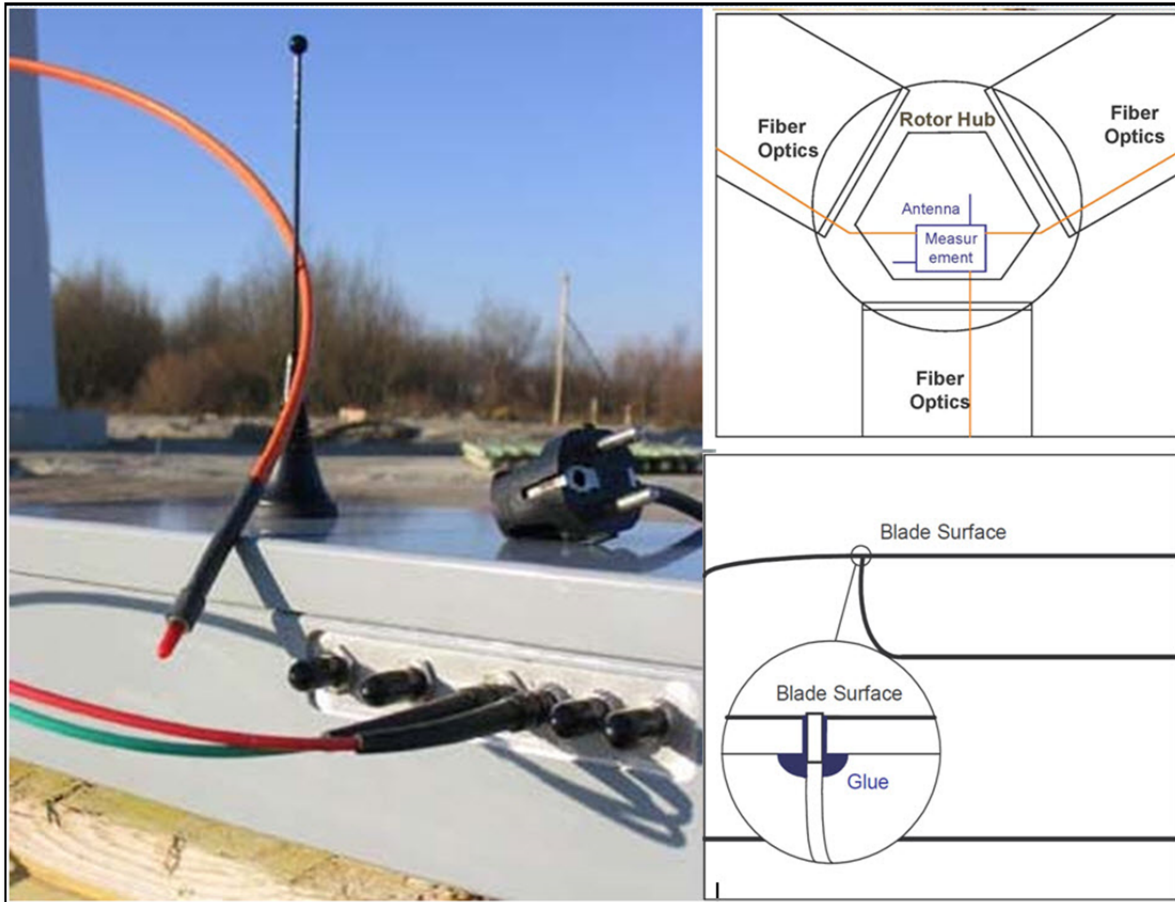


Figure 1.8: (Left) Infralytic Sensor tip with sender/receiver, (Right top) Sketch of rotor hub, (Right down) Sensor location in the blade. Source Brochure: IcesensorInfralytic\_EN.pdf

The system using infrared spectroscopy has an advantage in that all electronics and serviceable components are mounted in the hub of the turbine, not on the blades. There are no extra conductors out to the blades, so no additional lightning risk is generated. The point detection is a slight disadvantage, but this can be corrected by having more points under observation. The greatest disadvantage is the difficulty in installing the system in existing blades. This is because the fiber optic cables must be installed during the construction of the blade. This system has already been built by Infralytic. It has been independently tested in an icing wind tunnel with good results (S. Kimura, T. Sato et al., 2005). In addition, the sensor is included in the Swiss Project ‘Alpine Test Site Gütisch: Meteorological measurements and wind turbine performance analysis’ which runs within the COST 727 Action ‘measuring and

forecasting atmospheric icing on structures', which will test a variety of sensors over a three year period .

#### **1.3.1.5 Reflected light from inside**

The ice detector system utilizes a light source, light detector and temperature sensor coupled together for providing signals representative of icing which may be utilized to provide an alarm to the cockpit of the aircraft. Built In Test Equipment (BITE) is also included in the detector system for system failure indication to the pilot of the aircraft.(Federow et Silverman, 1994)

Using reflected light from an ice covered window out from the blade is a very simple idea that would probably work well for rime ice, but is expected to have difficulties with very thin layers of clear ice, for example freezing rain. This is due to the fact that thin layers of clear ice need not disturb the optical path.

#### **1.3.1.6 Fiber optic cable with special clad**

Finally the last optical ice detection system which we found in the market is an ice sensor for the remote rapid indication of ice formation or the presence of ice is a fiber optic "switch", activated by ice but not by water, and based on the difference in optical properties between water and ice. The approach is to construct a "fiber optic" which itself is the ice sensor. The fiber optic sensor (FOS) is designed so that no light is transmitted when water is present but as soon as ice begins to form, light is relayed. Thus ice switches on the light- In addition, limited quantitative information can be made available on the rate of ice formation. Alternatively the sensor can be formed of another type optical waveguide instead of an optical fiber. The ice sensor is formed by placing spaced stripes of a clad material on a fiber optic core, or other waveguide structure, where the clad has a refractive index close to ice and the core has an index greater than the clad but less than water. It is best to index match the core to the clad for optimal transmission when ice forms in the gaps between the clad stripes. The advantages of the ice sensor include: specific, sensitive, real-time response,

small, lightweight, inexpensive, requires no line-of-sight, EMI immune, rugged and flexible.(Klainer et Milanovich, 1990)

The Fiber optic cable with special clad as Infrared spectroscopy has disadvantage such is the difficulty on installation the sensor in existing blades. This is because the fiber optic cables must be installed during the construction of the blade.

#### 1.4 Limitations or disadvantages of current ice detection systems

Icing detection of wind turbines has different requirements than detection of icing on aircraft or for meteorological equipment purposes. Many of detection methods developed for icing detection on aircrafts and this is evident when sensors considered for other purposes do not perform adequately when mounted on wind turbines.

The all mentioned sensors could detect ice formation within an **area or on the point** just if there was a sensor installed in the area. The sensing elements/electrodes have the difficulty in installing on existing blades. This is because the sensor or the communication cables must be installed during the construction of the blade. In addition mounting of icing sensor on the Blades requires several points should be considered during the design phase. Such as:

- Sensor Installation during turbine's blades manufacturing;
- Lightning protection;
- Difficult access to the failed sensor;
- Problems of mounting a sensor on the flexing blade's material.

By the previous reviews about the icing sensor for the wind turbine **any of the proposed methods *could not* detect:**

- Real distribution and volume of ice on the blade's surface;
- Shape & Geometry of ice on the blade;
- The real shape of Ice in time of measurement (Geometry of modified airfoil);
- Estimated *Mass* and *Thickness* of Ice in measuring time.

Thus installing the ice detection sensors for an existing wind turbine is *impossible or more costly* if applied.

Table 1-1 shows the brief review from the studied ice detection systems

Table 1.1: Optical ice detection system in market

Existing Optical ice detection system	System to be integrate in WT design and make	Thin ice detection	Sensor on the blade surface	Ice distribution on the blade's surface	Geometry of modified blade's airfoil
<i>Direct detection by Reflective Light Sensor, HoloOptics</i>	No. Can be installed on exiting WT	yes	No. to be installed on the nacelle	No	no
<i>Stereo imaging from web cameras</i>	No. Can be installed on exiting WT	Depend on the camera optical resolution and field of view, (Artificial light is needed)	No. to be installed on the nacelle	No	No
<i>Reflection of polarized infrared light, IceHawk®</i>	Yes. Costly or impossible to integrate for existing WT	Yes-range limitation of less than 30 m	yes	No	No
<i>Infrared spectroscopy</i>	Yes. Costly or impossible to integrate for existing WT	Yes-in sensor position	Yes	No	No
<i>Reflected light from inside</i>	Yes. Costly or impossible to integrate for existing WT	Yes-in sensor position	Yes	No	No
<i>Fiber optic cable with special clad</i>	Yes. Costly or impossible to integrate for existing WT	Yes-in sensor position	Yes	No	No

Chapter 2 is a literature review from related research on our proposed method and chapter 3 reviews a new methodology for measurement by photogrammetric scanning of an installed wind turbine's blades. By this methodology the real distribution of ice's mass on the blades surfaces is measured by verifying the shape and dimension of iced rotor blades against CAD or master data of rotor blades. CAD data of master model of wind turbine blade generated by 3D reverse engineering based on the photogrammetry measurement of clean installed blades with appropriate level of details.

This new approach, once completed, can be considered as a new ice detection system which has more advantages than all previous systems such as:

- A **cost effective way** for ice measurement that can be applied on any size of wind turbine.
- Extraction of real shape of ice in time of measurement (Geometry of modified airfoil);
- In the proposed method, the required retro targets (printed patterns) could be added any time to existing wind turbine's blades and no sensors need to be installed on flexible blade's material.
- Regarding the shape of blades and the measurement area, the photogrammetric object recording could be applied by dynamic camera (Camera on RC Drone) which is the proposed method in Chapter 3 for measurement of the thickness of ice on all cross sections of wind turbine blade. If the object recording is applied by fixed Camera Sensor on wind turbine hub or nacelle, the overlapped photos contain limited information and the results cover a small region of WT's blade. This option is out of scope of this study.

## CHAPTER 2

### INTRODUCTION TO CLOSE RANGE PHOTOGRAMMETRY & IMAGE BASE MODELING

Three-dimensional models are being actively used in various fields like CAD/CAM/CAE, quality inspection, urban planning, emergency response systems and cultural heritage documentation, as a handful tools. In reconstructing of these 3D models, a large variety of data from different sources is utilized such as aerial and terrestrial laser scanning, stereo image pairs, range images and set of overlapping images. The basic of all these methods is **Photogrammetry**.

**Photogrammetry is the science of making measurements from photographs.**

'**photo**' – light;  
'**gram**' – drawing;  
'**metry**' – measurement.

The output of photogrammetry is typically a map, drawing, measurement, or a 3D model of some real-world object or scene. Many of the maps we use today are created with photogrammetry and photographs taken from aircraft (**Aerial Photogrammetry**). (Wikipedia, 2015)

In **Close-range Photogrammetry**, the camera is close to the subject and the output is drawings, 3D models, measurements and point clouds. Nowadays cameras are used to model and measure buildings, engineering structures, forensic and accident scenes, mines, earth-works, stockpiles, archaeological artifacts, film sets, etc. This type of photogrammetry (CRP for short) is also sometimes called Image-Based Modeling.

Image-Based 3D modeling has been described by (Remondino et El-Hakim, 2006) as a photogrammetry process that begins with data collection and finally results in 3D models capable of being visualized and analyzed interactively on a computer for various operations. Our research on *“Ice Measurement on the Wind Turbines’ blades by Close-Range*

*Photogrammetry Methods*” focuses on the ice modeling process using point clouds obtained through structure from motion to reconstruct the shape of ice on the blades as a polygonal mesh model. This is a new topic of research in ice detection methods of the wind turbine generators and computer but now because of operational complexity for accessing to the real case study, there is still a long way to go in making the process completely free from user interaction. Here there is a brief review of the photogrammetry process and the technical requirements for photogrammetric process.

## **2.1 The photogrammetric process**

Photogrammetry encompasses methods of image measurement and interpretation in order to derive the shape and location of an object from one or more photographs of that object. In principle, photogrammetric methods can be applied in any situation where the object to be measured can be photographically recorded. The primary purpose of a photogrammetric measurement is the three dimensional reconstruction of an object in digital form (coordinates and derived geometric elements) or graphical form (images, drawings, maps). The photograph or image represents a store of information that can be re-accessed at any time. It is therefore necessary to describe the optical process by which an image is created. This includes all elements that contribute to this process, such as light sources, properties of the surface of the object, the medium through which the light travels sensor and camera technology, image processing and further processing.

Figure 2.1 simplify and summarizes this sequence. The left hand side indicates the principal instrumentation used whilst the right hand side indicates the methods involved. Together with the physical and mathematical models, human knowledge, experience and skill play a significant role. They determine the extent to which the reconstructed model corresponds to the imaged object or fulfills the task objectives.

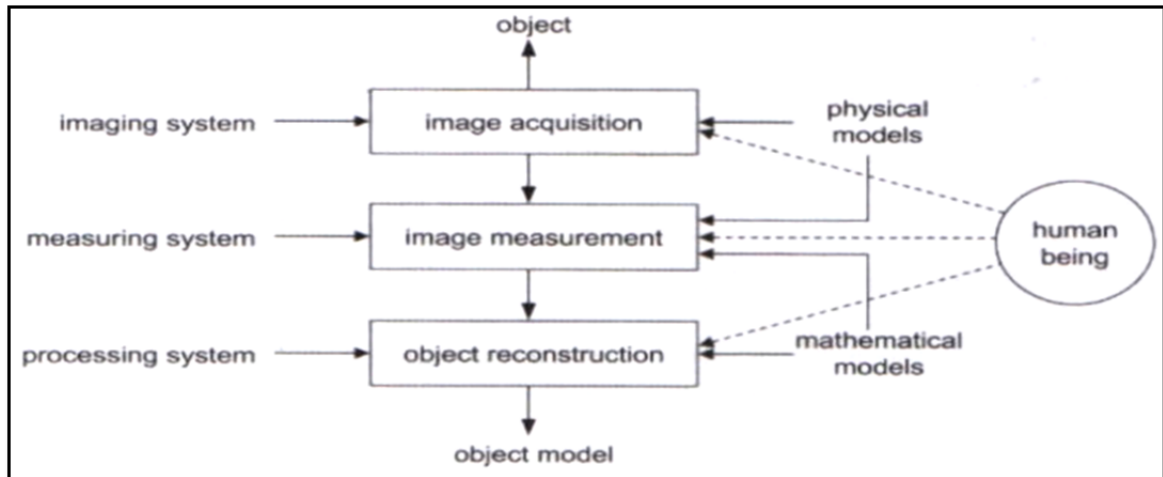


Figure 2.1: The photogrammetric process: from object to model  
 ((Luhmann, Robson et al. 2006), page 3)

The photogrammetric procedure has changed fundamentally with the development of digital imaging systems and processing. By utilizing appropriately targeted object points and digital on-line image recording, complex photogrammetric tasks can be executed within minutes on-site. A fully automatic analysis of the targeted points replaces the manual procedures for orientation and the special photogrammetric measuring instruments are no longer required and are replaced by standard computing equipment. The high degree of automation also enables non-specialist users to carry out the photogrammetric recording and data evaluation.

Close range photogrammetry based on digital image processing of the scanned imagery, offered the potential of measurement precision to 1:500,000 with respect to the largest object dimension. Particularly for outsized volume objects (e.g. >10 m diameter) with a high number of object points, photogrammetry could become a standard method for complex 3D measurement tasks (Luhmann, 2010).

### 2.1.1 Photogrammetry, recording and analysis procedures

In general, photogrammetric systems supply three dimensional object coordinates derived from image measurements. From these, further elements and dimensions can be derived, for

example lines, distances, areas and surface definitions, as well as quality information such as comparisons against nominal design dimensions (master CAD data) and machine control data (measured data). In addition, the recorded image is an objective data store, which documents the state of the object at the time of recording. The visual data can be provided as corrected camera images or graphical overlays (Figure 2.2).

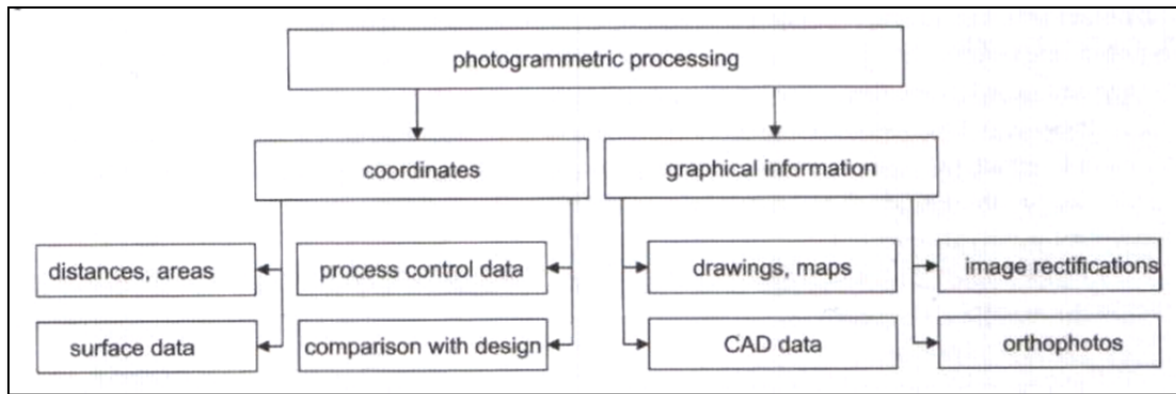


Figure 2.2: Typical photogrammetric products ((Luhmann et al., 2006), page 12)

(Luhmann et al., 2006) show the principal procedures in close range photogrammetry for both Digital & Analogue photography in Figure 2.3 which the four step of this process (Recording, Preprocessing, Orientation & Measurement & Analysis) are briefly summarized in the Annex I.

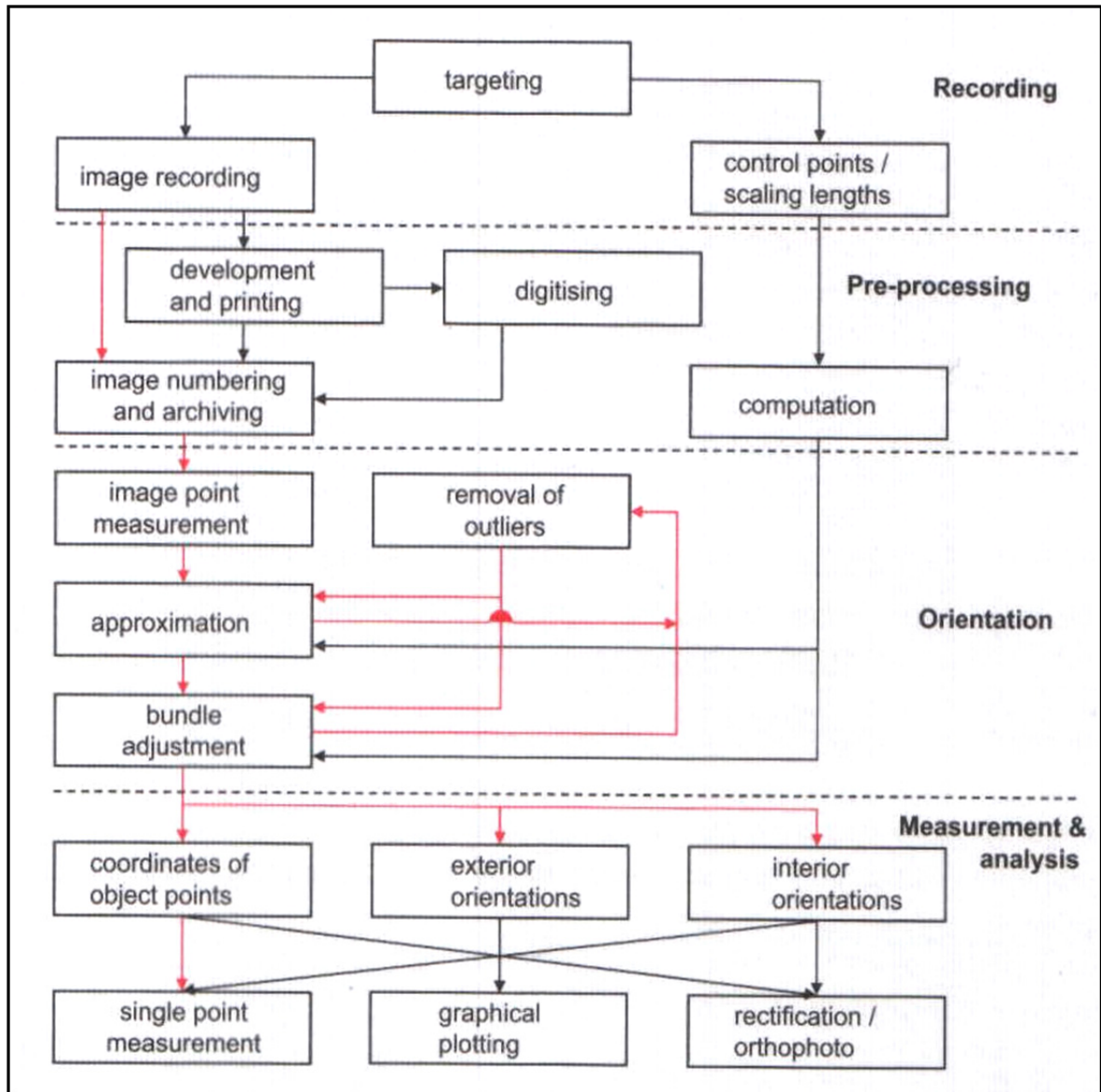


Figure 2.3: Recording and analysis procedures (red: can be automated in a digital system) ((Luhmann et al., 2006), page 3)

### 2.1.2 Technical components of photogrammetric process

The successful use of photogrammetry in industry requires a number of technical components that form an efficient and economic system. The following list summarizes these components and related technical issues (Luhmann, 2010):

- imaging sensor: resolution (number of pixels), available lenses, acquisition and data transfer speed, camera stability, synchronization, data compression, etc;
- targeting and illumination: representation of interesting object features, target shape and size, wave length of light sources, restrictions to object access, illumination power and measurement volume;
- imaging configuration: number of camera stations, desired measurement accuracy, network design, redundancy, robustness, self-calibration ability, datum definition and object control, self-control of orientation and calibration;
- image processing: automation of target recognition and identification, sub-pixel measurement of target center, multi-image matching approaches, feature tracking, and handling of outliers and scene artifacts;
- 3D reconstruction: methods for determination of 3D coordinates (e.g. spatial intersection, **bundle adjustment**) and error statistics; • data interfaces: integration into CAD/CAM environments, machine and data interfaces, user interaction and displays, etc; and
- Verification of accuracy: reference bodies, reference data, standards and guidelines, and acceptance tests.

The above listed topics show that appropriate design, setup and operation of close-range industrial photogrammetry systems form a complex task. The feasibility of a solution is not only a question of technical issues but also a function of required cost-performance ratio, system support, documentation, quality assurance and interdisciplinary skills. In the following, the **image base modeling** and structure from motion as chosen photogrammetry methods for our project are reviewed.

## 2.2 Introduction of image base modeling

Image based modeling is an off-line Photogrammetry process by which information from two or more images is extracted to produce a three dimensional model for an object. Image based modeling provides flexibility in terms of different viewing angles and positions while being very economic. Color and texture information is also captured in the data. Images can be acquired using complex cameras or sensors applied in photogrammetry or using consumer cameras.

Three-dimensional reconstructions are commonly visualized as mesh models. These models may have roughed boundaries in case of sparse point cloud, resulting in a model that is difficult to edit. Figure 2.4 show the sample of three-dimensional reconstructions of a complex object in form and surfaces.

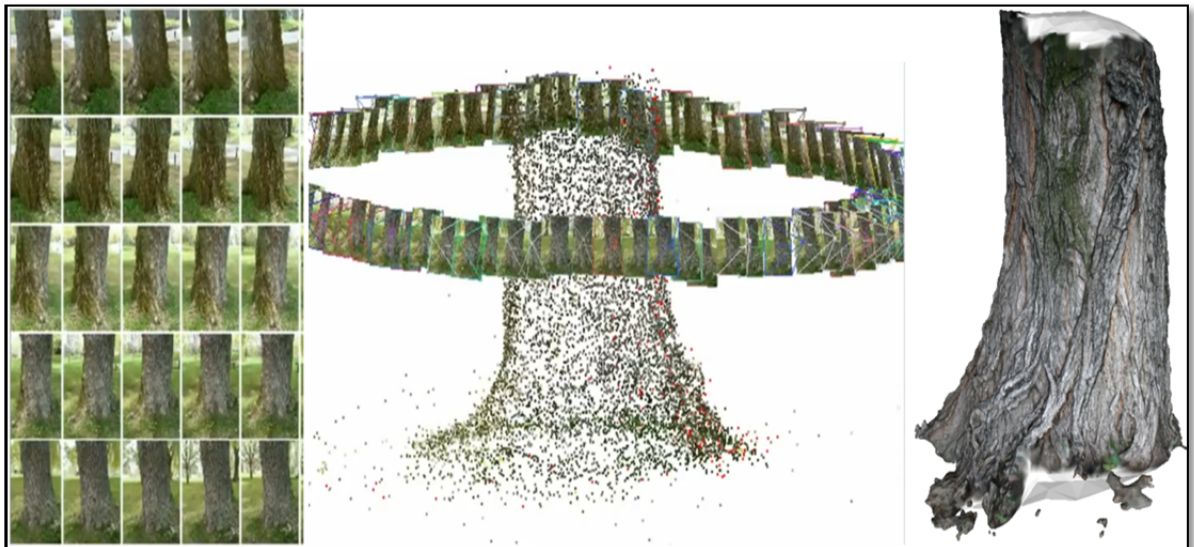


Figure 2.4: Three-dimensional reconstructions by image base modeling and Structure from Motion (SfM). Left: overlapped sequential images, Middle: Camera position and Camera path & direction in image recoding, Right: Textured mesh of object. (Horning, 2012)

### 2.3 Structure from Motion

The Structure from Motion (SfM) is described with the recovery of the three dimensional geometry of the scene (the structure) when observed through a moving camera (the motion). Sensor data is either a video or a set of pictures; additional information, such as the calibration parameters, can be used if available. The result is generally an unstructured 3D point cloud, consisting of the key points, which were identified and tracked, in the scene and a set of camera matrices, identifying position and direction of each picture with respect to an arbitrary reference frame. In image base modeling by Structure from Motion (SfM), the point clouds could have the properties of color and texture may be increased the accuracy of the results which are not available in laser scanning.

In traditional photogrammetric approach, 3D location and camera position were required as a priori information. SfM solves this problem by using key points in the images for estimating scene geometry, camera position and orientation. The key points are the common features invariant to scale and illumination that could be identified in the image pairs by applying a method called “*Scale Invariant Feature Transform*” SIFT (Lowe, 2004). However, generally SfM results are as point cloud in an optional coordinate system with no scale information. Hence, transformation to absolute coordinate system is achieved by 3D similarity transform using the primitive features in the blade (Cylinder axis in base of blade as pitch axis) and the coded retro targets in place of transformation constraint points as Ground Control Points (GCP).

The reconstruction of surfaces from oriented points has a number of difficulties in practice because of non-uniform sampling points in positions and normal are generally noisy due to sampling inaccuracy and scan misregistration. (Kazhdan, Bolitho et Hoppe, 2006) have shown that surface reconstruction can be expressed as a Poisson problem, which search for the indicator function that best fits with a set of noisy, non-uniform observations as accreted ice, and have demonstrated that this approach can robustly recover fine detail from noisy real-world scans.

## 2.4 Poisson surface reconstruction

The reconstruction of a point cloud, with oriented points, to generate its mesh is well-studied problem that has multiple approaches. The main problems when we have a point set and we want to reconstruct the mesh are:

- The vertices on the point set are not uniformly distributed over the model surface.
- The position of the vertices and its normal are generally noisy because of the Inaccuracy of the tools or inherited errors during the scanning.
- There are parts of the model surface that can be empty of data. Typically, when the tool can get that information because it is not accessible.

One of existing approaches that tries to deal with these difficulties is the Poisson Surface Reconstruction. (Kazhdan, Bolitho et Hoppe, 2006) express the Poisson Surface Reconstruction can also infers the topology of the unknown surface, fits the noise on the data accurately and fills the holes that are not holes in the initial model. The results of a Poisson Surface Reconstruction tend to be smooth and watertight. In contrast, of other approaches, the Poisson Surface Reconstruction is a global solution that considers all the data at once without using heuristic techniques or blending.

(Chauve, Labatut et Pons, 2010) showed that in 3D reconstruction, most often the three-dimensional model, the point cloud index or render efficiently by Poisson Surface Reconstruction. Therefore, if simplified geometry is derived from the mesh models, we risk increasing the already existent error on further processing. Moreover, mesh models for the iced zone tend to look unpleasant when input point cloud has high noise level (Schindler, Worstner et Frahm, 2011). Our case study is the iced blades, which the shape of blades as master data are invariant but the accumulated iced on the surface, have arbitrary and random shape due the position and climate condition.

## 2.5 Point cloud reconstruction

Point Cloud data is used as input in our research to reconstruct the ice geometry on the blades. This Point cloud is obtained through a sequence of images. In this section, we talk about the process of generating point cloud from sequence of images.

A sparse 3D scene structure is derived from a sequence of overlapping images through Structure from Motion (SfM). (Westoby et al., 2012) have described in their paper implementation of SfM in geosciences applications for generating Digital Elevation Model (DEM) from overlapping images. Traditionally, 3D location and camera position were required as a priori information for scene reconstruction. SfM solves this problem by automatically estimating scene geometry, camera position and orientation. This is achieved by identifying common features across image pairs. These features, also called key points, are detected by applying robust feature-point detection algorithms, like Scale Invariant Feature Transform (SIFT) (Lowe, 2004) and Speeded Up Robust Features (SURF) (Bay et al., 2008). Both algorithms can detect features without being affected by variation in scale, rotation, translation and illumination. The detected features are matched in image pairs using Approximate Nearest Neighbors (ANN) algorithm and Random Sample Consensus (RANSAC) algorithm removes the outliers (Schnabel, Wahl et Klein, 2007) . Using these detected features in image pairs; image or camera orientation is recovered by applying Epipolar geometry (Figure 2.5 (a)). This relationship between the two views is represented in matrix form, referred as Fundamental matrix. Fundamental matrix can be computed by 8-point correspondence algorithm (linear solution) or 7-point correspondence algorithm (non-linear solution). Using fundamental matrix we can compute relative projection (rotation and translation) matrix for each camera pose. The location of common features after applying the projection matrix is triangulated which results in a sparse 3D scene reconstruction (Musialski et al., 2013).

The described process could be scaled to generate sparse cloud for multiple photographs, as shown in the figure 2.5 (b). This is referred as Structure from Motion from 3D scene

structure which is created from images taken by a camera in motion (Joshi, 2014; Musialski et al., 2013). The 3D data reconstructed through SfM is in arbitrary coordinate system with no scale information. Transformation to absolute coordinate system is achieved by 3D similarity transform using Ground Control Points (GCP). 3D similarity transformation requires seven parameters, which consist of three rotation angles, three translations, and one scale parameter.

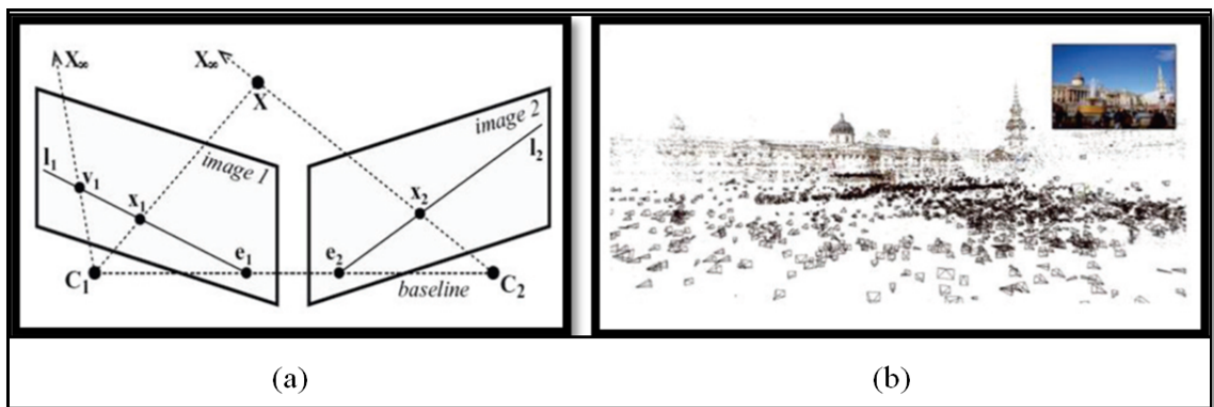


Figure 2.5: Right: Schematic of epipolar geometry (Musialski et al., 2013), left: Generated sparse point cloud from unordered images (Furukawa et al., 2009)

There are existing solutions, which deal with the reconstruction of a scene from a given set of images, some of them are open source solutions and others are free only for aCADemic purposes. We will discuss those applications that we consider more relevant for this project, but plugins for other applications such as MATLAB are out of the scope of this report. In Annex III we will explain with more detail Bundler, Sift, CMVS (Furukawa, 2012), PMVS (Furukawa et Ponce, 2010) and 3DF Zephyr pro which are the programs we selected for our “Structure from Motion” pipeline to reconstruct the 3D models.

## 2.6 Image base modeling by DSLR camera comparison with laser scanners

In Laser scanning, as a very popular method in three-dimensional modeling, the point’s coordinates have been derived using cross sectioning or time of flight methods as on-line

photogrammetry system. This real-time methods work well on the objects with Lambertian surfaces (matte). Because of type of laser beam used in commercial laser scanners (Red spectrum with wavelength between 600 to 700 nm), Ice in static conditions is generally birefringent at about 4 °C and wavelength of 624 nm. It means that laser beam incident to ice as birefringent material, is split by polarization into two rays taking slightly different paths. Figure 2.6 shows birefringence optical property on the calcite crystal.

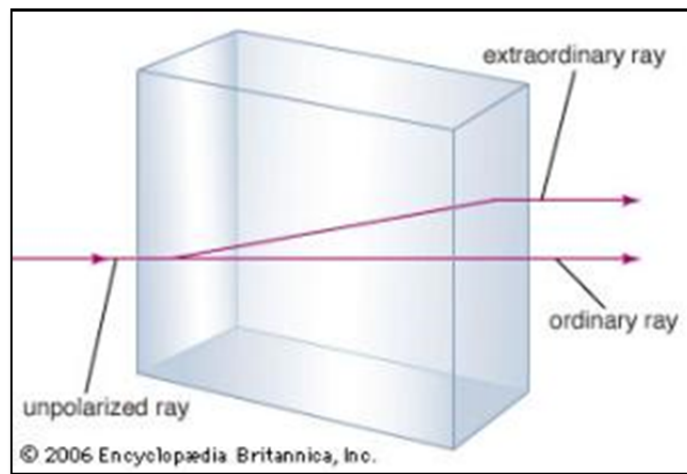


Figure 2.6: Birefringent (double refraction) optical property. when a single light ray strikes a calcite crystal at a right angle to one face, showing two rays emerging. (Britannica, 2015)

Birefringent property of ice at the wavelength between 600 to 700 nm (red spectrum), affect the accuracy of the result point cloud by commercial laser scanners that are far from the real shapes of ice.

As parts of this research, the author has proposed a customized laser scanner for measuring the ice thickness by using the optical properties of ice vs. the different wavelength. Ice exhibits strong absorption in the ultraviolet (UV) at wavelengths 170 nm. With increasing wavelength, the absorption becomes extremely weak in the visible, with a minimum near 400 nm. In the wave length of 405 nm-460nm the ice have merely solid opaque characteristics (Warren, 1984). In this case if we use the UV laser in visible wave length 405 nm-460nm, we

could measure the shape by laser scanning methods (Ackermann et al., 2006). Please refer the Annex II “**Laser Light Sectioning Camera**” of this thesis for presentation of system and complementary information. Figure 2.7 shows the proposed validation prototype for **Ice Laser Light Sectioning Camera**.

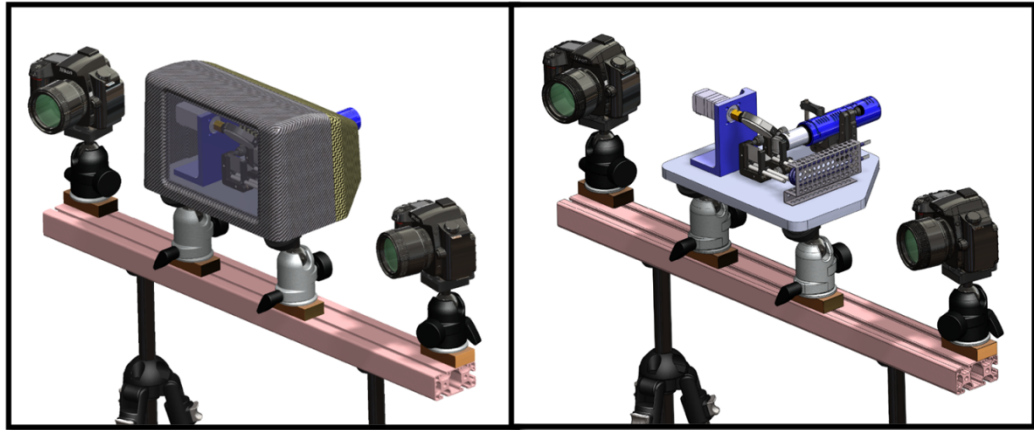


Figure 2.7: Customize laser scanner equipped by laser beam at wavelength 405-460 nm

(Kersten et Lindstaedt, 2012) compared in their works the result of different image-based recording and modeling procedures. They show that the results from some software packages, e.g. Bundler/PMVS2, using images from SLR digital cameras and standard parameter settings in the software are comparable with results from expensive terrestrial laser scanners. Object recording with cameras is simple, very fast, very flexible and economical. The entire procedure is largely automated and works even without targets as control points. Objects can be scaled through the inclusion of a single scale bar in object space. The results presented that the open-source software Bundler/ PMVS2, VisualSfM and the web service Photofly and/or 123D Catch Beta can generate equivalent 3D models when compared with terrestrial laser scanners, although the exact results depend upon the size and shape of the objects.

(Remondino et El-Hakim, 2006) & (Haala et Kada, 2010) in their work reviewed the Image based modeling as popular topic of research. These methods can reconstruct significantly

accurate models at low cost as compared to laser scanning (Westoby et al., 2012). In laser scanning, the initial cost of equipment itself is quite high in case, whereas, image-based modeling requires only a good quality camera. In case of photography of wind turbine blades, we should consider the cost of access on blades' surfaces to have a suitable angles view for capturing the required images. The possible methods of image capturing for photogrammetry of the wind turbine blades and required retro targets and pattern for better accuracy, are reviewed in chapter 3.

## **2.7 Structure from Motion & the accuracy of image base modeling**

Structure-from-motion methods estimate simultaneously the scene structure and the camera motion from images of a scene with little prior information about the camera. A modular processing chain, developed locally at Institute for Photogrammetry of University of Stuttgart, by (Abdel-Wahab, Wenzel et Fritsch, 2012) intended to automatically and accurately process unordered sets of images to determine relative image orientations and sparse point clouds of tie points without prior knowledge of the scene.

They presented in their research, adding more images in the SfM process can improve the scan alignment due to the stable image geometry as well as the increase in the redundancy, where more features will be used for the calculation of transformation parameters. Nevertheless, large number of images require more time for processing. Fortunately, latest developments in the SfM methods are able to resolve the time issue.

The pipeline used by (Abdel-Wahab, Wenzel et Fritsch, 2012) consists of four processing steps:

- 1) Employing fast image indexing to avoid costly matching of all possible image pairs, which dominates computational complexity along with the multiple bundle adjustment steps,

- 2) generating tie points by means of feature extraction and matching where the required automatic measurements are realized at maximum accuracy and reliability,
- 3) building and optimizing a geometry graph based on the image network, whereby the dataset can be split into reliable clusters of neighboring images that can be processed independently and in parallel within the reconstruction step,
- 4) merging all clusters and then finally adjusting the full model with integrating the ground control points if available. The number of unknowns within the SfM process can be reduced by using the interior orientation determined in the test field calibration.

Accordingly, the images are rectified by removing the distortion. A detailed description of the individual processing steps and accuracy analyses of the SfM implementation is given in (Abdel-Wahab, Wenzel et Fritsch, 2012) .

Chapter 3 implement the pipeline in 3d modeling of processing steps to create the 3d mesh models from frosted Ice accumulated wind turbines' Blades. The methodology of this study is explained in next chapter.



## CHAPTER 3

### METHODOLOGY

#### 3.1 Introduction

Photogrammetric scanning of the icing blades with Image base modeling and Structure from Motion in order to measure **the thickness** and **extract the real shape of ice with its distribution on the blades** is completely new in wind turbine ice detection and measurement methods. When the rotor blades were mounted on the wind turbine tower, ice thickness inspections became nearly impossible to be performed in the past, now by image base modeling of iced blades, geometry extraction are possible.

The present study started for measuring the ice shape & thickness on the blades of the two installed REpower MM92 turbines at "Site Nordique Experimental en Éolien CORUS" (SNEEC). This measuring operation was intended to do by the commercial Photogrammetric systems in the markets. As described before, the First step of Photogrammetric Measurement is object recording that consist the Targeting, Control points determination & Image recording, which all need the direct access to the operational wind turbine on site.

The limited financial resources for required equipment, high traveling charges in time of icing, difficult access to the wind farm and also security reason change the focus of the present work to develop appropriate method of ice detection and modeling by simulating the icing condition on the prototype blades.

In this phase, the current study focuses on reconstruction of three dimensional polygonal mesh models by images captured from a prototype of wind turbine blade with a similar configuration of digital SLR cameras for the real case study. This simulation process is described in the Section 3.6 of this chapter.

Regarding to the importance of the validation of the proposed method in real case study, all requirement for successful photogrammetric measurement the ice shape & thickness on the blades turbines at SNEEC are proposed in Section 3.9. This stage can be realized as a complete measuring project by collaboration of Wind Energy TechnoCentre in future at SNEEC. The required financial support for travel & equipment, the facility for access to the wind farm in icing period in secure manner are essential for validation and measurement the real case studies. Figure 3.1 show the view of one of the REpower MM92 turbines at SNEEC.



Figure 3.1: "Site Nordique Experimental en Éolien CORUS" (SNEEC), Gaspé, near Rivière-au-Renard, Quebec, Photo from the top of the second wind turbine. (eolien.qc.ca, 2015)

### 3.2 Image-based modeling & 3D object reconstruction procedures

The Icing problem associated with wind power generation in cold climates such as Canada is an active field of research. The humid climate is a particular challenge for the turbine technology to prove their value, even in moist Canadian weather conditions with lots of ice and snow that accumulate on the operational generators and interrupted the energy production. Creating the 3D images of icing blade and documentation of this information could help to design better wind turbine for arctic and alpine regions.

Figure 3.2 illustrate the comparative methods for resolve the real shape and distribution of ice on the blades surfaces in time of image recording. The measurement extracted by verifying of the shape and dimension of icing rotor blades against CAD or master data of rotor blades. Master model of wind turbine blade could be generated by 3D reverse engineering base on the Photogrammetry measurement of clean installed blades with appropriate level of details.

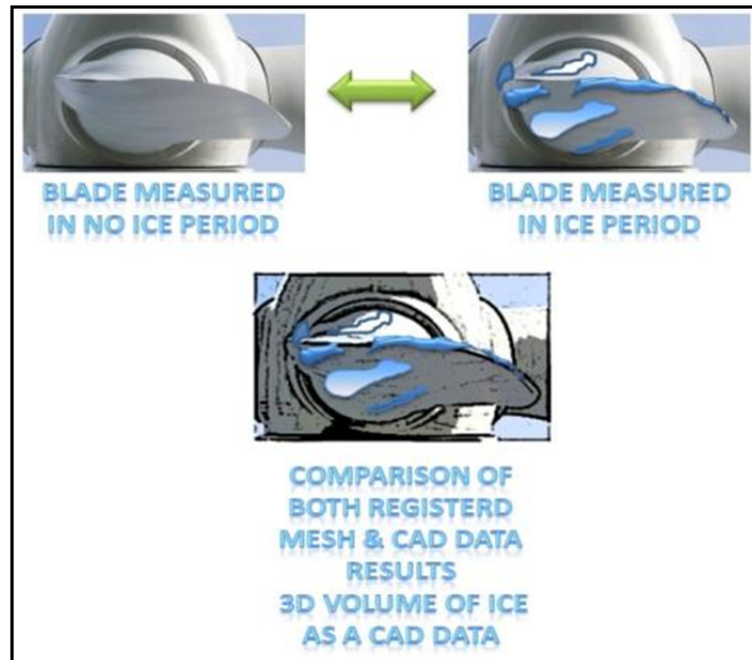


Figure 3.2: Image base modeling and comparison for extraction of ICE on Blade as CAD DATA

In the Section 2.1.3 (Luhmann et al., 2006) show the principal procedures in close range photogrammetry for both Digital & Analogue photography. Section 2.7 reviewed the pipeline procedure for Structure from Motion method used by (Abdel-Wahab, Wenzel et Fritsch, 2012) in order to have automatically and precisely process for creating accurate mesh from unordered sets of images. Figure 3.3 show the flow chart of our methodology for 3D modeling of iced blade by Structure from Motion method.

Each stages of workflow are detailed at follow.

- Recording

Photogrammetric object recording

- Targeting & illumination;
- Digital photography;
- Camera position to Object;
- Camera Movement for 3D Object.

- Preprocessing

- Image orientation & camera calibration
- Camera Calibration parameter;
- Image rectification for Radial & Tangential distortion;
- Partitioning the images in cluster.

- Orientation & 3D Mesh Modeling

- 3D Point Cloud by Dense Image Matching;
- 3D Transformation Control Point/Scaling;
- 3D Meshing & Texture Mapping.

- Measurement & Analysis

These steps are explained at following for prototype simulation process by considering the requirement for measuring the real case study.

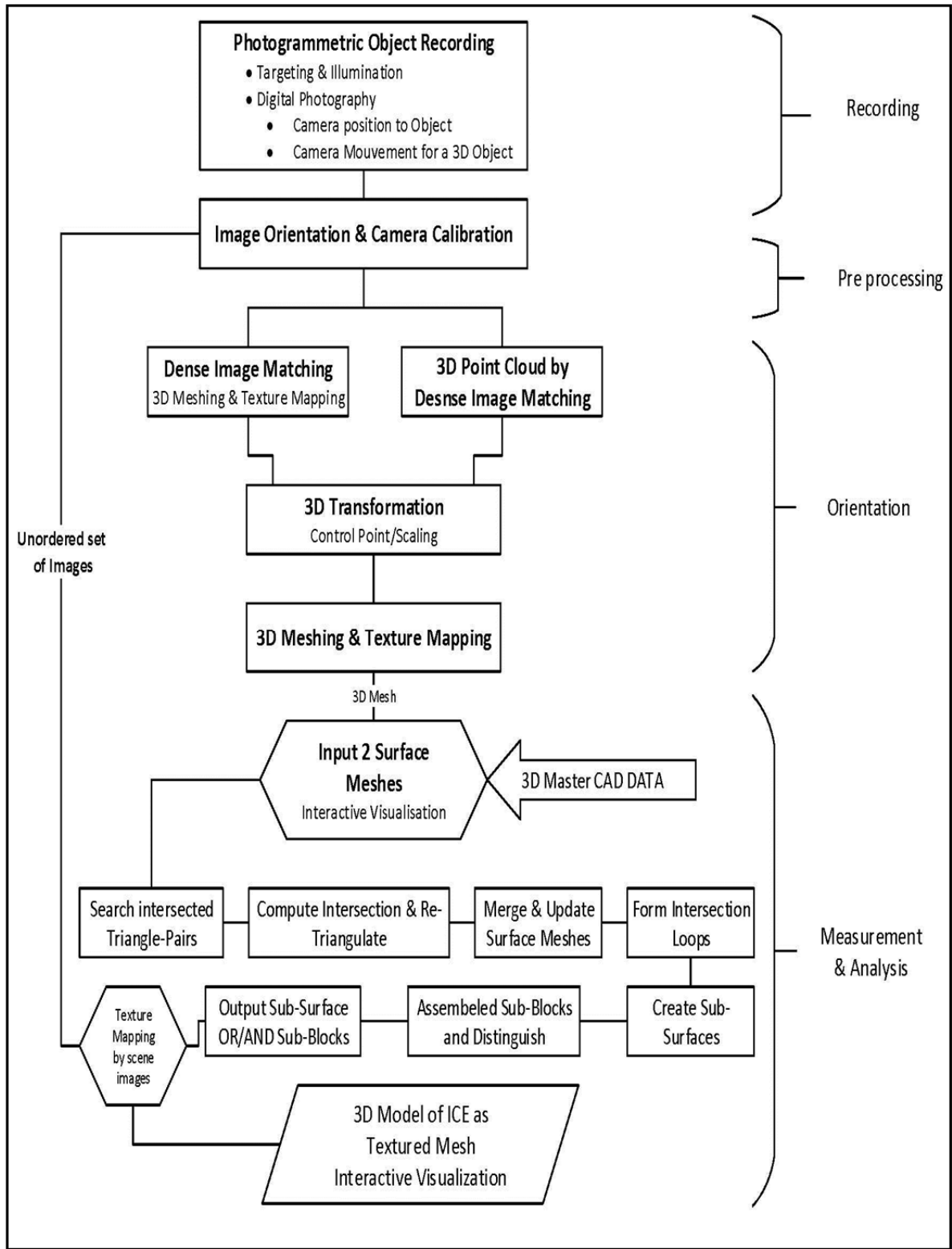


Figure 3.3: Workflow for Image-Based Modeling & 3D object reconstruction procedures

### **3.3 Photogrammetric object recording**

In photogrammetric object recording the size and shape of the object should be considered. A blade, whose outer contour is designed from aero dynamical considerations, is built to be sufficiently strong and stiff. The majority of wind turbine blades today are built using glass-fiber-reinforced plastics (GRPs). A thin film of so-called gel coat is first laid in the mould that gives a smooth white finish to the blades and therefore it is not necessary to paint the blades afterwards. The shape of the blades as a large object needs to have installed targeting that support fast image matching and image orientation in process of 3D mesh generation. The next section expresses the specification for the targeting and illumination. In real case study, this preparation phase for image recording of the wind turbine has the technical and economic issues that are reviewed in Section 3.11.

#### **3.3.1 Targeting object**

A target is a point in a scene or on an object that can be easily identified and easily marked when viewed in an image. Typically, a target is a high contrast dot or filled circle. Such a target can be marked with high precision with the sub-pixel marker (manual or automatic). When a surface is curved or has an arch, targets allow you to identify points with greater ease in the photographs. In addition, when you require maximum accuracy, targets are the way to go.

The different type and format of targets and retro reflective used base on the subject of photogrammetry. Annex IV describe the advantages of retro targets and coded retro targets in photogrammetry process. In validation segment of our study, we used the small solid circles that are placed on curved surfaces to provide points for marking. Figure 3.4 shows rows of circular dot targets placed on surface for marking purposes:

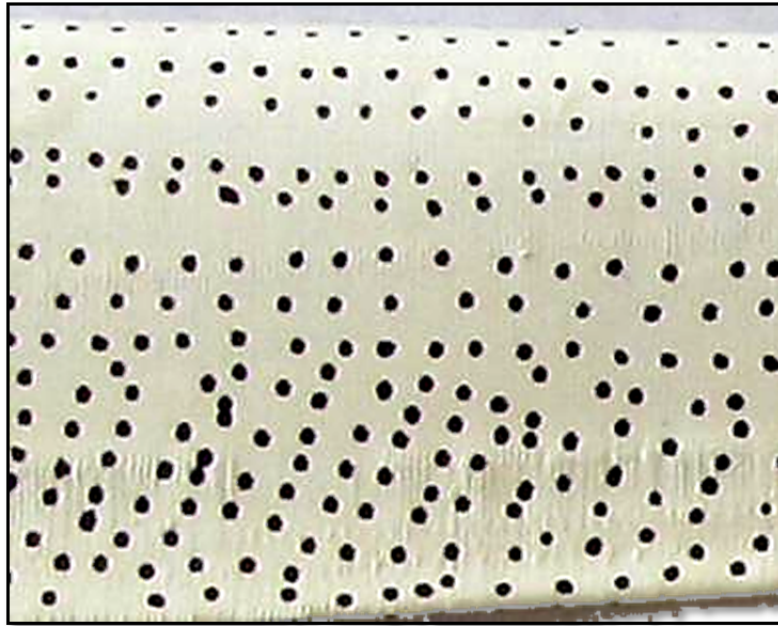


Figure 3.4: Curved surface with rows of circular dot targets

Any type of surface, from a Wind turbine Blade to Wind turbine Nacelle can be targeted in this fashion but some care has to be taken in deciding on the color and size of the targets. In order for accurate measurements to be made, the diameter of the circular target images needs to be suited to the target detection and measurement process to be used. For digital processing systems, it is generally accepted that target images should be **at least 5 pixels in diameter**. The color chosen should contrast well with the surface being measured. As long as the target is relatively high contrast (black on white, white on black, dark on light, or light on dark) and shows up in the image ideally about 8-10 pixels across the sub-pixel marker will work well.

### 3.3.2 Light and illumination

Digital photography is simple when there is plenty of light and the conditions are ideal. Nevertheless, in arctic region, lighting conditions for digital photography are not always as the process needs. In digital image recording it is essential that we work with light as much as humanly possible otherwise disappointing results may occur.

The flash is the major resolution to low light digital photography. However the problem with this is that not all situations can benefit from using the flash. The flash can appear in the digital images as reflect of light in form of shiny spot on the object. This is especially true for a flash that is built-in on digital cameras. The built in flash (and a flash in general) has the effect of lighting your subject on the front only, which compresses the depth in your digital photos. Compressed depth can really decrease the beauty of your subject in your digital photography. Generally in the photogrammetric object recording the “Ring flash” on DSLR camera (Figure 3.5) is used and helps to illuminate from viewing direction of camera without the reflect effect on the images. Another source of light in photogrammetry is the ambient light refers to any source of light that are already available naturally (e.g. the sun, moon, lightning) or artificial light already being used (e.g. to light a room). The ambient light has the key role in Image base modeling and texture mapping of the object.



Figure 3.5: Ring flash on DSLR camera helps to illuminate from viewing direction of camera, source: [www.capture3d.com](http://www.capture3d.com)

In Section 2.6 the proposition of customized laser scanner equipped the laser beams with wavelength between the violet (405 nm) and blue (460 nm) spectral ranges (Figure 3.6) have been described. The behavior of ice for this wavelength range could help in photogrammetric object recording. The similar idea for enlightenment with artificial ambient light for the objects, which are covered by different type of ice, is a new choice for better and performance object recording. Through using the light in this wave length for illuminating the area of photogrammetry regarding the optical properties of ice, the ice have merely solid opaque characteristics which help to the have the maximum of ice texture and also the shape of transparent ice as a solid surface, during the image recording. This illumination method in case of illumination by ring flashes needs the color filters in the wavelength of 405 nm-460 nm and in case of light projector the digital the video projector with color generator software is the fast way to enlighten the object by color light during photogrammetric object recording.

In this study the iced object illuminated during the object recording by a video projector, which enlighten the object by the violet blue light. The mean value between the wavelength 405 nm & 460 nm is chosen and illuminated the object by light with  $\lambda=432$  nm. The mean value chose to insure the light color  $\lambda$  is in the desire spectral range due variation in light color in video projectors. The RGB color code for this  $\lambda$  is Red 51, Green 0 & Blue 255 (Figure 3.8). These values extract by SPECTRA free software (Figure 3.7). The process for object recording is done without using of flash because of missing equipment such as color filters for flashlight. The number of detected features in bundle adjustment increased significantly. Chapter 4 compared the 2 mode of illumination.

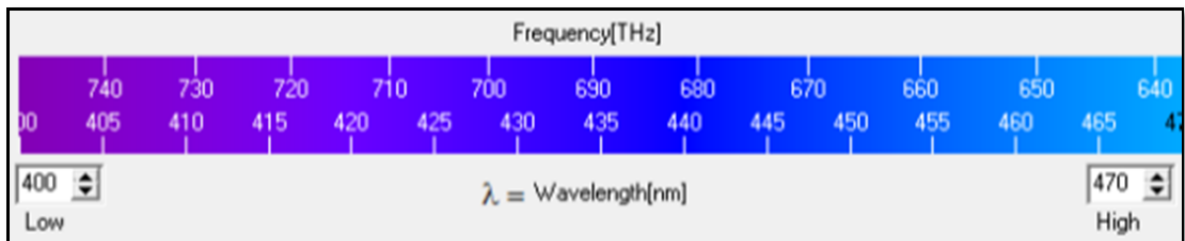


Figure 3.6: Spectrum of Blue Violet light,  $\lambda$  between 405 nm to 460 nm

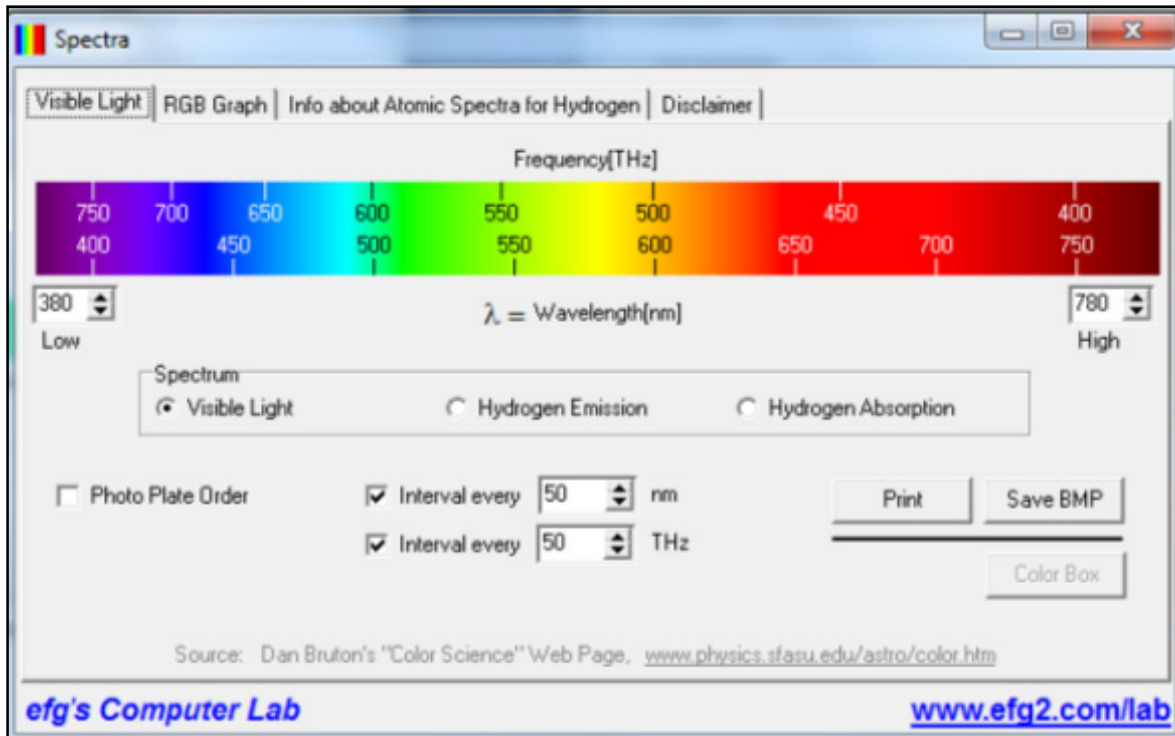


Figure 3.7: Spectra software for light color extraction from wavelength  $\lambda$

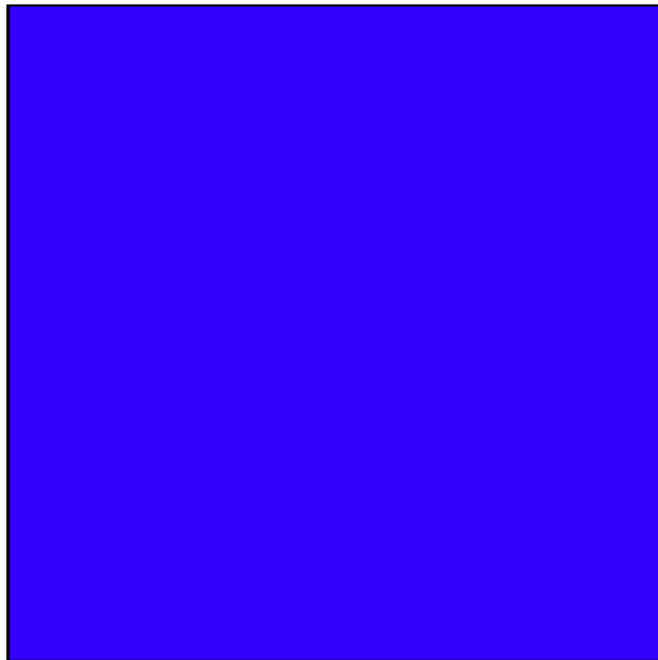


Figure 3.8: Color block with wavelength 432 nm-  
Code RGB (51, 0, 255)

### 3.3.3 Digital photography

Digital Photography is the practice of creating durable images by recording light electronically by means of an image sensor. The condition and the position of light have the direct effect on the quality and result of photogrammetry. High-resolution digital SLR cameras are now available with sensors between 10 and 60 Mpixel and image formats between approximately 20 x 14 mm and 54 x 45 mm. Such cameras are designed for (semi-) professional photographic work with a range of exchangeable lenses, high-capacity storage devices and powerful batteries. The data used in this project is a set of overlapping photographs mainly taken by Nikon D5200 24.2 MP Digital SLR Camera with DX18-55VR II Lens (Vibration Reduction lens) & Canon PowerShot SX10IS 10MP Digital compact Camera (Figure 3.9). The mechanical stability of both camera are usually poor in terms of high-accuracy photogrammetric requirements, and camera calibration is therefore an important step in the complete process chain (Shortis, Robson et Beyer, 1998).



Figure 3.9: Left: Nikon D5200, Center & Right Canon PowerShot Digital Camera

In process of Structure from Motion (SfM) additional information, such as the camera's intrinsic and extrinsic parameters and the calibration parameters (Annex III) is used in workflow. The used software in this study takes the camera/lens parameters from the EXIF tags in the jpegs images. EXIF (Exchangeable Image File Format) (Wikipedia, 2014) register

the information about the camera parameters (focal length, width of the sensor model of the camera, etc.).

Table 3.1: EXIF table tags information in the jpegs images

Id	Field	Data
1	File name	IMG_8617.JPG
2	Last modification	28/02/2015 1:08:44 PM
3	ImageDescription	
4	Make	Canon
5	Model	Canon PowerShot SX10 IS
6	Orientation	1
7	XResolution	180/1
8	YResolution	180/1
9	ResolutionUnit	2
10	DateTime	2015:02:28 13:08:45
11	YCbCrPositioning	2
12	ExposureTime	1/80
13	FNumber	28/10
14	ISOSpeedRatings	80
15	ExifVersion	30 32 32 31
16	DateTimeOriginal	2015:02:28 13:08:45
17	DateTimeDigitized	2015:02:28 13:08:45
18	ComponentsConfiguration	01 02 03 00
19	CompressedBitsPerPixel	3/1
20	ShutterSpeedValue	202/32
21	ApertureValue	95/32
22	ExposureBiasValue	0/3
23	MaxApertureValue	95/32
24	MeteringMode	5
25	Flash	16
26	FocalLength	5155/1000
27	MakerNote	1A 00 01 00 03 00 30 00 00 00 2
28	UserComment	00 00 00 00 00 00 00 00 00 00
29	FlashPixVersion	30 31 30 30
30	ColorSpace	1
31	PixelXDimension	3648
32	PixelYDimension	2736
33	InteroperabilityIndex	R98
34	InteroperabilityVersion	30 31 30 30
35	RelatedImageWidth	3648
36	RelatedImageLength	2736
37	FocalPlaneXResolution	3648000/241
38	FocalPlaneYResolution	2736000/181
39	FocalPlaneResolutionUnit	2
40	SensingMethod	2
41	FileSource	03
42	Tag A401	0
43	Tag A402	0
44	Tag A403	0
45	Tag A404	3648/3648
46	Tag A406	3
47	Compression	6
48	XResolution	180/1
49	YResolution	180/1
50	ResolutionUnit	2
51	JPEGInterchangeFormat	5108
52	JPEGInterchangeFormatLength	2702

### 3.3.4 Camera position & movement for 3D object

The process of photography for a set of overlapping photographs from object needs to know the geometry of object, the access viewpoint for taking the images and existing invariant features in the overlapping images pair. As for the flat object, record at first the 4 calibration images from the top. The object view from the top is not mandatory but desirable. Otherwise, select a position out of which, as many coded reference points as possible can be recorded that are well spread out across the image. For the now following all around measurement of the three dimensional object, hold the camera in medium object height (level 0), walk around the object and record images at a distance of  $45^\circ$  from each other. Then, record the same number of images from below (level -1) and finally from above (level +1). Figure 3.10 shows the position of camera path of movement around the 3D object.

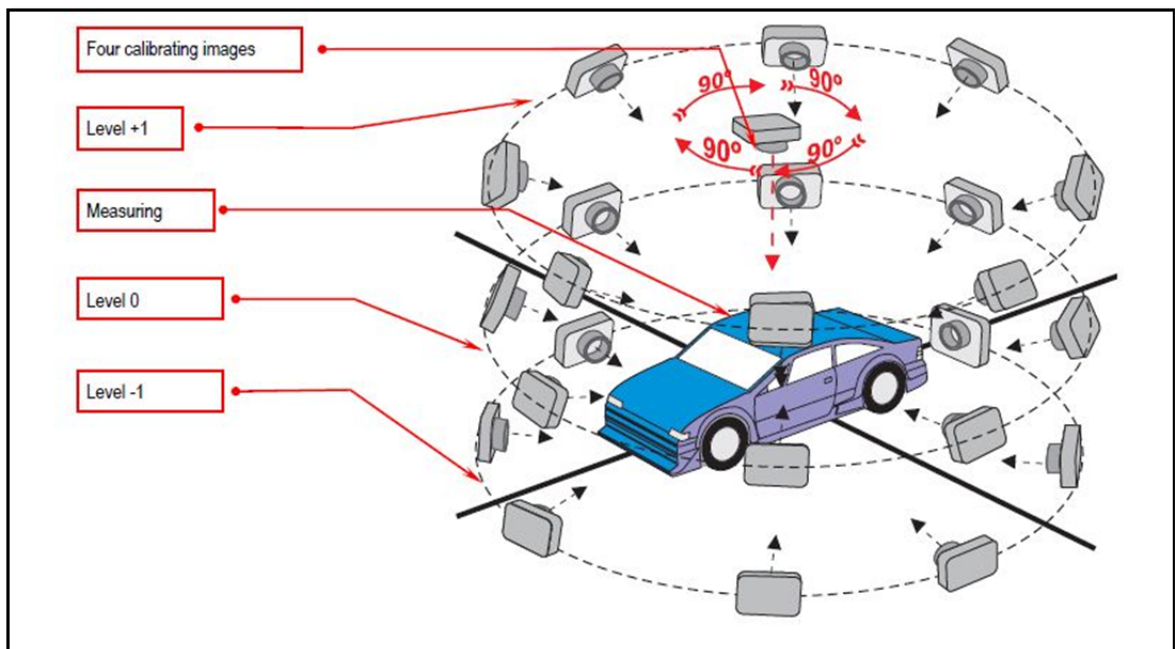


Figure 3.10: Camera position for large Object images recording.

As a proposition for measuring the ice on the existing wind turbines by this process, we need to add suitable retro targets and surface printed patterns on the object before object image

recording. For image capturing, in case of installed blades, the camera should turn around the blades and take the image. The strategy of image capturing strongly is related to the methods of access to blades and implemented equipment. These methods are reviewed in Section 3.9.

### 3.3.5 Camera movement for a large 3D object

For measuring a large 3D object, we normally need to adapt the size of the reference points to the object size. In certain applications, large marks are not desired. In this case, use small reference points and record the object in sections. This procedure is called "tiling"(Figure 3.11). The tiling procedure determines the size of reference point on the surface. The size of the reference points need to be adapted to the camera resolution (image pixels) and to the lens setting (see Annex II targeting and illumination). The optimum reference point's diameter is 10 image pixels due the tiling image size.

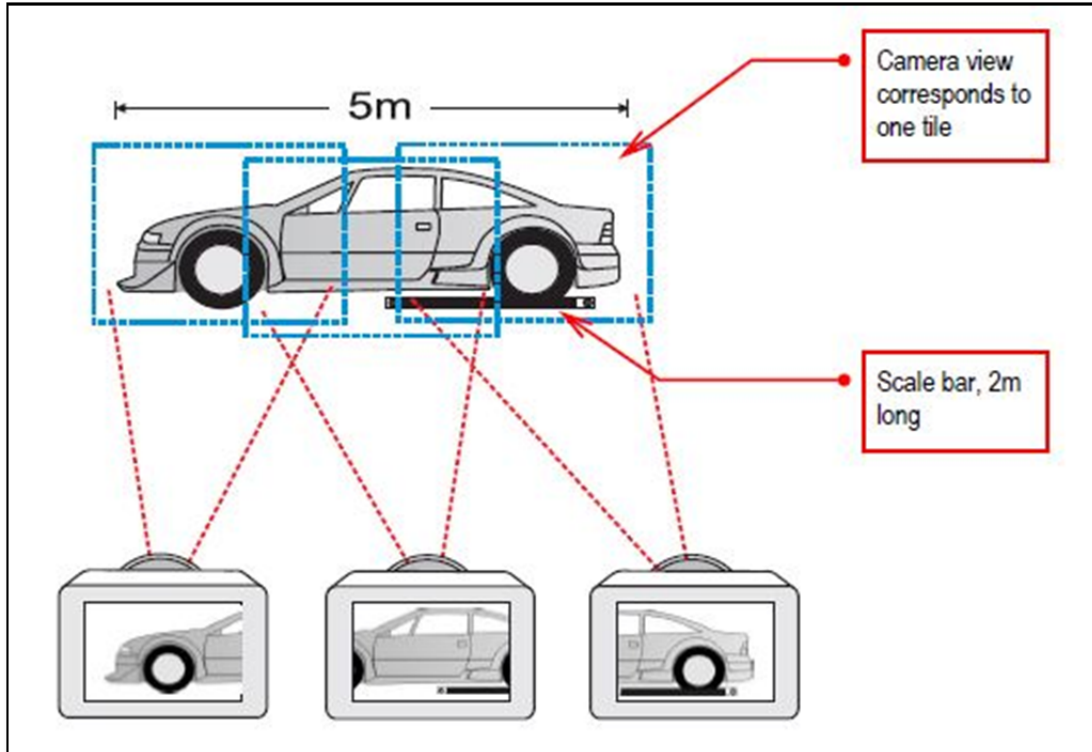


Figure 3.11: Tiling procedure for large object.

In this example, the digital camera records a maximum object length of approx. 3 m. For an object to be measured having a length of 5 m, images are recorded that are overlapping in the marginal areas. For this shooting technique, connecting images are of particular importance, e.g. views from the top, images that connect the right and the left side with each other, etc. These images prevent accumulated errors when evaluating the image set.

Some points, which are considered for acquiring photos for this study, are as follows:

- 1) Sharpest aperture setting should be used for the lens (often f/8).
- 2) Lens should be fixed to infinity focus.
- 3) Fastest Shutter speed should be used.
- 4) In case of low light condition, ISO should be increased as necessary.
- 5) Approximately 80% overlap should be ensured to obtain good quality output.

### **3.3.6 Image orientation & camera calibration**

Camera calibration is an essential part of photogrammetric systems in industrial application since measurement accuracy usually is usually related to sensor quality and correct modeling of the interior orientation. The standard models for camera calibration include the 3D position of the perspective center in image space (principal distance and principal point), parameters for radial and decentering distortion, and possibly corrections for affinity and shear within the sensor system. These parameters are calculated through a self-calibrating bundle adjustment in a multi station convergent network of images. This study used **3DF Lapyx** as a free software utility to perform automatic camera calibration, that extracts the typical intrinsic camera parameters used in Computer Vision. The software using the Brown-Conrady model (Hugemann, 2010) which can extract and export the camera focal length (in pixels and mm), optical center, skew and radial distortions parameters. See Annex III for description of Camera Calibration parameters.

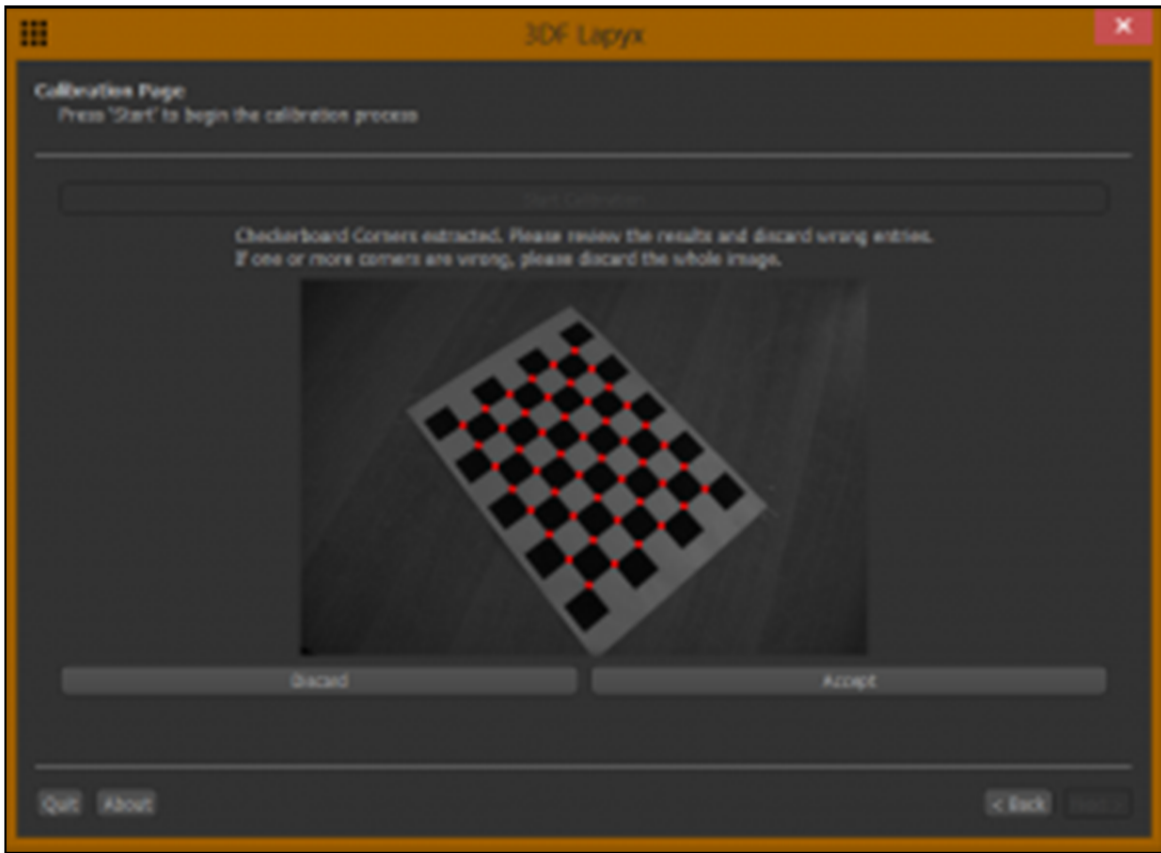


Figure 3.12: 3DF Lapyx automatic camera calibration software that extracts the typical intrinsic camera parameters used in Computer Vision

The first step after images acquisition is importing of the images into the particular processing software to correct lens distortion in arbitrary photographs automatically. In this study **PTlens** software has been read the EXIF information from the digital image, look up the camera in its database and apply its lens correction, all of it with minimal user interaction. All images are rectified for radial & tangential distortion by **PTlens** as Image rectification software (Figure 3.14). This practice optimizes significantly the time of process and quality of point cloud reconstruction. Figure 3.13 show the different type of lens distortion. Figure 3.15 shows the rectified Photo from Same photograph which distortion is corrected.

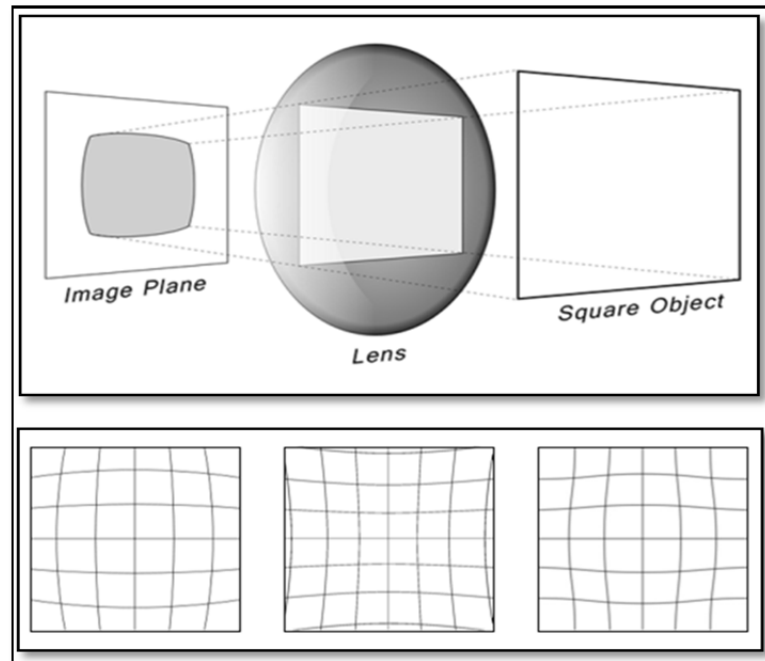


Figure 3.13: Top: Image distortion by simple lens, Down: Different type of Lens Distortion order from left to right; Barrel. Pincushion & Moustache Distortion  
 (<http://www.photocritic.org/articles/everything-about-camera-lenses>)

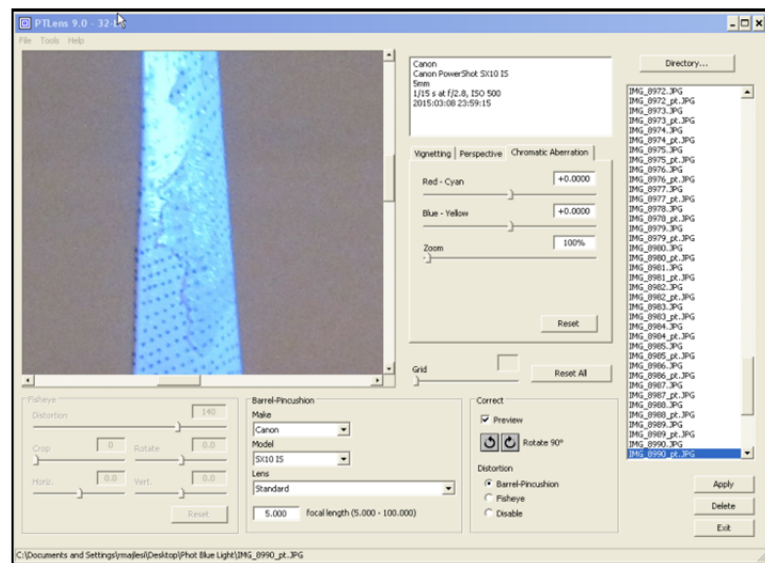


Figure 3.14: PTlens interface

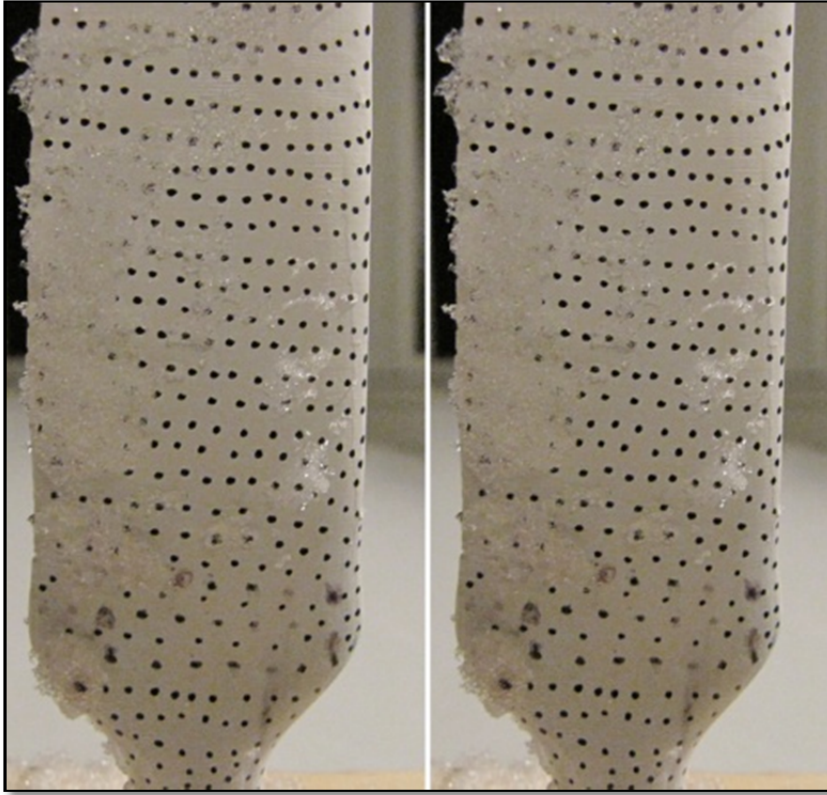


Figure 3.15: Left: Original Photo, Right: Rectified Photo from Same photograph, distortion corrected

The image orientations are computed automatically by Bundler/PMVS2 and VisualSfM software as applied software for automatic generation of 3d point clouds. The software support camera calibration data (focal length  $f$  from EXIF data and two radial distortion parameters  $K_1$  and  $K_2$ ) from set of images. Bundler/PMVS2 and VisualSfM software could work for cameras with a low distortion but it could not work properly for cameras with large distortion therefore the image rectification in previous step is necessary for our process.

For large scale reconstruction, clustering and optimizing on the image network is essential. Reconstruction is too expensive when the number of images grows. In large-scale reconstructions it is thus important to partition the images in clusters, covering different parts of the scene. This results in two benefits - reduced runtime on a single machine due to the

smaller dimensions of the clusters and the possibility to split the processing across multiple machines for even further speedup.(Mauro et al., 2013)

### **3.4 Orientation & 3D mesh modeling**

The first step after images orientation & Camera calibration is generation of 3D point clouds or 3D surface models in full automatic mode by selected software for our study. Only for the 3D transformation of the point cloud & meshed model into a super ordinate coordinate system, the user needs to measure control points interactively. The derived 3D model is automatically textured using the original image data. The CAD model be constructed from a transformed and geo-referenced, colored 3D point cloud, manual processing has to be carried out in a CAD program, e.g. CATIA. This 3D CAD model can later be manually textured in visualization software as a 3D image of real shape of ice on the blade.

The result of Structure from Motion (SfM) is generally an unstructured 3D point cloud, consisting of the key points, which were identified and tracked, in the scene and a set of camera matrices, identifying position and direction of each picture with respect to an arbitrary reference frame.

There are existing solutions, which deal with the reconstruction of a scene from a given set of images, some of them are open source solutions and others are free only for aCADemic purposes. The following section investigates the applied software that we used in this project for automatic generation of 3D point clouds and 3D surface models from image data.

### **3.5 Applied software**

For this investigation into the automatic generation of 3D point clouds and 3D surface models from image data the following software packages were used:

- 1) **3DF Lapyx** as a free software utility to perform automatic camera calibration,
- 2) **PTlens** software to correct automatically lens distortion in images,

- 3) Sparse cloud point and dense cloud reconstruction by open-source software **VisualSfM/SIFT/CMVS & PMVS**,
- 4) **Dassault System CATIA** software used for 3D Similarity Transform of generated cloud points and meshes generation. CATIA suite software is calculated the variation between master CAD data and generated mesh model.

### 3.5.1 VisualSfM

The VisualSfM is a GUI application developed by Changchang Wu (Wu, 2011b) and it is used to reconstruct 3D models. This application includes some of his previous works:

- 1) Sift on GPU (SiftGPU) (Wu, 2011a).
- 2) Multicore Bundle Adjustment (Wu et al., 2011).
- 3) Towards Linear-time Incremental structure from motion (Wu, 2013).

Once we have all the images, we reconstruct the point cloud using VisualSfM (Wu, 2011b). (Falkingham, 2013) has provided a brief overview about working with VisualSfM. Images resolution is selected depending upon the available memory for processing. If very high-resolution images are used, memory consumption will be more, which causes slow processing of images. Most suitable image dimension is 3200 resulting in sufficient information extraction without taking a lot of time. Once all the images are added in the software, GPU-accelerated feature matching is performed that is based on SIFT (Lowe, 2004). Next processing step in VisualSfM is to reconstruct a sparse point cloud, which is followed by dense cloud reconstruction using the PMVS binary files (Furukawa et Ponce, 2007). VisualSfM outputs other information as well along with the dense cloud data, such as, coordinates of camera center in arbitrary system, focal length, principal point, etc for each image. If all the images have sufficiently large overlap and features are matched effectively, then VisualSfM results in single model. Otherwise, it may result in multiple models.

These are the main characteristics of VisualSfM:

- 1) It exploits the multicore capabilities of the computers.
- 2) SiftGPU uses the architecture CUDA of Nvidia to speed up the process for some binaries of windows.
- 3) It has a graphical interface where we can see where the cameras are located and the resulting point set. Users can configure the options of the reconstruction.
- 4) It is prepared to run PMVS/CMVS among one of its options.
- 5) It also supports external binaries of Sift (for instance David Lowe's Sift or the VLFeat version).
- 6) It contains a command line program to perform the operations that are done with the GUI.
- 7) It allows us to specify the pair-list for matching. This means if we already know the pairs of cameras that have features in common, we can specify in a TXT file these pair of images and save time instead of realizing a full-pairwise matching.
- 8) We can use our own feature files for the images and we can also define our own feature detector.
- 9) It can store animations of our movements inside the application for future presentations.
- 10) The reconstruction can be intervened manually. The process is performed incrementally, so we can pause it or delete the current work in each iteration.

The author also presents some problems and solutions that the program can have:

- SiftGPU tries to fit the memory available in the GPU so, for GPU with not much memory will provoke that SiftGPU downscale automatically the images and consequently, the reduction of features for the images.
- There is only one radial distortion parameter that could work for cameras with a low distortion but it could not work properly for cameras with large distortion. This issue considered and resolved in this study by rectifying the images (see Section 3.3.6).
- Some binaries of 32 bits can run out of memory because the limitations of the OS.



Figure 3.16: 3D Reconstruction - Using the VisualSfM GUI

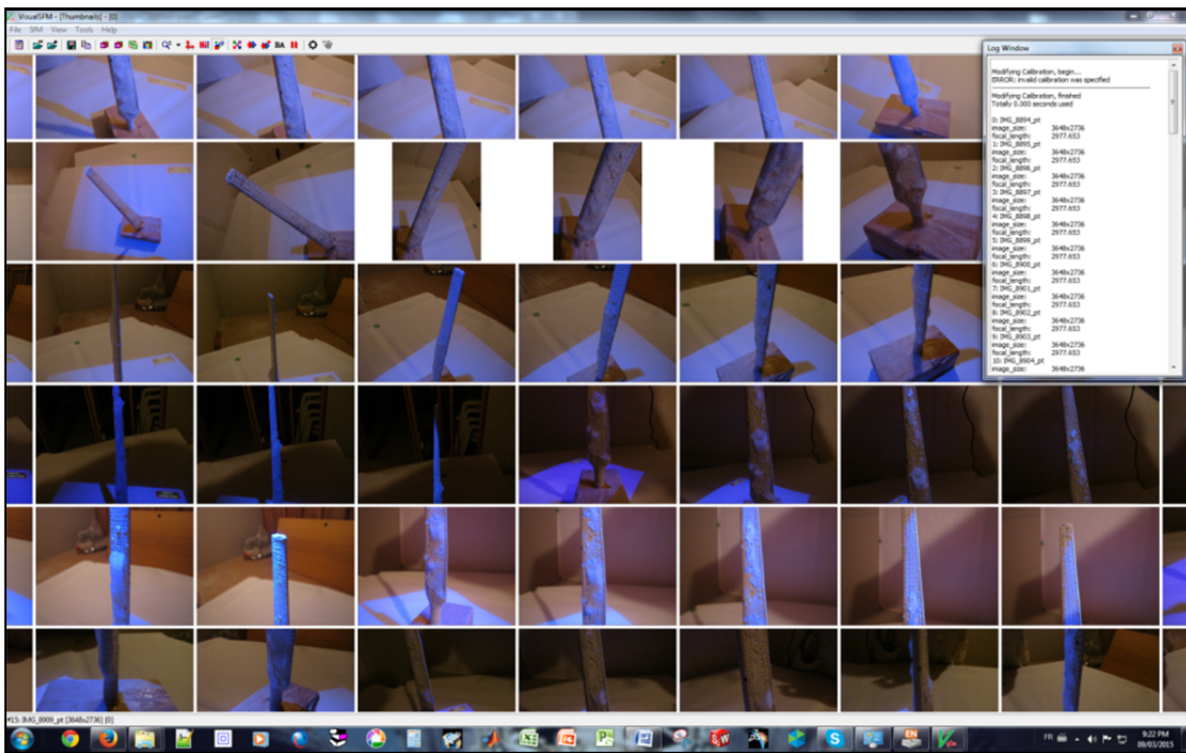


Figure 3.17: VisualSfM with rectified images from PTlens software

Annex IV (SIFT/Bundler/CMVS & PMVS) explain with more detail Bundler, Sift, CMVS (Furukawa, 2012), PMVS (Furukawa et Ponce, 2010) which are the programs inside the VisualSfM GUI to reconstruct the 3D cloud points.

### **3.6 Process simulation of ice measurement on the wind turbines' blades by close-range photogrammetry methods**

This research topic focuses on reconstruction of three dimensional polygonal mesh models by images captured from wind turbine blade with a configuration of digital SLR cameras. As explained before, the main objective of this study is to identify the volume and shapes of iced accumulated areas on the wind turbine blades in arctic regions. Comparison of these polygonal mesh models with the master CAD data of clean blade without ice, could be extracted the geometry of iced regions. This section; explain a low cost laboratory simulation method for validating the process before measuring the real case study.

#### **3.6.1 Digital-mock-up of master CAD data**

In validation process, CAD data of master model of wind turbine blade is generated by 3D reverse engineering with appropriate level of details. This CAD data is used on our process of Photogrammetry measurement as installed ice-free blade on the wind turbine. As discussed before, the CAD data of the blades is properties of the Wind Turbine makers and unavailable for us, thus the author created digital Mock-Up of wind turbine blades base on the available information of Airfoils S823 in root and S822 on tip. The shape of this blade is similar to the mid-size operational wind turbine. Figures 3.18 & 3.19 shows the 3D model of this CAD data, which modeled on CATIA software.



Figure 3.18: Rendered view of master CAD data of prototype blade

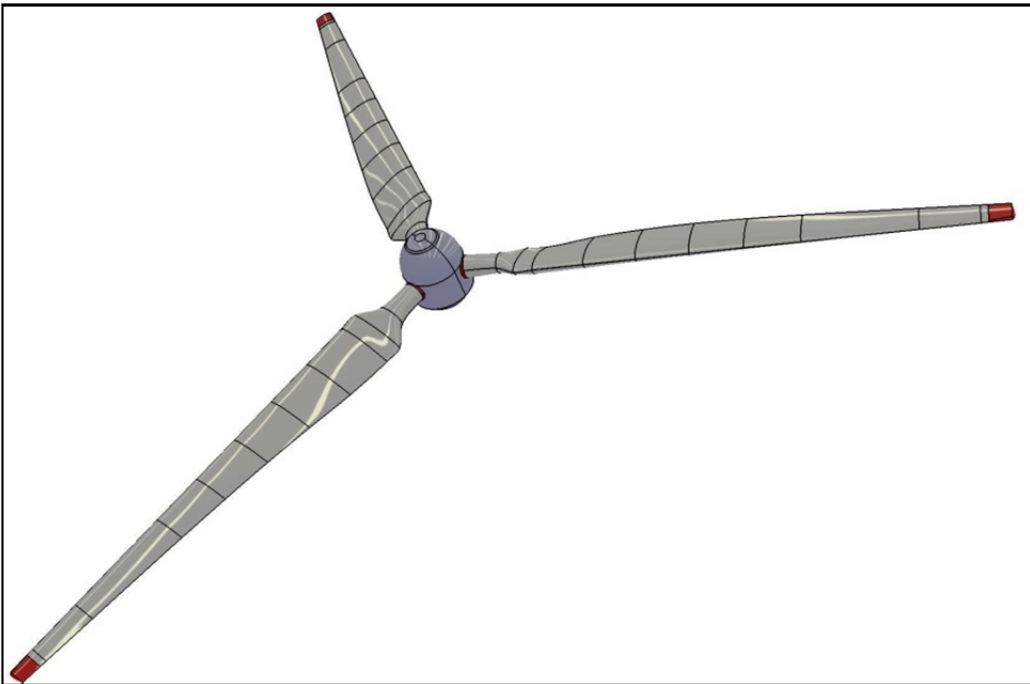


Figure 3.19: Digital mock-up of the prototype of wind turbine blades on hub

### 3.6.2 Rapid prototyping of scaled wind turbine blade by 3D printing

[3D printing or additive manufacturing (AM) refers to any of the various processes for printing a three-dimensional object. Primarily additive processes are used, in which successive layers of material are laid down under computer control. These objects can be of almost any shape or geometry, and are produced from a 3D model or other electronic data source. A 3D printer is a type of industrial robot]. (<http://en.wikipedia.org>, 3D printing)

In this research, the master CAD data is scaled for the available size in 3D printer machine at École de technologie supérieure. 3D printer made simple prototype of a **wind turbine blade without ice from master CAD data**. The prototype blades regarding the 3D printer specification are equal in size and relating to the precision and material used for these prototype blades, these parts are very fragile to mechanical loads especially in low temperature. During the process of measurement, some of the blades have been broken and they are repaired for rest of project.

### 3.6.3 Targeting & determination of control points

In Section 3.3.1 the type and size of the targets described. All of the blades fin sanded and painted in white. In order to choose the suitable targeting, surface pattern and illumination, on each blade pattern has drawn differently. These different patterns help to understand the best target shape and size, adapted to object access and measurement volume.

These prototypes in comparison of the real blades are too small to use the coded retro targets as Ground Control Points (GCP). In this case, the 3D model has the cylindrical feature in the base of model as axis of the blade (see Figure 4.9, 4.10 & 4.11) and a steel ruler with known length are used for scaling and transformation of cloud points to absolute coordinate system (Figure 4.13). In 3D modeling of the prototype blades the connecting base created by primitive cylinder feature as axis of pitch rotation of blades. These pitch axis are one of the design parameters in wind turbines.



Figure 3.20: Up: Render view of Master CAD data, Down: Prototype blades with different surface patterns and targeting layout, From top Pattern 1 to 3

In order for accurate measurements to be made, the diameter of the circular target images needs to be suited to the target detection and measurement process to be used. As described in Section 3.3.1 for digital processing systems, it is generally accepted that target images should be **at least 5 pixels in diameter**. The black target spots contrast well with the surface being measured.

#### 3.6.4 Prototype & photogrammetric object recording

In this study, multiple overlapping photos capture the object from different positions, whereby coverage of common object parts should be available from at least three but preferably five photographs from different camera positions. However, the prototype are too small in comparison of real case study and the tiling procedure (Section 3.3.5) can happen

just only when the photos has been taken by SO mode (Small Object). This mode of photography generally needs the particular Macro lens type, but with regular lens, there are only two things that we need to control to get good pictures – the light and keeping things still. Figure 3.20 show three prototype blades during the ice generation on the blades' surface in cold temperature  $-20^{\circ}\text{C}$ .

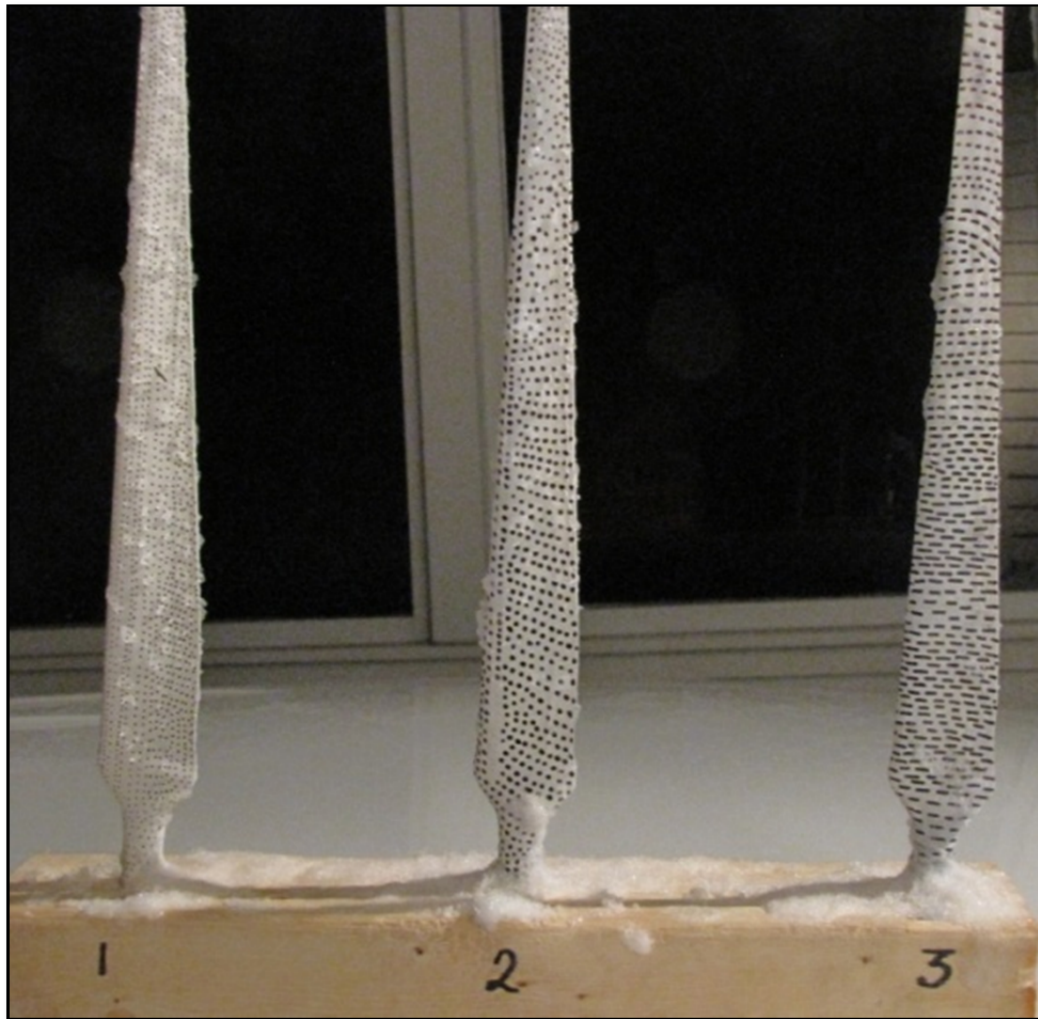


Figure 3.21: Blades with different target pattern.

As described before the three different retro target pattern added to the blade surfaces. Because of the small size of the object, no coded retro target used in photogrammetric object recording. The object illuminated by light with  $\lambda=432\text{ nm}$  base on the color box (Figure 3.8)

with Code RGB (51, 0, 255) which projected by video projector. The camera is fixed still by a tripod and captured the sharp and clear photo from small prototype blade.

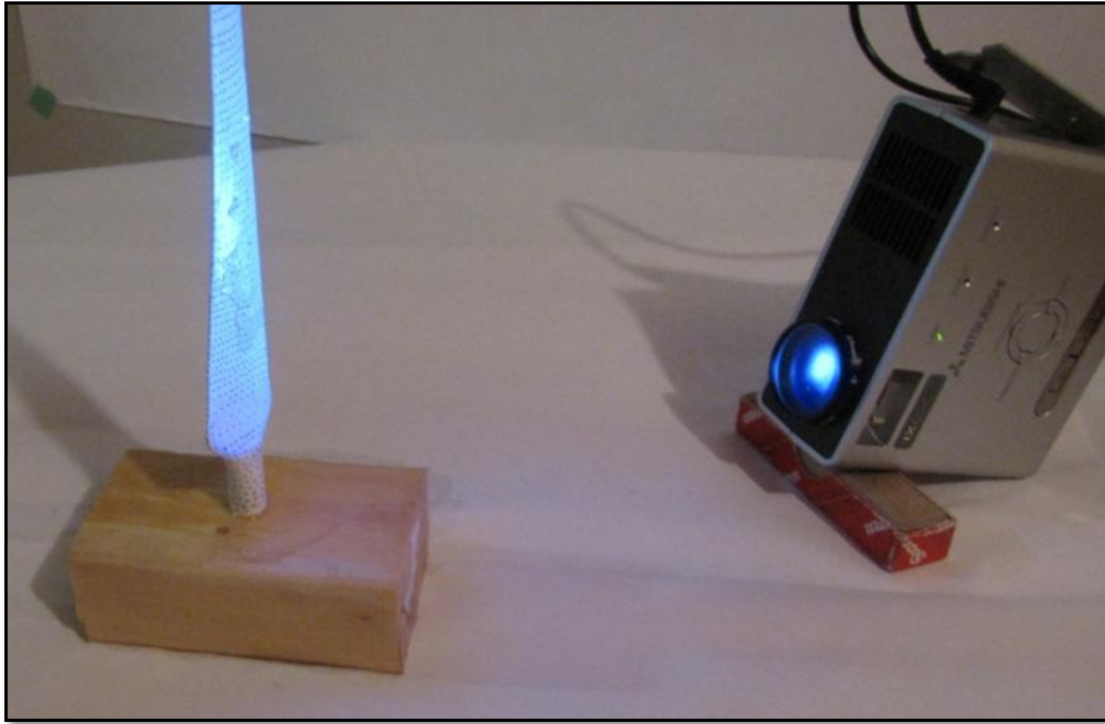


Figure 3.22: Prototype blade illuminated by color light with  $\lambda=432$

As reviewed in 3.4, the typical intrinsic camera characteristics extract by 3DF Lapyx software which used in the Fixed Calibration option of VisualSfM. The related parameters for our camera are listed in below :(fx cx fy cy r):

Focal (pixels) - Fx: 3078.41 Fy: 3078.07, Optical center - Cx: 1863.04 Cy: 1320.21 &

Radial distortion (Brown's Model) K1: -0.17812 (see ANNEX IV).

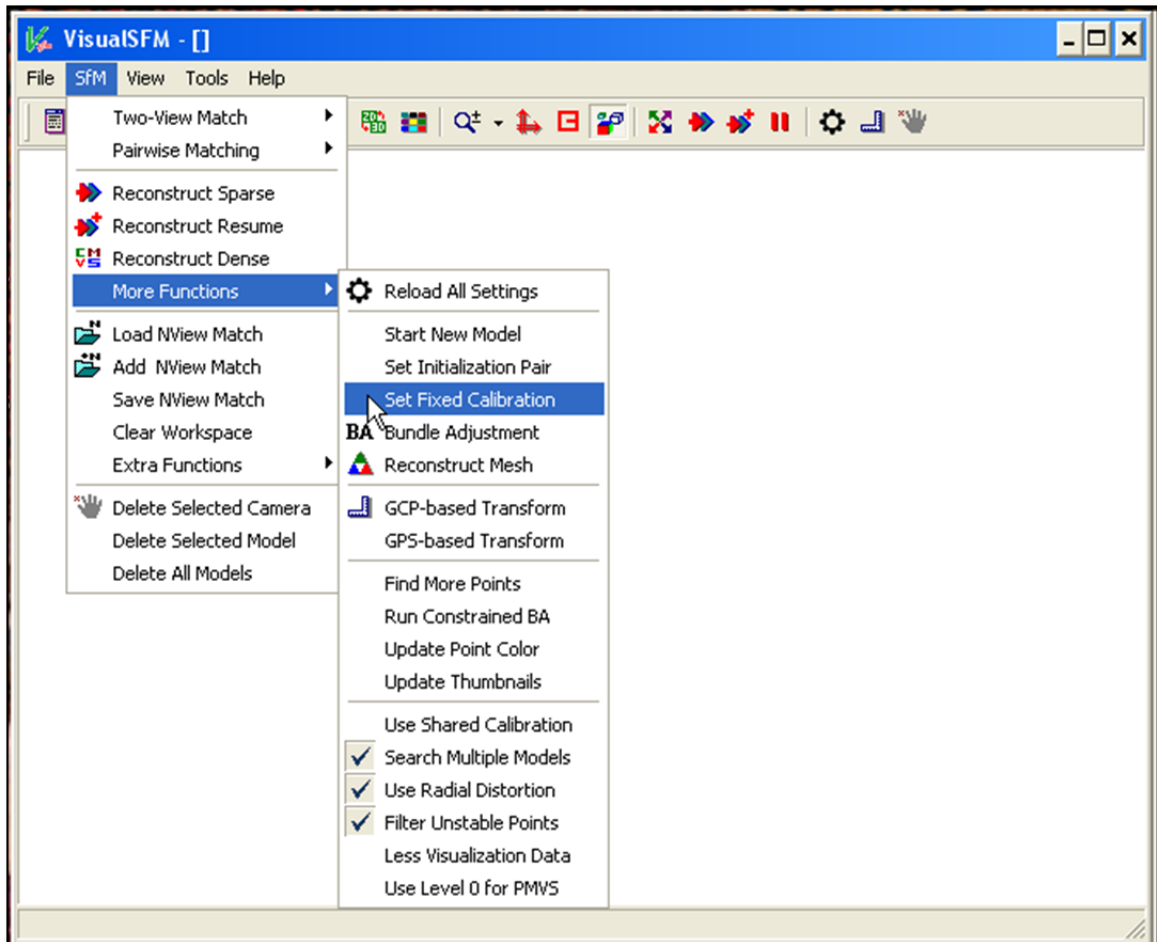


Figure 3.23: Camera calibration parameter in VisualSfM

Once all image rectified for Radial & Tangential distortion, the images are added to VisualSfM the GPU-accelerated feature matching is performed that is based on SIFT (Lowe, 2004)(Lowe 2004)(Lowe 2004)(Lowe 2004). Next processing step in VisualSfM is to reconstruct a sparse point cloud, which is followed by dense cloud reconstruction using the PMVS binary files. Refer to (Falkingham, 2013) for a brief overview about working with VisualSfM.

Resulted cloud points (.ply format) are transferred to CATIA. After reducing the noise and distortions a cloud of point was produced for each ice model. The process of aligning the cloud points with master CAD data and inspection is illustrated in chapter .4.

### **3.7 Brief history of project case study and Wind Energy Technocentre**

REpower Systems AG and Renewable Energy Systems Canada Inc. (RES Canada) have completed the construction of a test wind farm in the Gaspé region on 2010. The joint pilot project "Site Nordique Experimental en Éolien CORUS" (SNEEC) consists of two REpower MM92 turbines, each with 2.05 MW nominal power. The Wind Energy Techno Centre is the developer and owner of the project.

Constructed in the town of Gaspé, near Rivière-au-Renard, the SNEEC project uses two special cold climate versions (CCV) of the REpower MM92. These have been designed for the demanding conditions of the Canadian 60-Hertz network. Previous experience of the Wind turbine test facility in Inner Mongolia was one of the reason to prove that these 2 special cold climate versions Wind Turbine can be used reliably, even at extreme temperature fluctuations and temperatures as low as -40 degrees C. The humid climate (compared with China) is a particular challenge for the turbine technology to prove their value, even in moist Canadian weather conditions with lots of ice and snow.

Together with the owner of SNEEC, the Wind Energy Techno Centre, as much experience as possible is now to be gained from the test run and collaboration between the project partners. A REpower Systems AG team will monitor the turbines intensively over the operation periods

### **3.8 About Wind Energy TechnoCentre:**

The Wind Energy TechnoCentre is a non-for-profit organization that promotes the development of an industrial wind energy network in Québec, able to compete on North American and world stages, while valorizing the Gaspé Peninsula and Magdalen Islands as being central to this emerging niche of Québec's economy.

Surrounded by wind parks in high altitude in the Gaspé Peninsula, the Wind Energy Techno Centre is dedicated to research, development and technology transfer. Its location make the research center a unique natural laboratory to study the impact of the Nordic environment for

the use of wind energy. The Wind Energy Techno Centre is a member of the Wind Energy Strategic Network (WESNet) which includes 16 Canadian universities and industrial partners and is recognized as a College Centre for the Transfer of Technologies (CCTT).

### **3.9 The methods & equipment for blades access and photography**

As a part of this study, the author tries to find the best solution for access and photography of project's default case study. In following sections, all required considerations as technical components of photogrammetric process are proposed. The methods of access to the blades' surfaces, type and size of adapted targeting and illumination for real case study is explained.

#### **3.9.1 Using of the crane for accessing to the blade surfaces and marking the blade**

In this method, the installation of retro targets and photography can be done in place. This is a safe and conventional method for accessing the blade surface and it is flexible to measuring all views of the blade. The process needs that crane be ready in icing time. Concerning to availability of crane in this period, economical reason (the required crane size is very expensive for renting) and besides the possibility to transferring and access the wind farm during the winter, we need to find another alternative solution.



Figure 3.24: RE POWER MM 92 & Crane Withdraws (source: <http://myrenaultzoe.com/index.php/2013/02/17/>: image: T. Larkum)

### 3.9.2 Using of the blade access suspended platforms

This suspended platform shown on Figure 3.25 from “spider staging Co.” is a good solution for 360° access to the wind turbine blade. By this equipment, the photography can be done in place. This is a safe and conventional method for accessing the blade surface and has the flexibility to measuring all views of the blade. This platform in North America are available to purchase or rent from manufacturing company.



Figure 3.25 : Suspended access equipment for Wind Turbine ([www.spiderstaging.com](http://www.spiderstaging.com))

### 3.9.3 Using of the maintenance access man hole in the wind turbine hub

In this method a trained technicians with suspended access equipment can mark on the blade the desire sections and stuck retro-reflecting targets when there is no Ice on the blades. Regarding the close access to blades' surfaces, same person in icing period could do the image acquisition. Figure 3.26 show the access hole on the Wind Turbine's blade.



Figure 3.26: Access to the blades' surfaces by access man hole in the wind turbine hub  
(source : <http://www.frontierpro.com>)

### 3.9.4 The photography of the objects by remote controlled drone

Images acquisition could be done by a radio controlled Helicopter that equipped by DSLR camera. The camera's viewfinder display is transmitted over a 5.8GHz wireless connection for video assist or to be recorded by the wireless video base station and/or handheld controller.

The JR GSR260 Voyager Gas Helicopter (Figure 3.27) with modifications to lift 12 lbs. of payload has enough payloads for carrying the weighted DSLR Camera and its accessories

such as flashes and battery and longer flight time in comparison to the electrical RC helicopter, take us a good flexibility for shooting the wind turbine components.



Figure 3.27: Remote controlled Helicopter for WT image acquisition (Source: <http://www.airfoilsycam.com>)

### **3.10 Recommended procedure for photogrammetric object recording via remote control drone**

Between the methods of access to wind turbine blade and photogrammetric object recording, this study recommended the photogrammetry object recording by remote controlled drone (Section 3.10.4). This method, concerning to the progress of controlling system of the drone and available accessories in the market could cover the requirements for our proposed method. The drone has the enough flexibility to be applied in different positions and also they are able to position the camera in required angle of view with different distances from object. Parts of Sections 3.3.3 & 3.3.4 described the general prerequisite for an efficient photogrammetry object recording.

In future works for selection of equipment, the quality and resolution of camera sensors, lens type, lighting and illumination of object and other requirements during the process should be determined by real condition and dimension of objects.

The effective bundler adjustment by SfM methods requires the random targeting on whole wind turbine blade surfaces with rows of non-coded retro targets (dot targets) and coded retro targets should be added to the blade surface as described in Section 3.7. Figure 3.28 shows the proposed camera movement around the blade during object recording. The camera distance from object should be evaluated in future works by technical specification of image capturing sensors and also the size of the object. Please refer to ANNEX IV for the size of the retro targets on the object.

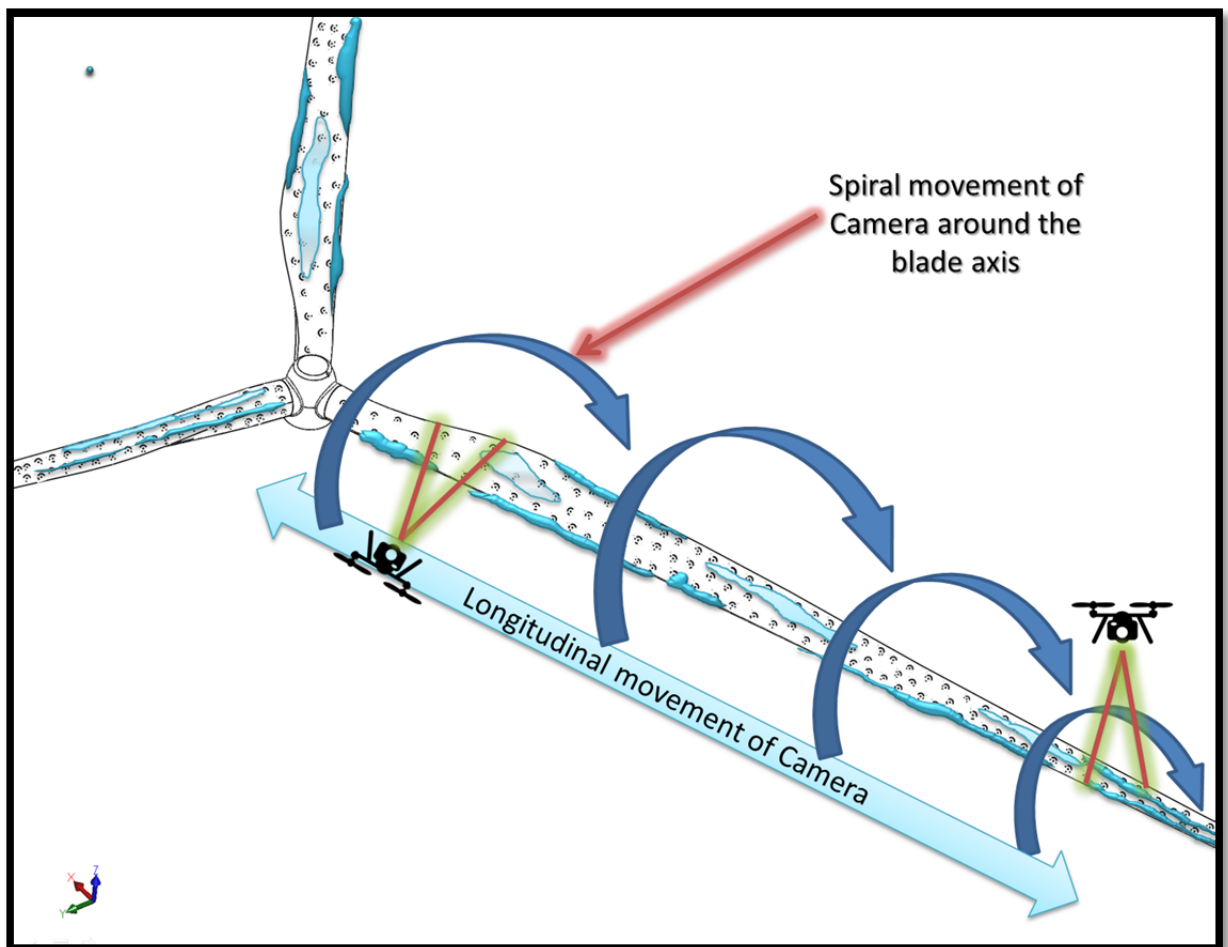


Figure 3.28: Proposed camera movement around the blade by Remote controlled drone

### 3.11 The equipment for marking the measuring surfaces

For accelerating the sticking of Un-coded references on the surface, in some cases, we could use the self-inking stamps instead of paper reference points. Self-inking stamps are made with a built-in ink pad. The pad is easily replaceable and provides thousands of quality impressions. These stamps are perfect for fast repetitive stamping.



Figure 3.29: Self-inking stamp for coded and non-coded retro target

### 3.12 The economic challenges in ice measurement on the wind turbines' blades

In previous sections, by default the probable access to SNEEC wind farms, we proposed different access methods to the installed RePOWER MM92 located at “Wind turbine Techno Center” wind farm field in Gaspésie peninsula. The Preparation process of wind turbine for photogrammetric measurement process such as another dimension measuring methods needs to turn off the wind turbine and stopping the blades. During the operational periods when the generators are working, this process has an economic impact for the owner of wind turbine for loss of the power generation’s revenue.

In maintenance periods is a good opportunity for preparing the blades for photogrammetric measurement. The Spots and Coded retro targets (simple and retro-reflective type) could be installed on the existing wind turbine blades and has no impact in performance of generator.

During Atmospheric icing of the wind turbines, the generators should be stopped for security and damaged preventing actions for the reasons such as:

- power reduction by disrupt the aerodynamics airflow;
- overloading due to delayed stall;
- increased fatigue of components due to imbalance in the ice load;
- and damage or harm caused by uncontrolled shedding of large ice chunks.

In one or combination of the above reasons, the wind turbine should be cleaned and prepared for restarting. At this time, the photography & image acquisition could be implemented by one of the proposed methods such as photography by a remote controlled Drone.

Chapter 3 describes the complete workflow of the study and description in details, about data , hardware and software tools used. This chapter also proposed the important notice & details recommendation in Photogrammetric measuring of Ice for the real case study base on the author knowledge and the experiences from this study.



## CHAPTER 4

### RESULT AND CONCLUSION

In this section, the obtained results based on the methodology explained are discussed. In first part, results are discussed and in the second part, accuracy assessment of the models is carried out.

#### 4.1 Points cloud reconstruction

After preparing the iced blade mockups, several photos were captured respecting the methodology previously explained. The photographs were then processed by VisualSfM software and after reducing noises and distortions a point cloud was produced for each iced blade. Figure 4.1 and 4.2 depict the dense reconstruction point cloud generated by VisualSfM.

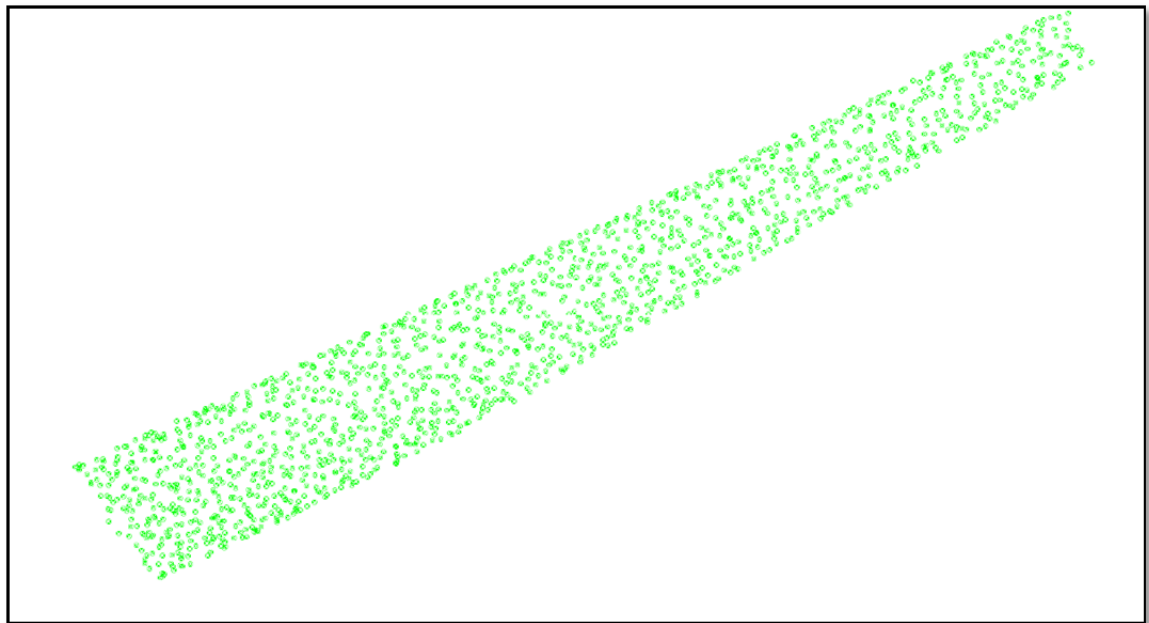


Figure 4.1: Generated point cloud of the iced blade-regular light

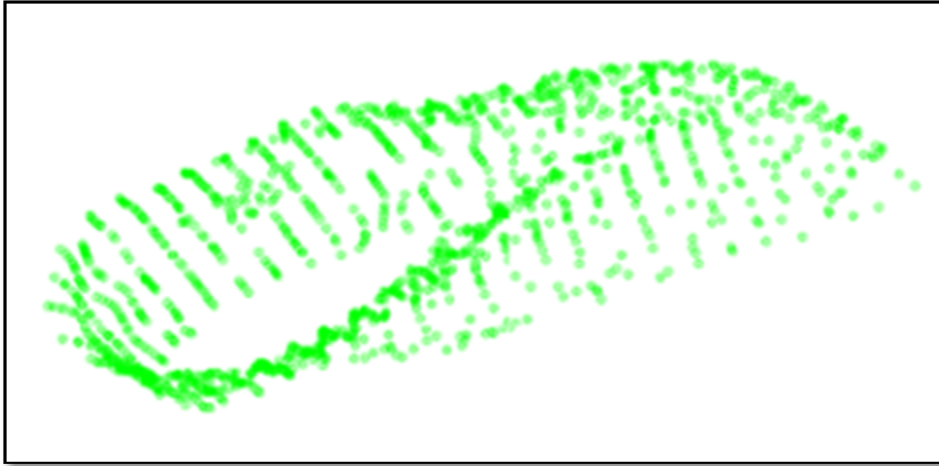


Figure 4.2: Point cloud view from pitch angle axis

## 4.2 Mesh generation

The generated point clouds were then transferred to the Digitized Shape Editor Environment of CATIA for further process and measurements. Since the point cloud consists of discrete points in the space it cannot directly be used to for alignment in order to achieve a continuous model, in the same environment meshes of parabolic triangular patches were generated using the point clouds. Figures 4.3 and 4.4 show the mesh generated using the point cloud of the first blade with normal lighting.

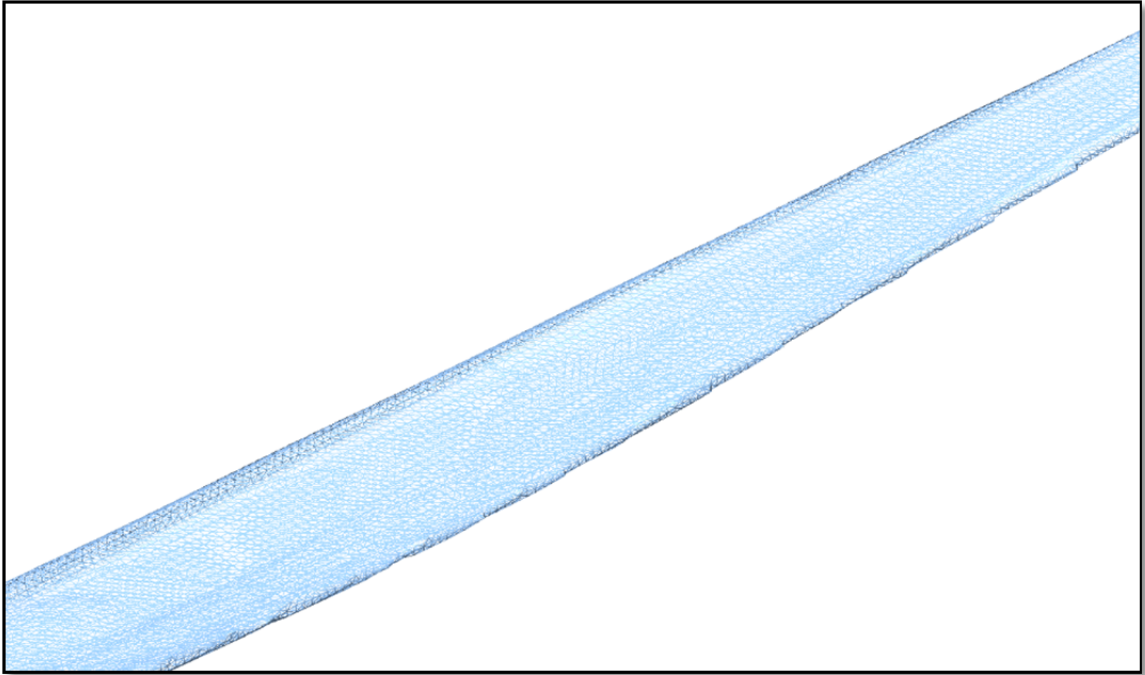


Figure 4.3: Generated mesh of 1<sup>st</sup> blade (recto view). Extracted point cloud from normal lighting

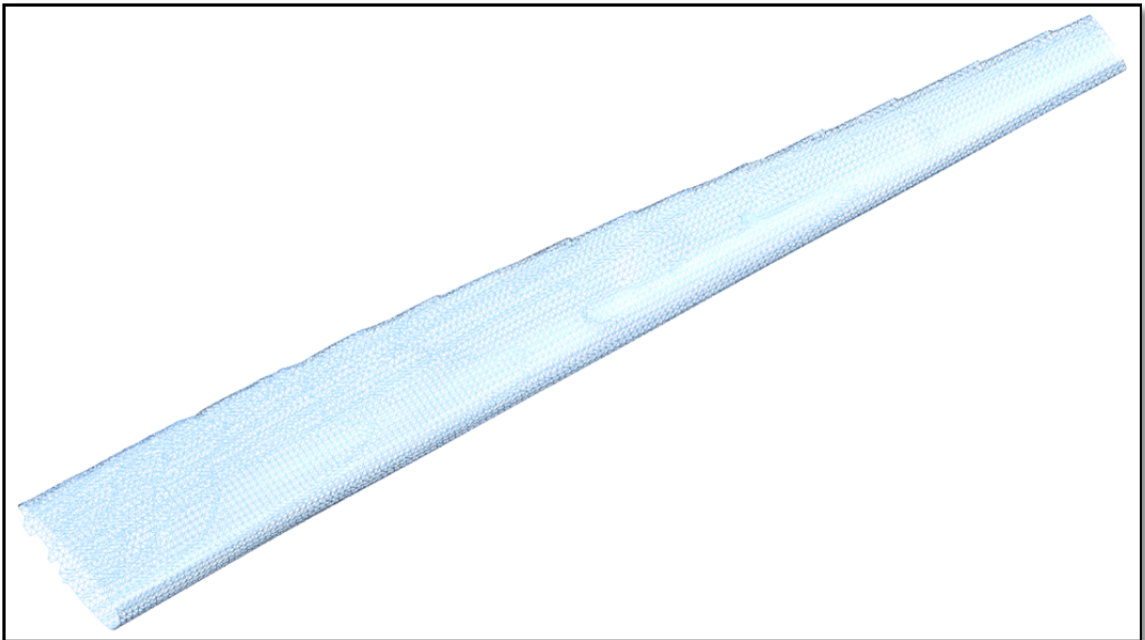


Figure 4.4: Generated mesh of 1st blade (verso view). Extracted point cloud from normal lighting

Figures 4.5 and 4.6 demonstrate the mesh generated using the point cloud of the same specimen scanned under the light with  $\lambda=432 \text{ nm}$ .

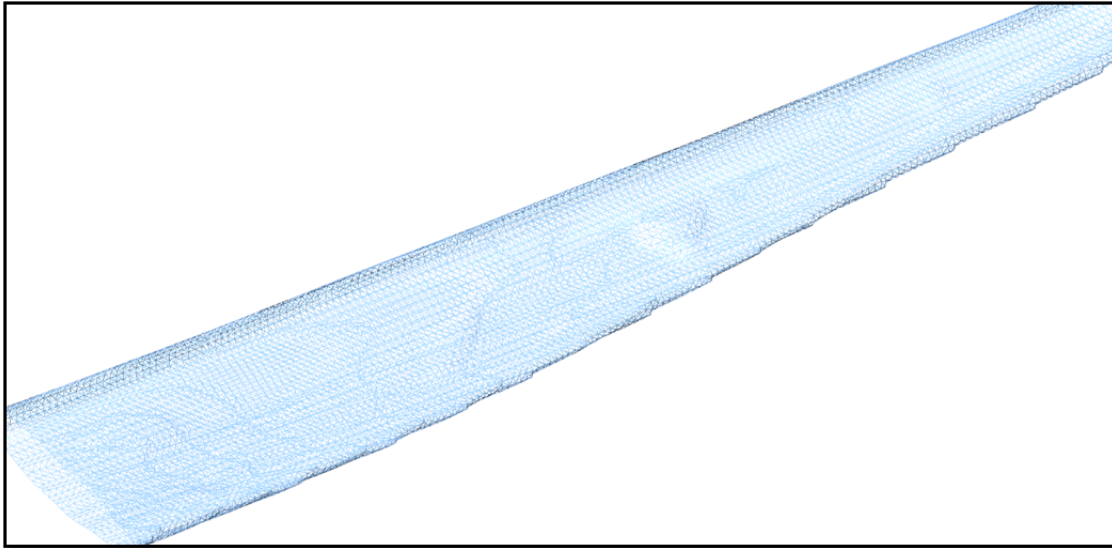


Figure 4.5: Generated mesh of 1<sup>st</sup> blade (recto view). Extracted point cloud from light with  $\lambda=432 \text{ nm}$

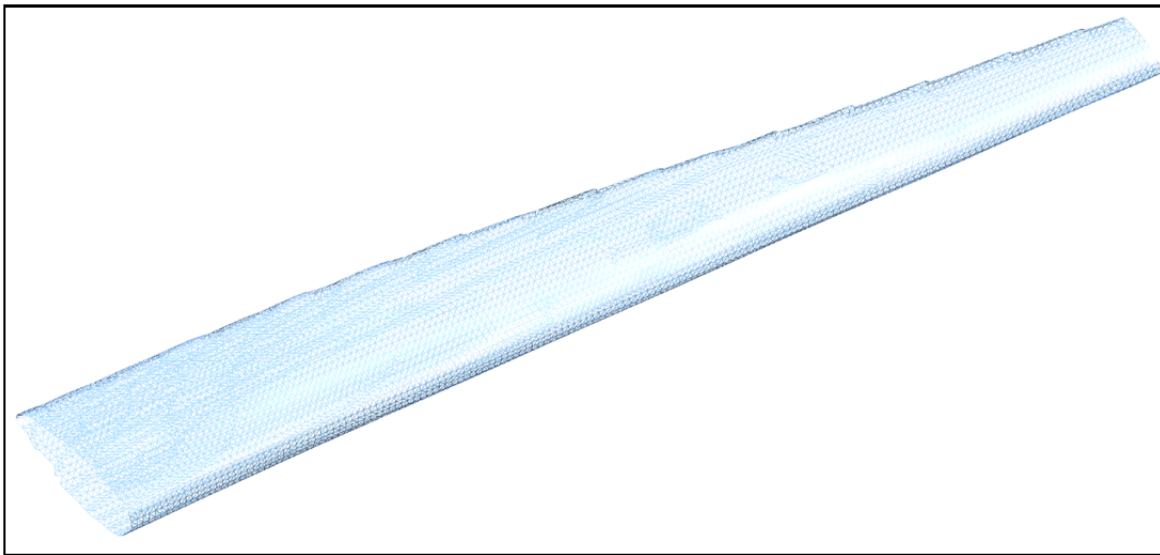


Figure 4.6: Generated mesh of first blade (Verso view). Extracted point cloud from light with  $\lambda=432 \text{ nm}$

Figures 4.7 and 4.8 show the mesh generated for the second blade with smoother ice covering.

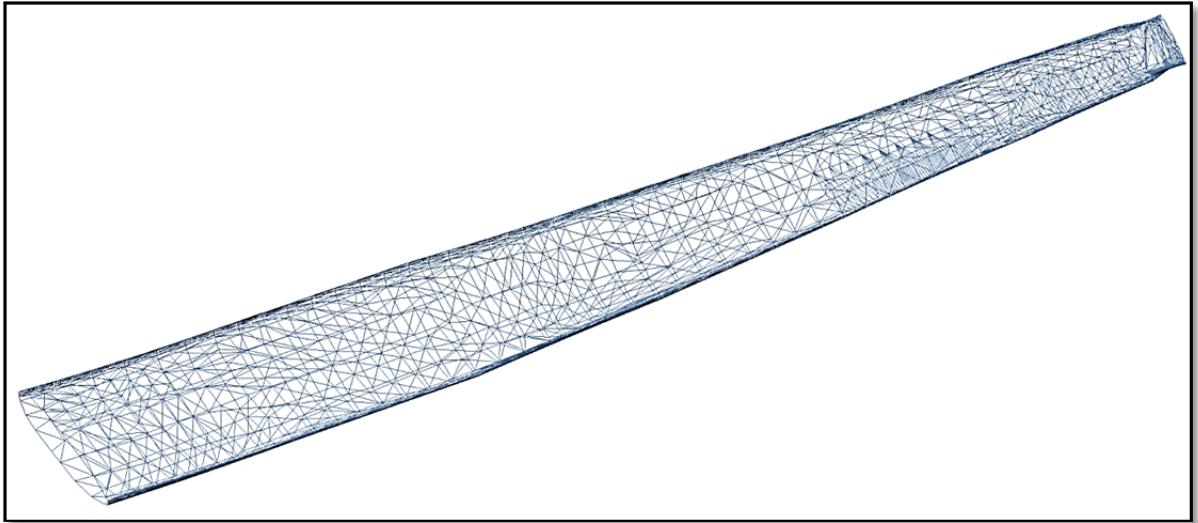


Figure 4.7: Generated mesh of second blade (Verso view). Extracted point cloud from light with  $\lambda=432 \text{ nm}$

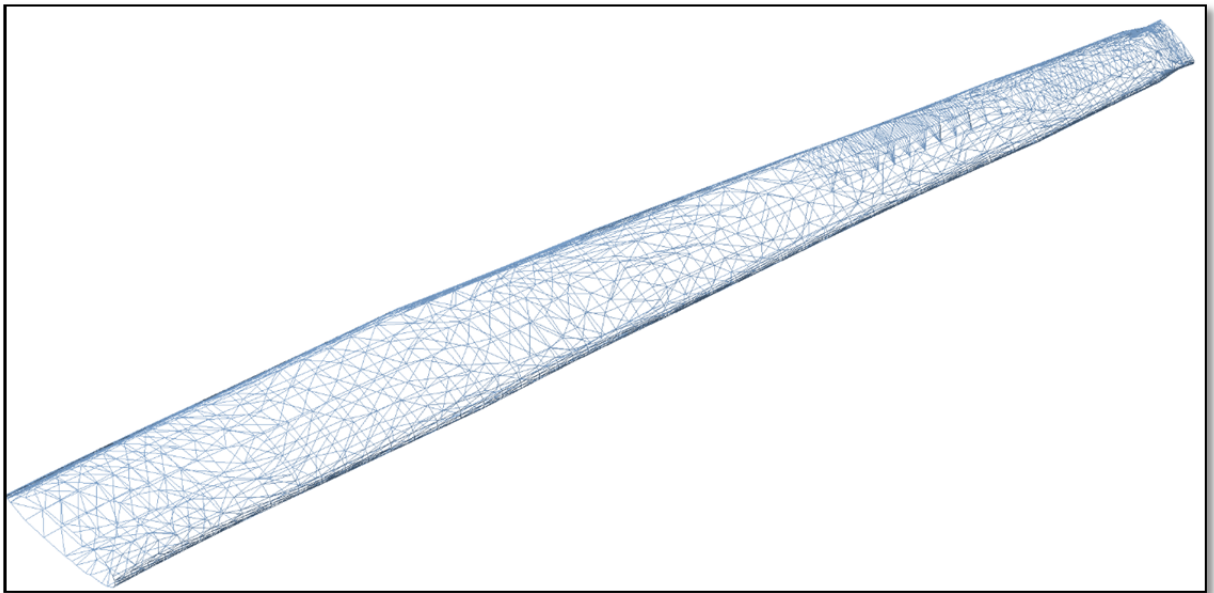


Figure 4.8: Generated mesh of second blade (Verso view). Extracted point cloud from light with  $\lambda=432 \text{ nm}$

The visual observations of the generated meshes showed that as it was expected one weak point of this method is the capability to capture sharp edges. In all experiments with different geometric and lighting conditions it was clearly observed that the sharp trailing edge was not scanned with an appropriate concentration of points.

Moreover, visual comparison of the meshes generated for the same model once photographed under normal lighting and once under Blue light, showed that the point clouds generated using photos captured under the aforementioned blue light included more details about the surface roughness. In fact under normal lights transparent ice protrusions were hardly captured.

Table 4.1: Illumination effect on Ice feature detection

<b>Lighting in Photogrammetric Object Recording</b>	<b>Point cloud from normal lighting</b>	<b>Point cloud from light with <math>\lambda=432\text{ nm}</math></b>
Numbers of photos	53	53
Numbers of detected points	24273	30867
Ice texture detection in photos	Normal	BETTER
Triangles Mesh in each model	52691	61906

One very important issue that is necessary to be noted is the scale less nature of photogrammetry. Unlike laser scanning, the resultant point cloud has no absolute scale. So it is required that an object of known dimensions (e.g. a scale bar) be present next to the object being photographed. This object of known dimensions should be incorporated in image processing, so that it can be used in bringing the whole model in the real scale.

### 4.3 Scaling and alignment of the model

The first thing to note of importance is that photogrammetry is a scale-less method as well as the resultant point cloud has no absolute scale. It is imperative that an object of known dimensions (e.g. a gauge bar) is present next to the subject being photographed, and this

known scale are taken as part of the process of photogrammetric object recording, so that the scale ends up in the final 3D model. The length of this reference feature should be large enough to have small scaling errors on the all cloud points' results.

In the current work, a steel ruler was used as a reference for scaling the point cloud. The length of this reference scale bar used as the reference for scaling the meshed cloud points. Figure 4.9 show the position of the scale ruler (Scale Bar) in the images and figure 4.10 shows generated point cloud from the images. Also for alignment purpose, the cylinder like base of the prototype blade model was cleaned from Ice before the process of object recording was applied.

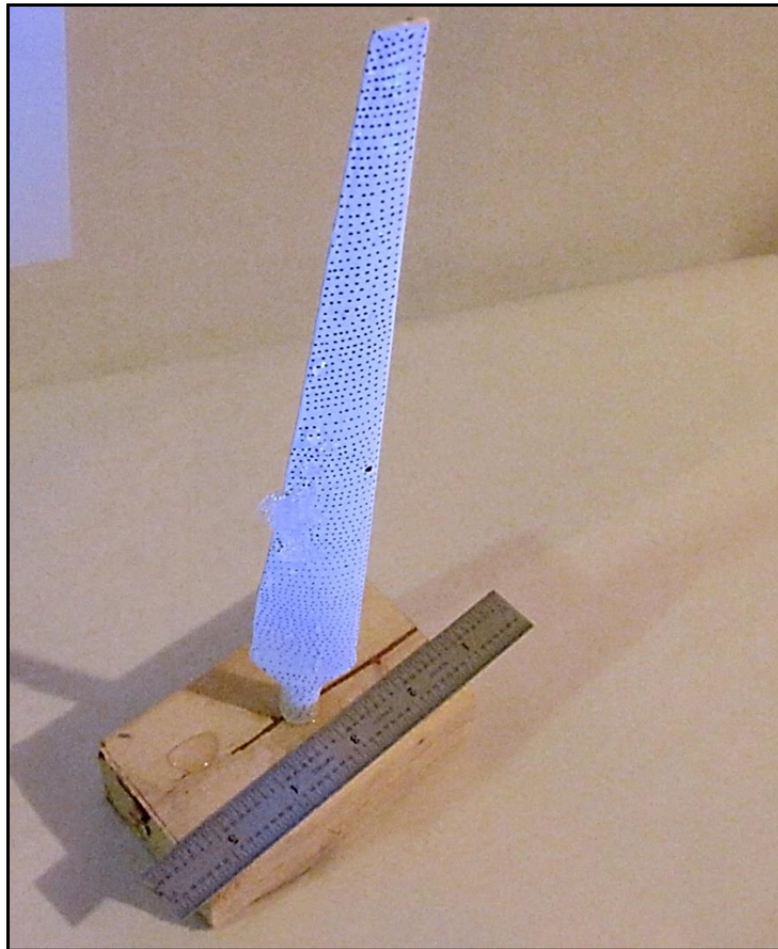


Figure 4.9: Steel ruler as Ground Control Points (GCP).

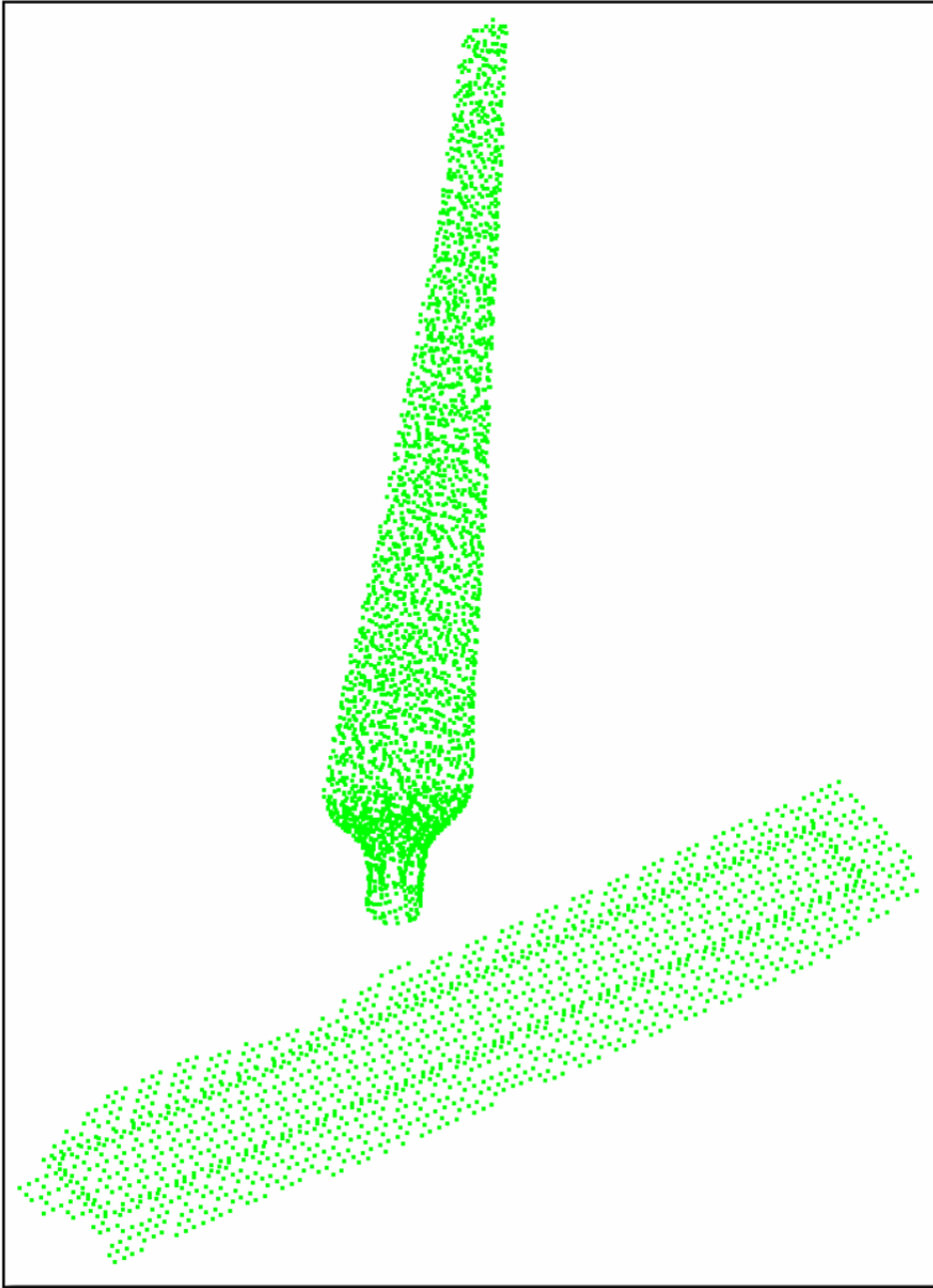


Figure 4.10: Scale Bar in the point cloud

After mesh generation (Figure 4.11) and scaling the mesh using the length of the known scale bar, the standard features required for aligning the mesh with the original CAD model were distinguished. Figure 4.12 depicts the cylinder fitted to the root of the blade which is used as

the first and the most important feature of alignment. This picture shows the location of the cylinder with regard to the complete blade.

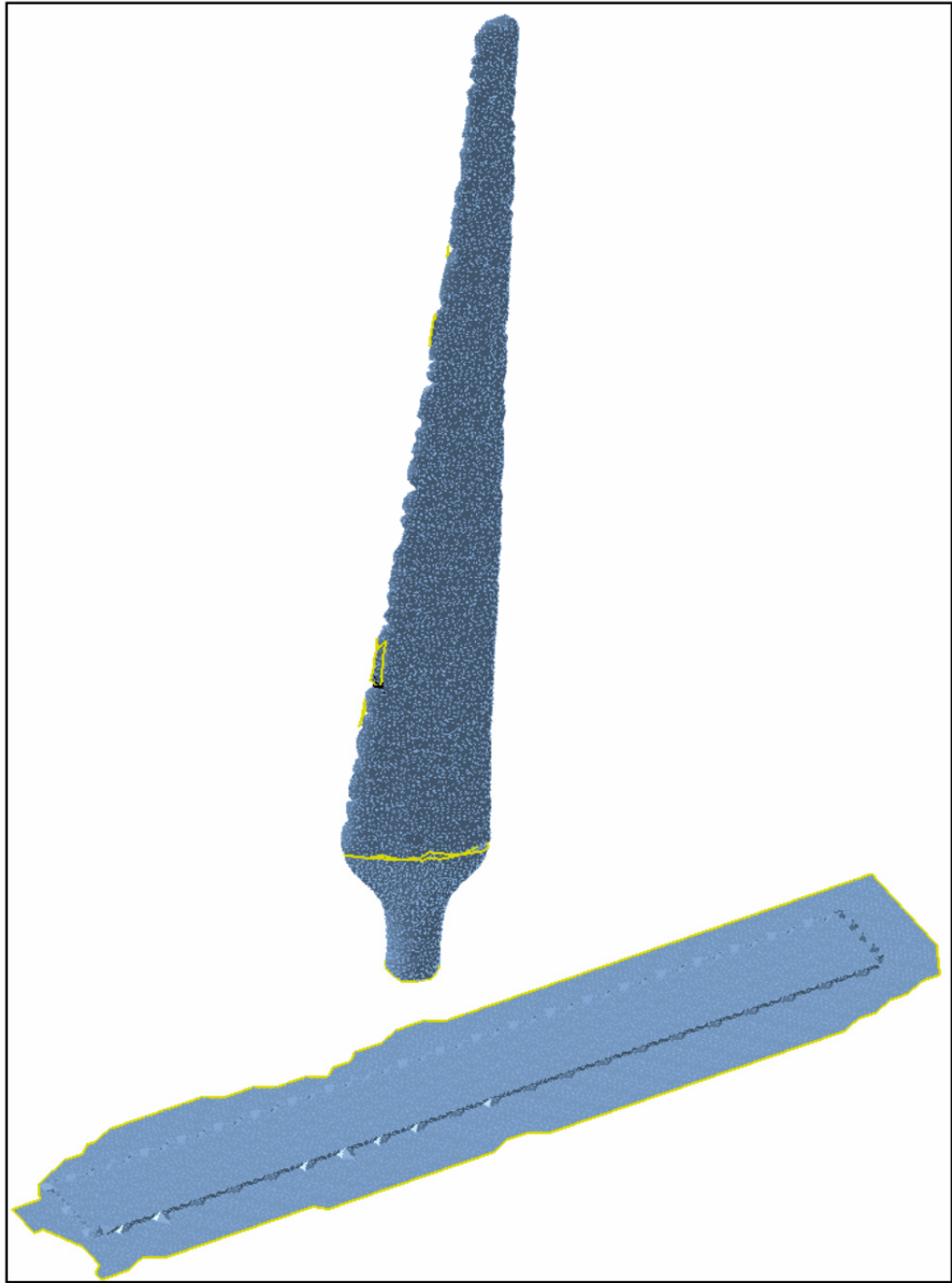


Figure 4.11: Generated mesh in Digitized Shape Editor Environment of CATIA

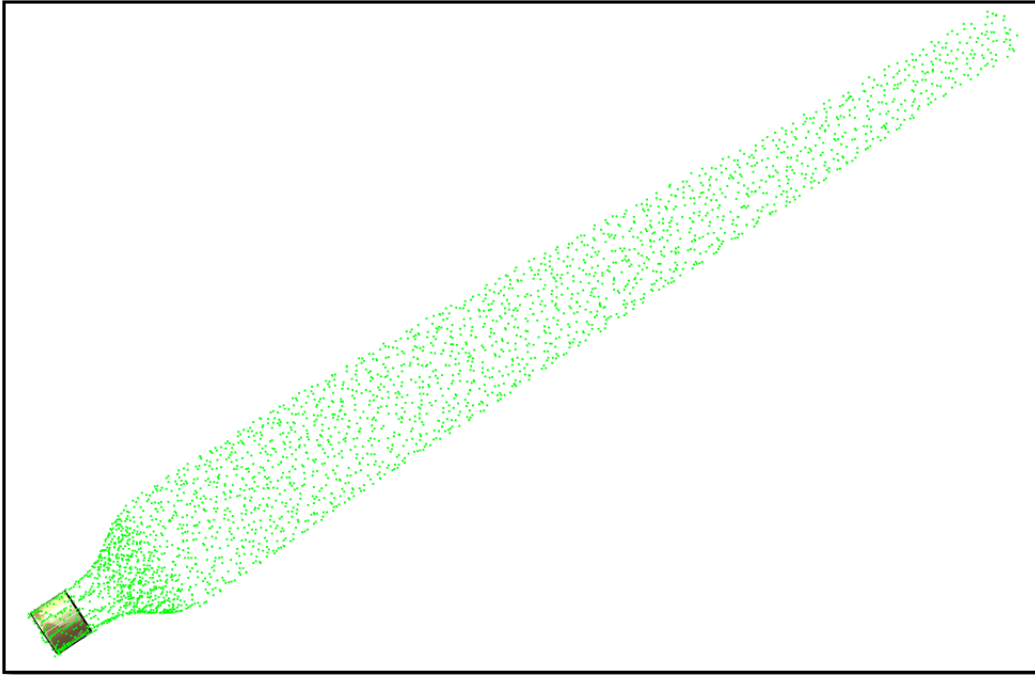


Figure 4.12: 3D Similarity transform feature is positioned on the blade

Using the recognized features and by minimizing the gaps and the overlaps the generated meshes were matched to the original CAD model. However since divers sources of numeric errors exist in the process of generation of point cloud and consequently the meshes and recognized features, the methodology employed could not guarantee the exact alignment and the alignment errors should be considered in the measurement of the ice layer. Figure 4.13 shows aligned CAD model and cloud point.

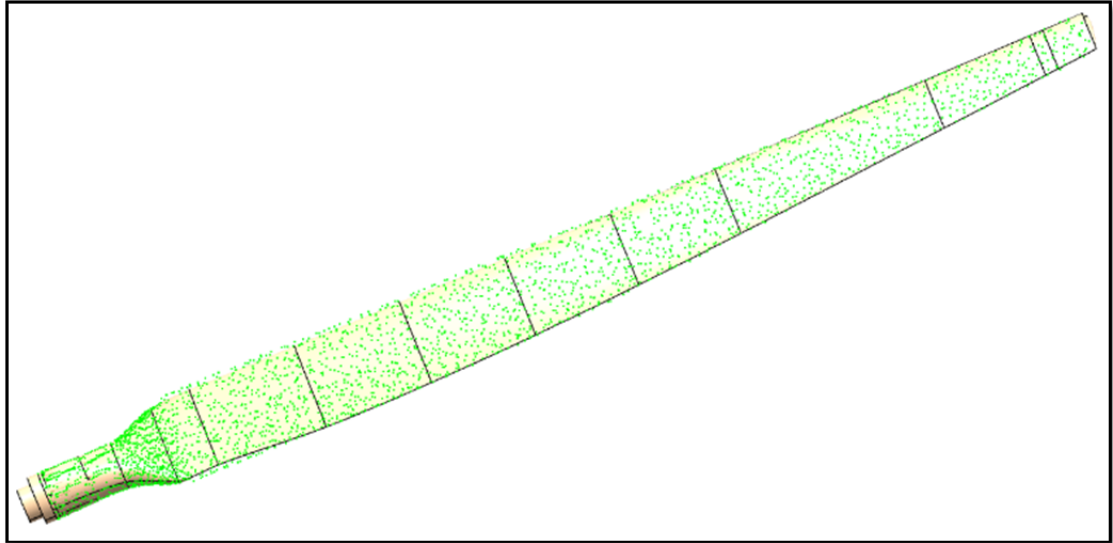


Figure 4.13: CAD model aligned with the generated cloud point

#### 4.4 Measurement system analysis

After alignment, the generated meshes were geometrically compared with original CAD model and the results were reported as contours of deviation. This deviation is regarded as the thickness of the ice. Figures 4.15 & 4.16 show the ice thickness contours for the first blade photographed under normal light. Moreover, Figures 4.14 & 4.15 show the contour the same blade under blue light ( $\lambda=432 \text{ nm}$ ). As well as it was previously observed the contour of the specimen scanned under blue light shows more variation in ice thickness which is an evidence for higher precision of scanning under blue light (Figures 4.18 & 4.19). In order to verify the results, the thicknesses of ice in certain places were measured using manual feeler gauge tools and were compared to contour values at the same place. Figure 4.17 shows the location of manual ice thickness measurements and Figure 4.16 shows the composition of the used feeler gauges. Table 4.2 shows the manual measurement on the blade surface and the result in the area with no ice-covered by glaze & Rim Ice. Regarding the small dimension of prototype blade the available feeler gauge and the caliper penetrate easy in the ice layer which was impossible to measure the thickness in the points.

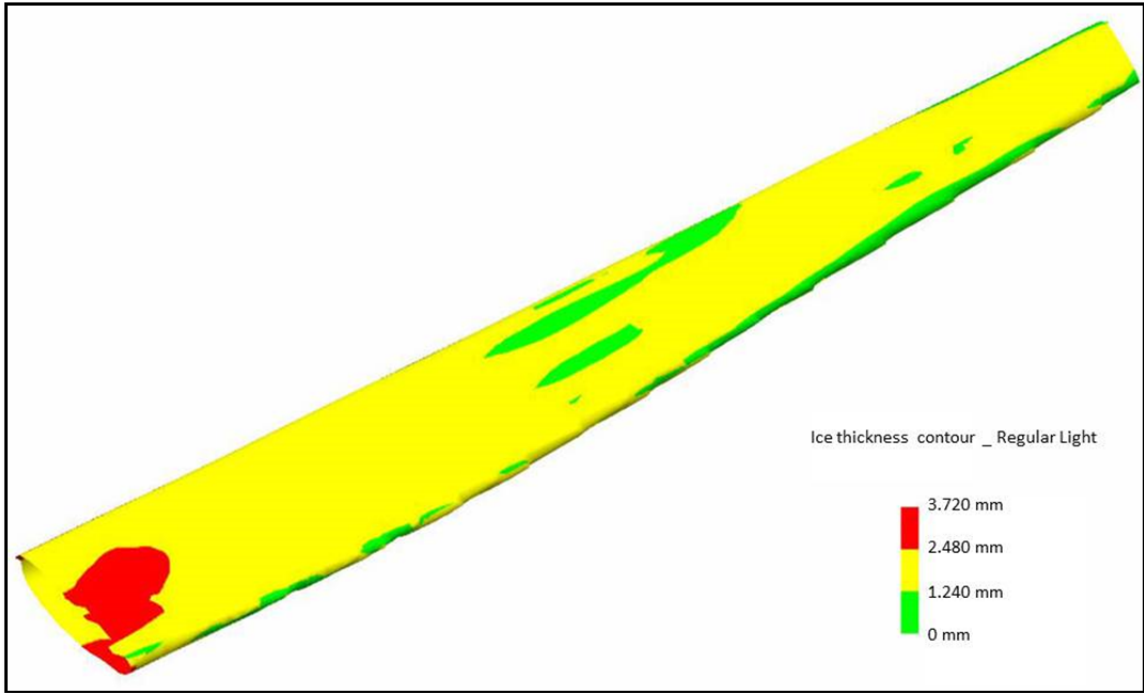


Figure 4.14: Ice thickness contour of first blade (recto view). Extracted point cloud from regular light

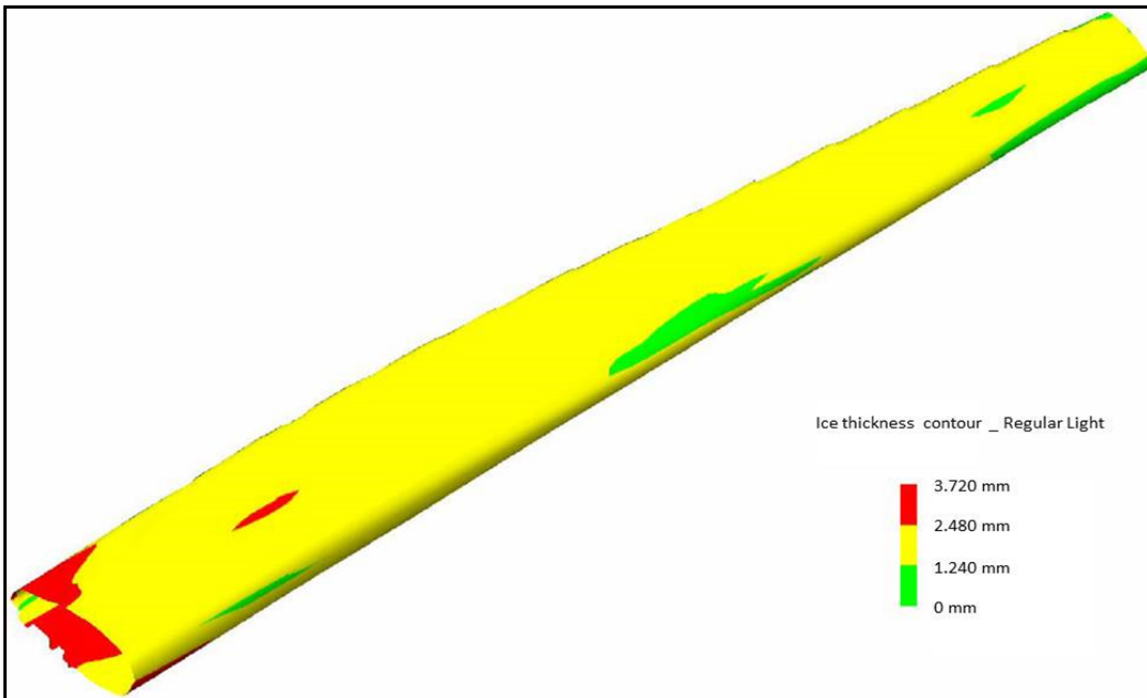


Figure 4.15: Ice thickness contour of first blade (verso view). Extracted point cloud from regular light

Table 4.2: Comparison of manual measuring and digital mesh results

	<b>Manual thickness Measuring (mm)</b>	<b>Thickness detected on mesh model lighting by regular light</b>	<b>Thickness detected on mesh model lighting by light with <math>\lambda=432\text{ nm}</math></b>
No Ice Zone	0	0.2-0.5	0.1-0.3
Glaze Ice Zone	0.9	1.54	1.3
Rim Ice Zone	2.99	3.72	3.89

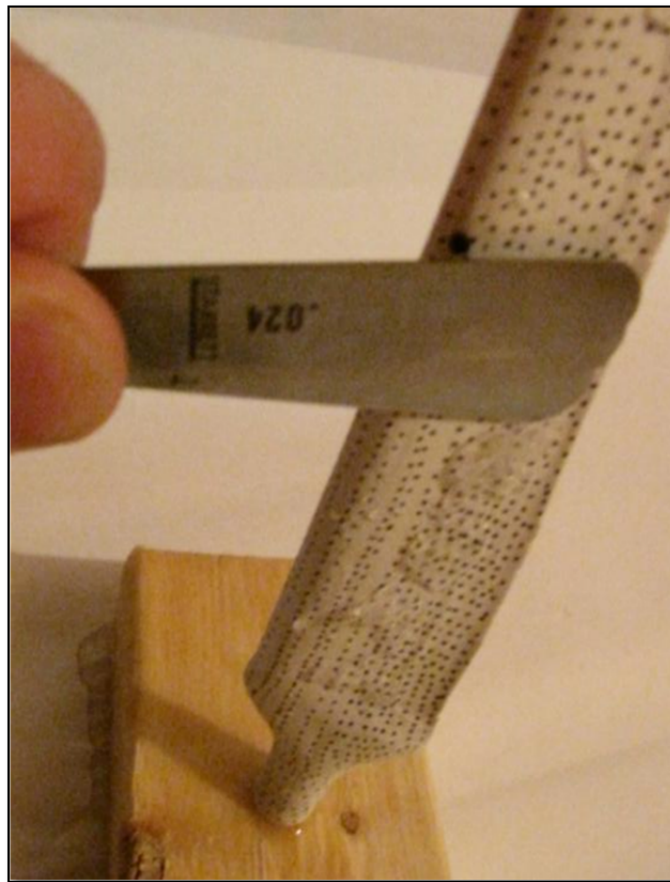


Figure 4.16: Manual measurement of iced region.  
Filler gauge shows  $\approx 2.9\text{ mm}$  in area

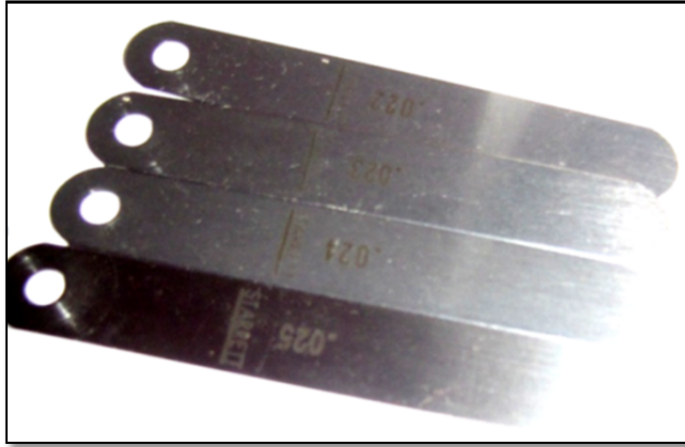


Figure 4.17: Composition of used feeler gauges in measurement

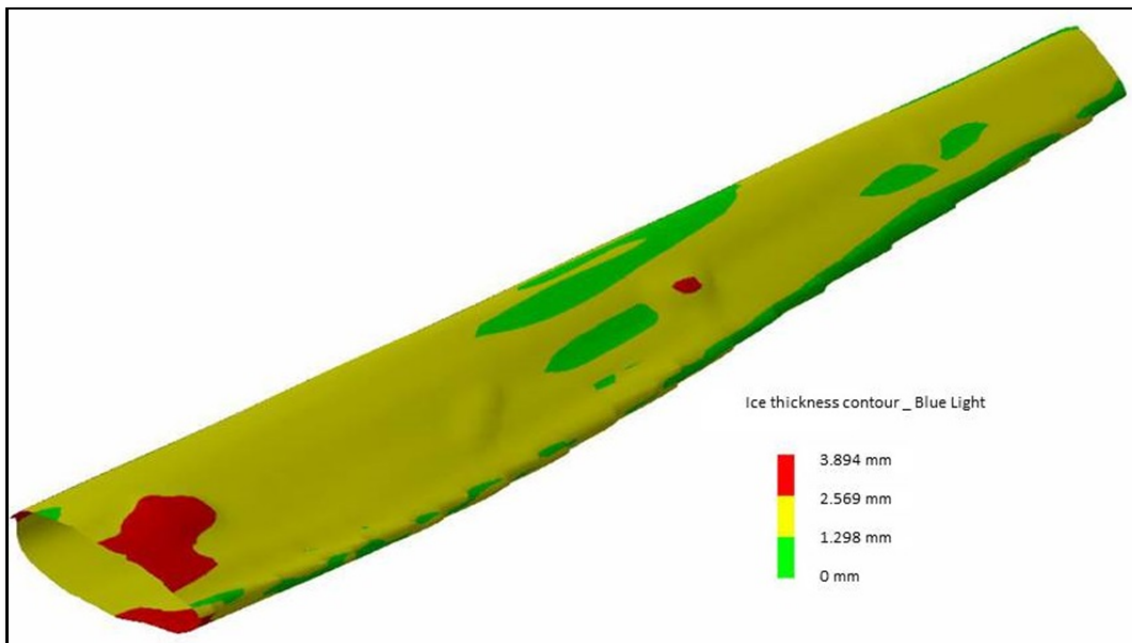


Figure 4.18: Ice thickness contour of first blade (recto view). Extracted point cloud from light with  $\lambda=432$  nm

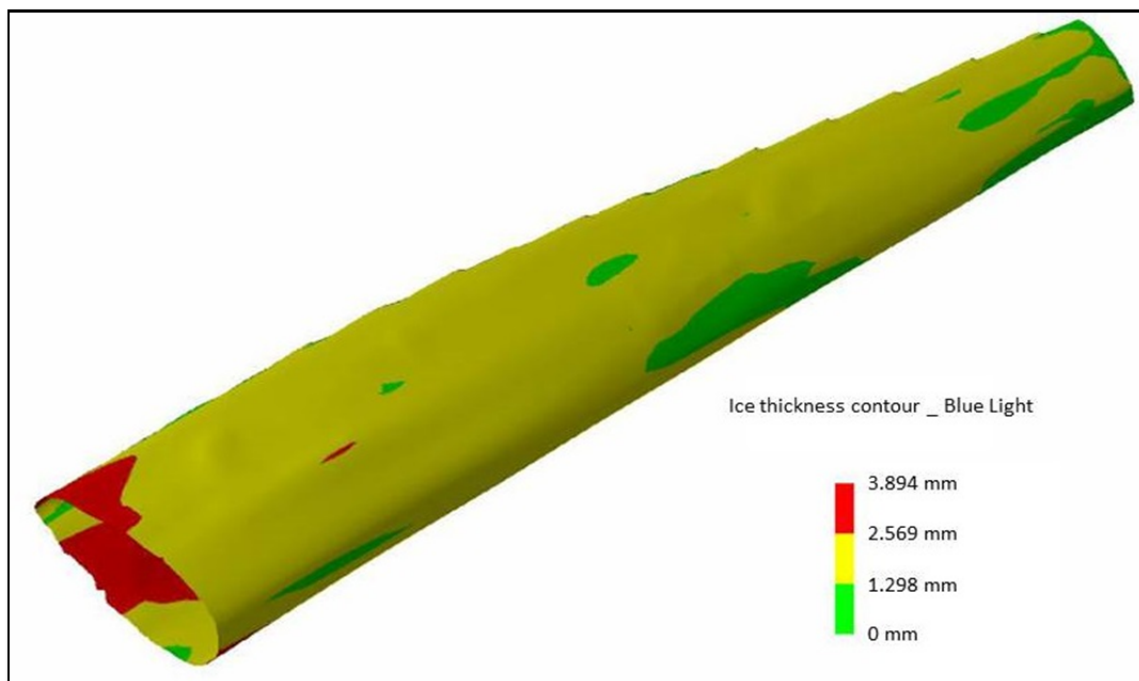


Figure 4.19: Ice thickness contour of first blade (verso view). Extracted point cloud from light with  $\lambda=432$  nm

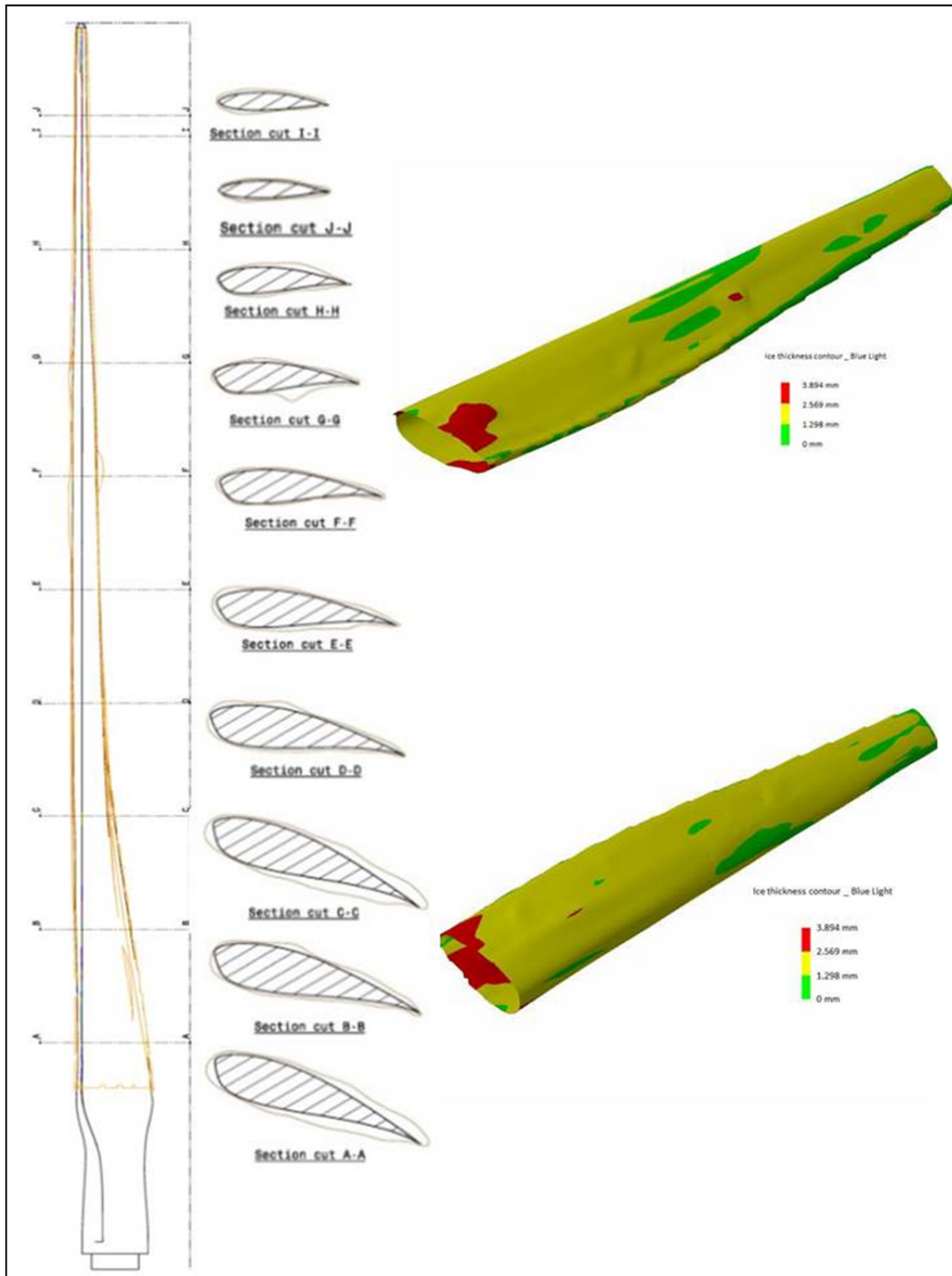


Figure 4.20: 2D ice profile shape on the blade in different span wise of object. The hatched profile is the blade real cross section. Brown show the margin of the ice volume on the blade

#### **4.4.1 Prototype process simulation, limitation and consideration**

The real case study and measuring object of this project was a giant RePOWER MM92 wind turbine “2-MegaWatt power plant with 92 meter rotor diameter” installed in the cold windy area of wind farm field in Gaspésie peninsula. The MM92 has a “3 blade rotor hub” by blade length of 45.2 meter each and with hub height of 80 meters.

During the prototype simulation, we have used the small blades which can be considered as rigid object in term of dimensional measurement because there is no deformation or distortion on its shape during the photogrammetry object recording. On the contrary, the real wind turbine blades are a non-rigid body which deform by the external and gravity forces during operation and as well as in time of measurement. These dimensional variations need to be studied during photogrammetric object recording of large blades since the result point cloud comes from the captured images of deformed blade resulting in deformed cloud points of object. The behavior of WT blade is such as a cantilever beam which when subjected to a structural load, the cantilever carries the load to the support. The deformation of blade surface increases from blade root's to the tip. In other hand as described in Section 1.2 & 1.3, the tip of blades is one of important region in measurement which has the maximum rate of ice accretion and a significant effect in loss of power of the wind turbines. Our proposed method in close range photogrammetry is able to cover these variations in measurement of real case study.

The large blade can be measured as a rigid body in smaller sections which have the similar behavior as rigid body behavior. The length of rigid body segments on the blades can be varied by the geometry and the cross sections shape on the blade. As describe in Section 3.3.1, the effective bundler adjustment by SfM methods require the random targeting on whole wind turbine blade surfaces with rows of non-coded retro targets (dot targets).The coded retro targets should be installed on the blades' surface for 3D similarity at Ground Control Points (GCP) as explained in Sections 2.3 & 3.6.3. This GCP is used for aligning the produced cloud points to the related sections of blades CAD data.

In large-scale reconstructions, it is thus important to partition the images in clusters, covering different parts of the scene as partial rigid body. This results in two benefits - reduced runtime on a single machine due to the smaller dimensions of the clusters and the possibility to split the processing across multiple machines for even further speedup. Figure 3.24 shows the variation in length of rigid body sections on the blade. Photogrammetry image capturing for each section need to be clustered and processed as shown in workflow for Image-Based Modeling & 3D object reconstruction procedures (Figure 3.3)

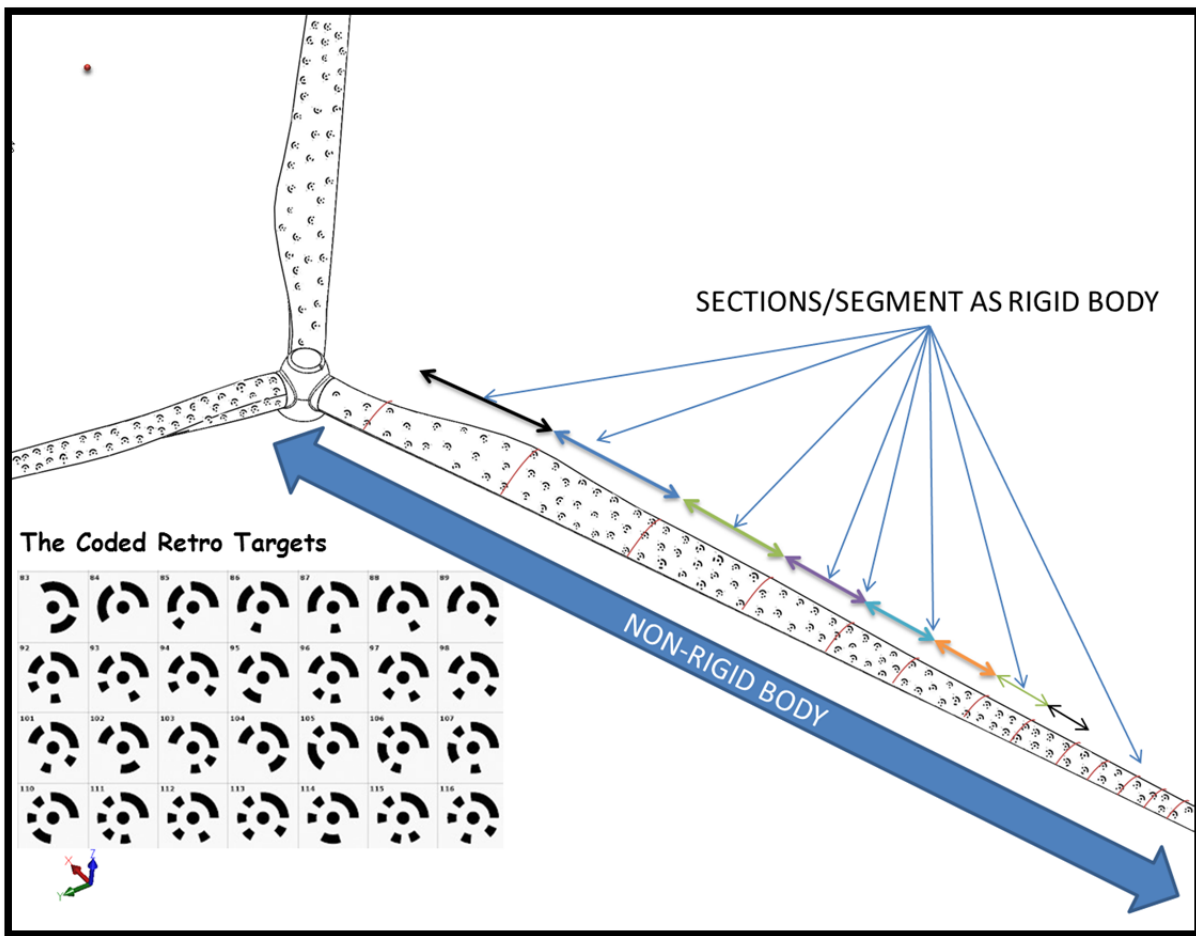


Figure 4.21: Wind turbine blade as with coded retro targets on surface

## CONCLUSION

This study focused on the feasibility of reconstruction of 3D polygonal mesh models by images captured from a wind turbine blade with a configuration of digital SLR cameras. The main objective of this reconstruction is to identify the volume and shape of ice-accumulated areas on the wind turbine blades in arctic regions. Geometrical comparison of these triangular mesh models and the non-iced blade CAD could reveal the geometry of accumulated ice.

### **Answers to the research questions**

#### ***1) What is the 2D ice profile shapes on the blades at different span-wise locations?***

By the proposed method, it is possible to extract the 2D ice profile shapes on the blades at different span-wise locations. When the meshed model aligned on the master CAD data, the approximate blade shape after the accumulation of ice can be extracted. This information could be used to identify the effect of ice on performance and life of the generators in cold climate area.

This research evaluated the possibility in extraction of volume of the ice accumulated at the time of object recording in order to calculate the mass of ice was proven. This mass can be approximated by subtracting the volume of the non-iced blade from the volume of iced blade and considering the density of ice. However identifying the density of ice that is strongly related to climate condition and atmospheric parameters needs more study and investigation.

Figure 4.21 show the section view of the iced blade and the aligned original CAD model which transformed in the same global coordinate system. The different span wise locations on the wind turbine blade are sectioned for depicts the variation in form of the air foil of blades. Considering the methods of the ice generation on the blade, the ice volume inscribed the blade profile in different span wise. The type of ice with different texture surfaces changed the detected points and the result of meshed model.

***2) What is the ice thickness (glaze ice & rime ice) on the surface of the rotor blades?***

In the studied case, the shape of blades as the master data were assumed invariant but the accumulated iced on the surface have arbitrary and random shape due the position and climate condition. These measurements showed that although the outline of the mesh generated from the iced surface is similar to the real iced surface the calculated thickness is not precise, but it was a success to measure the thickness of ice on the blade, which was not possible in a cost effective way.

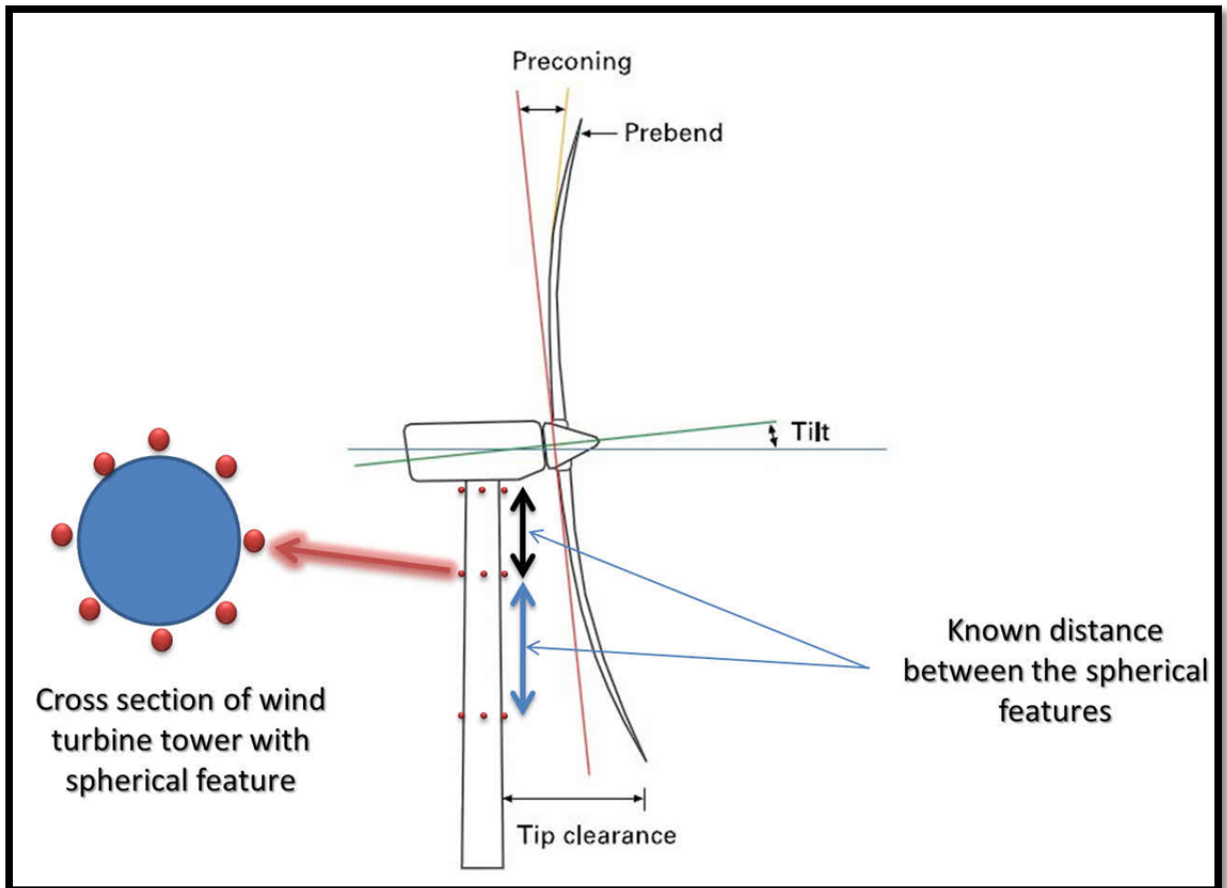
## RECOMMENDATIONS

Image-based modeling is widely used for reconstruction of three-dimensional models from two-dimensional images. In this research, a new approach to reconstruction of 3D models of frosted blades was described and implemented. In this process based on the presented workflow in Figure 3.3 (page 45), the proposed recommendations review are as follow:

1. The **targeting** and **illumination** are the two major parameters for photogrammetric object recording. The effective bundler adjustment by SfM methods require the random targeting on whole wind turbine blade surfaces with rows of non-coded retro targets (dot targets). Target images size, should be **at least 5 pixels in diameter** and to be easily identified and easily marked when viewed in an image the installed retro targets support the fast image matching and image orientation in process of 3D mesh generation. The coded retro targets should be installed on the blades surfaces for 3D similarity at Ground Control Points as explained in Sections 2.3 & 3.6.3. The optimum reference point diameter is 10 image pixels due the tiling image size.
2. In this study, multiple overlapping photos capture the object from different positions, whereby coverage of common object parts should be available from at least three but preferably five photographs from different camera positions. The clear and sharp photos with more than 70% coverage by recorded object in each frame support well the fast image matching and image orientation in our process.
3. In general Rime ice grows as droplets rapidly freeze and forms brittle, opaque, and milky-textured ice. In this study, the illumination by light spectrum with the wavelength between the violet (405 *nm*) and blue (460 *nm*) spectral ranges helps to boost the textured of ice in the captured images which were absent in photogrammetric object recording by the normal and ambient lights. In present of ambient light, the illumination by ring flashes equipped by available color filters in the mentioned wavelength is the fast way to enlightenment the object by color light during photogrammetric object recording.

4. Regarding the limited financial resource for this project, the author used the open source and free license software for cloud point generation. The VisualSfM support only one radial distortion parameter that could work for cameras with a low distortion but it could not work properly for cameras with large distortion. This issue considered and resolved in this study by rectifying the images by PTlens Software as low cost licensed software (See Section 3.3.6). The mechanical stability of the cameras in this study was really poor in terms of high-accuracy photogrammetric requirements. The photogrammetric object recording by a commercial Digital Photogrammetric System such as TRITOP optical CMM from GOM Company, recommended for real case study that support the Structure from Motion method with high level of accuracy
  
5. In Section 3.10, this study recommended the photogrammetry object recording by remote controlled drone (Section 3.9.4). The remote control helicopter (Figure 3.28) is proposed which has enough payloads for carrying the weighted DSLR camera and its accessories such as flashes, battery and in addition longer flight time that take a good flexibility for shooting the wind turbine components as explained in Sections 3.3.4 & 3.3.5. The photogrammetric object recording for three frosted blades, should be applied in the same time which the position of these blades based on the rotation axis of wind turbine is arbitrary.
  
6. The first thing to note of importance is that photogrammetry is a scale-less method as well as the resultant point cloud has no absolute scale. In prototype simulation, process a steel ruler is used as a reference for scaling the point cloud. As such, it is imperative that an object of known dimensions (e.g. a gauge bar) is present next to the subject being photographed, and that photographs incorporate this known scale in photogrammetric object recording, so that the scale ends up in the final 3D model. The length of this reference feature should be large enough to have small scaling errors on the all cloud points' results. The tower of wind turbine could be as scale bars for this important. The author recommended installing on tower, the spherical features in known distance between them. The spherical feature could detect in six degree of freedom as a point in

our photogrammetry method. The following image shows the general idea of this type of scale features. For integration of the resulted cloud points from the features on the tower, the presence of coded and non-coded retro targets on the tower surfaces are necessary to add this cloud points at any time to the generated cloud points from frosted blades.



### Spherical features as proposed Scale bars on the tower of wind turbine

Another possibility of proposed method in this study is to create the textured 3D model from frosted blades. As remarked in presented workflow in Figure 3.3 (page 44), the resulted mesh from our proposed methods could be mapped by the images of case study and shows the textured model of frosted blades. An example of this process shown in Figure 2.4 (3D textured model of a tree trunk). This process needs the texture mapping software such as Blender mapping which is out of scope of this research. These models could match with the

operational data of Wind turbine in cold climate and make a library from the cause and effect of icing.

## ANNEX I

### PHOTOGRAMMETRY, RECORDING AND ANALYSIS PROCEDURES

Luhmann (Luhmann, 2010) shows the principal procedures in close range photogrammetry for both Digital & Analogue photography in Figure 12 which are briefly summarized in this Annex.

#### 1) RECORDING

1. Targeting:  
Target selection and attachment to object features to improve automation and increase the accuracy of target measurement in the image
2. Determination of control points or scaling lengths:  
Creation of a global object coordinate system by definition of reference (control) points and/or reference lengths (scales)
3. Image recording:  
Analogue or digital image recording of the object with a photogrammetric system (DSLR Camera)

#### 2) PRE-PROCESSING

4. Computation:  
Calculation of reference point coordinates and/or distances from survey observations (e.g. using network adjustment)
5. Development and printing:  
Photographic laboratory work (developing film, making photographic prints)
6. Digitizing:  
Conversion of analogue photographs into digital images (scanning)
7. Numbering and archiving:  
Assigning photo numbers to identify individual images and archiving or storing the photographs

### 3) ORIENTATION

8. Measurement of image points:

- Identification and measurement of reference and scale points
- Identification and measurement of tie points (points observed in two or more images simply to strengthen the network)

9. Approximation:

Calculation of approximate (starting) values for unknown quantities to be calculated by the bundle adjustment

10. Bundle adjustment:

Adjustment program, which simultaneously calculates parameters of both interior and exterior orientation as well as the object point, coordinates which are required for subsequent analysis

11. Removal of outliers:

Detection and removal of gross errors, which mainly arise during (manual) measurement of image points

### 4) MEASUREMENT AND ANALYSIS

12. Single point measurement:

Creation of three dimensional object points coordinates for further numerical processing

13. Graphical plotting:

Production of scaled maps or plans in analogue or digital form (e.g. hard copies for maps and electronic files for CAD models or GIS)

14. Rectification/ Orthophoto:

Generation of transformed images or image mosaics which remove the effects of tilt relative to a reference plane (rectification) and/or remove the effects of perspective (Orthophoto)

## ANNEX II

### LASER LIGHT SECTIONING CAMERA

As parts of this research, the author has proposed a customized laser scanner for measuring the ice thickness by using the optical properties of ice vs. the different wavelength. Ice exhibits strong absorption in the ultraviolet (UV) at wavelengths  $170\text{ nm}$ . With increasing wavelength, the absorption becomes extremely weak in the visible, with a minimum near  $400\text{ nm}$ . In the wave length of  $405\text{ nm}$ - $460\text{ nm}$  the ice have merely solid opaque characteristics (Warren, 1984). In this case if we use the UV laser in visible wave length  $405\text{ nm}$ - $460\text{ nm}$ , we could measure the shape by laser scanning methods (Ackermann et al., 2006). Please refer the following images shows the concept of our proposed Ice Detection System and the final images show the concept design for proposed validation prototype for **Ice Laser Light Sectioning Camera**.

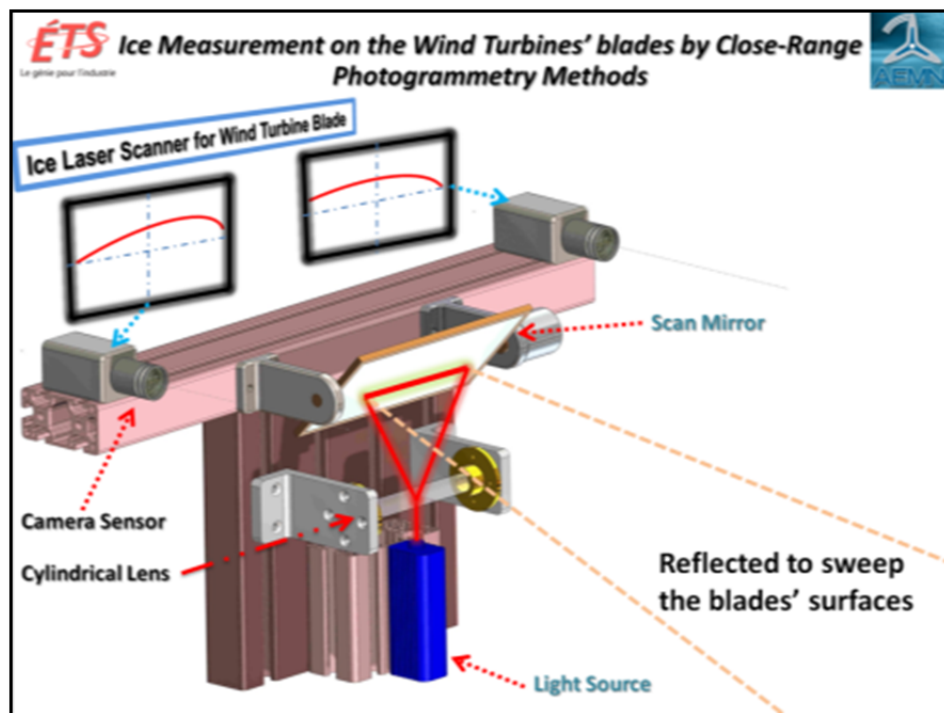


Figure A. 1: Principle of Ice laser Scanner for Wind Turbine

**ÉTS** *Le génie pour l'industrie* **Ice Measurement on the Wind Turbines' blades by Close-Range Photogrammetry Methods** 

March 12, 2015

**2 Main Components of our solution:**

**❖ Optical Ice Detection system**

- ❖ Base on Retro Target Scanning and image processing
- ❖ System save the laser tracks images as a Master DATAs (*learning*)
- ❖ The Bar codes that covered by ice show the situation of ice
- ❖ The laser beam image will show the type of ice (Rim, glaze Ice or Mix.)
- ❖ System detect the changes in images (*Comparing*)

**❖ Optical Measuring System**

- ❖ Base on Light-Section Method
- ❖ System Save the cloud of points of the clean blade as a Master DATAs (*learning*)
- ❖ Cloud point converted to the CAD DATAs Mesh (.iges & .stl CAD files)
- ❖ The iced region (Covered bar codes) scanned more precisely
- ❖ The icing Blades' cloud of points save also as a CAD DATA Mesh
- ❖ System detect the **ICES' volume and thickness** by *comparing* the CAD DATAs

Laser beams Angles ( $\alpha_1$ )  $\rightsquigarrow$  the region of measurement  $\Rightarrow r/R$

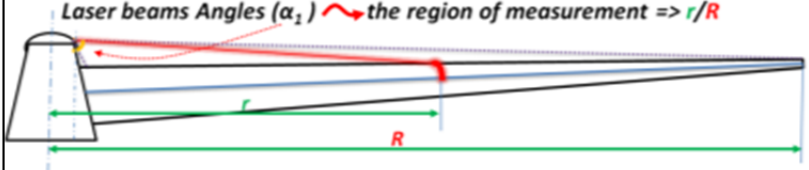
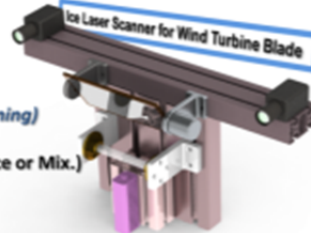



Figure A. 2: System Components

**ÉTS** *Le génie pour l'industrie* **Ice Measurement on the Wind Turbines' blades by Close-Range Photogrammetry Methods** 

**How system detect the type of ice?**

System use the optical properties of the accreting ice. Generally the optical properties of ice is dependent on the surface roughness and the gasses trapped in the ice volume, which alter the density of micro-bubbles and micro-cracks.

These imperfections scatter or reflect the light, giving the ice its characteristic transparent (glazed) or opaque white (rime) appearance.

**Rim Ice** **Glaze Ice**

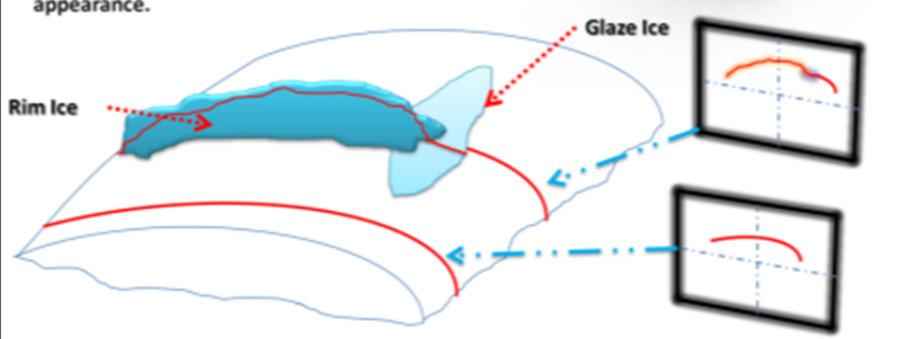
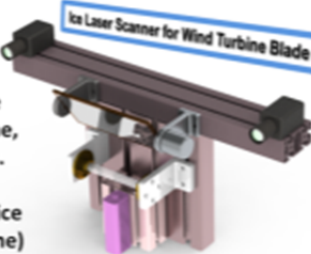



Figure A. 3: How systems detect the type of ice?

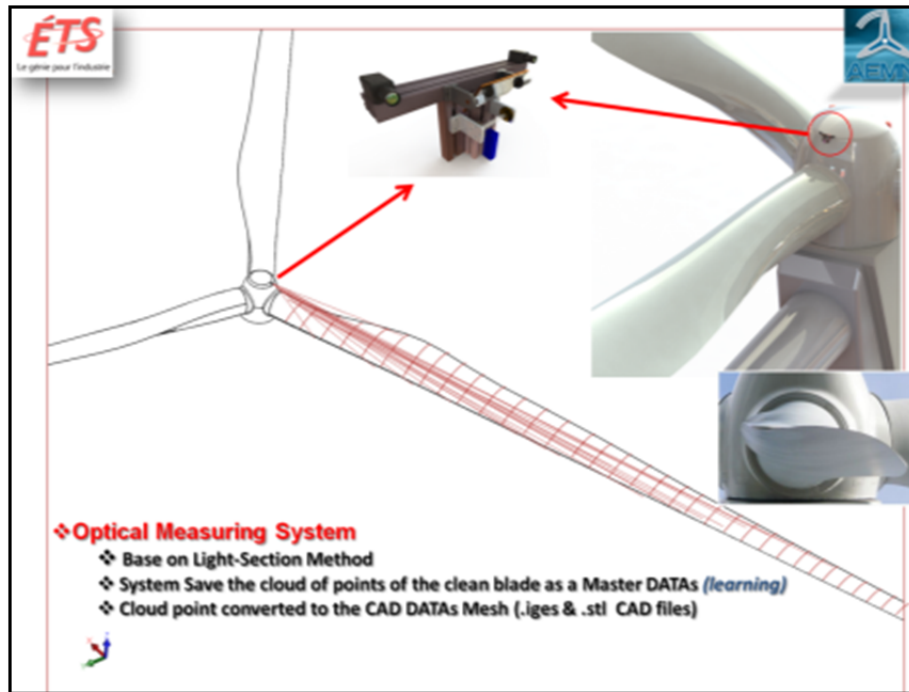


Figure A. 4: Installation position of system on the Wind Turbine Hub

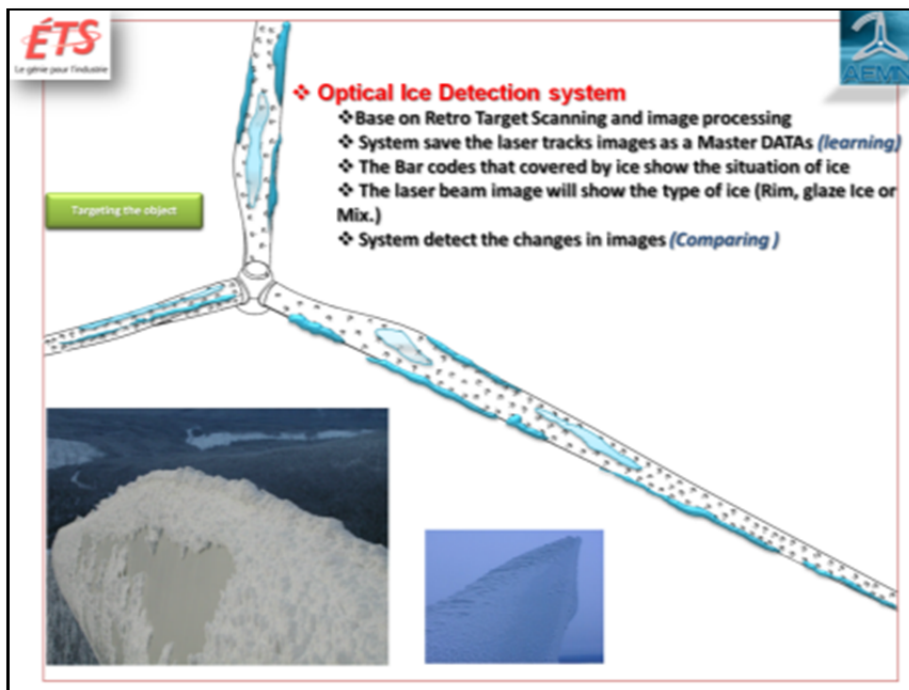


Figure A. 5: optical Ice Detection System based on retro target scanning



Figure A. 6: Validation prototype Concept design

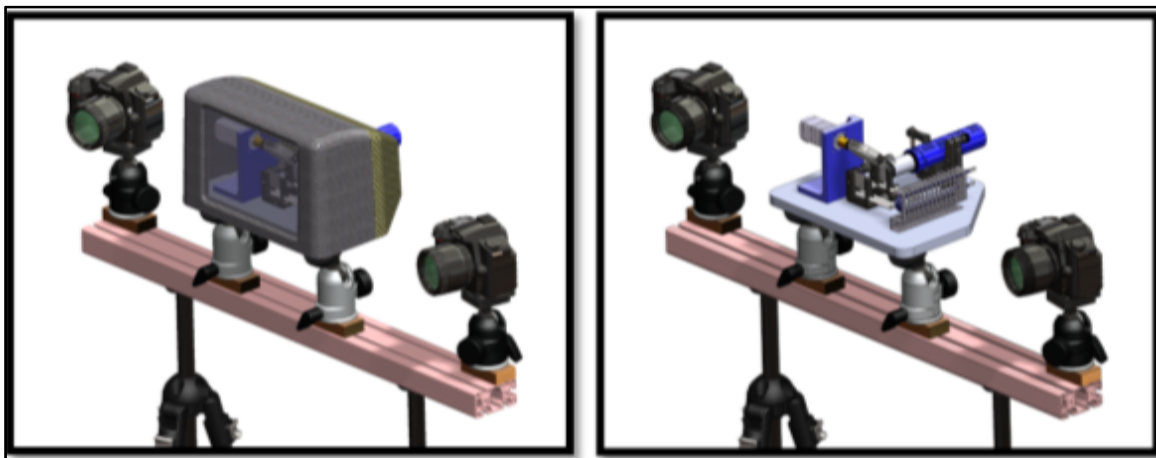


Figure A. 7: Laser Scanner Box Unite



Figure A. 8: Ice Measurement Laser Scanner Exploded View of Components

<i>Ice Measurement Laser Scanner</i>						
<i>ITEM NO.</i>	<i>PART NAME</i>	<i>Supply</i>	<i>DESCRIPTION</i>	<i>QTY.</i>	<i>Unity Price \$</i>	
1	Laser Scanner Box unit	Made		1	\$4,905.30	\$4,905.30
<i>Cameras &amp; Accessories</i>						
2	Nikon D90 Camera-Body	Buy		2	\$730.00	\$1,460.00
3	LENS 55-200 mm f/4-5.6G ED AF-S DX	Buy		2	\$230.00	\$460.00
3.1	LENS Filters with accessories	Buy		2	\$150.00	\$300.00
4	Manfrotto 410-Junior Geared Head	Buy		2	\$279.00	\$558.00
<i>System base Support</i>						
5	Adaptor-block-Joint-8020-2130	Made	AL6061- 76.20x38.10x19.05 mm	2	\$70.00	\$140.00
6	Profile AL-8x80x40	Buy	Profile 8 80x40 1N light natural L=550	1	\$50.00	\$50.00
7	Manfrotto 458B Tripod Assembly	Buy		2	\$200.00	\$400.00
7.1	Cabling & Fastener Joints	Buy		1	\$200.00	\$200.00
<i>Computer and Processing Unit</i>						
8	Dell Latitude E5420 Notebook	Buy	Dell Latitude E5420 - Core i5 2.5 GHz - 14" - 2 GB Ram - 320 GB HDD	1	\$760.00	\$760.00
8.1	Camera Control Pro 2-Software	Buy		1	\$225.00	\$225.00
8.2	Camera Calibration software	Made		1	\$0.00	\$0.00
8.3	DAVID-laserscanner 2.6.3-Software	Buy		1	\$200.00	\$200.00
					<i>Sum</i>	<i>\$9,658.30</i>
					<i>TPS(5%)</i>	<i>\$482.92</i>
					<i>TVQ(8.5%)</i>	<i>\$862.00</i>
					<i>Total (Tax included)</i>	<i>\$11,003.22</i>

Figure A. 9: Bill of Material with price (2011)

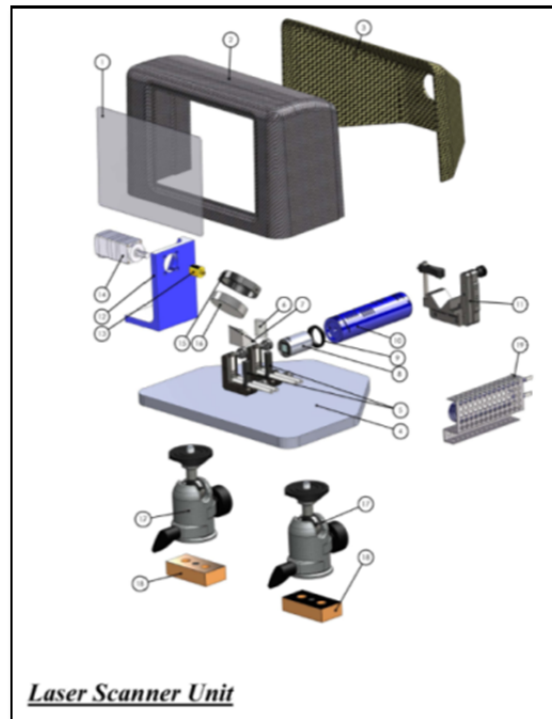


Figure A. 10: Laser Scanner Box Unit, Exploded view

<b>Laser Scanner Box unit</b>						
ITEM NO.	PART NAME	Supply	DESCRIPTION	QTY.	Unity Price \$	
1	Window-glass shield	Made		1	\$50.00	\$50.00
2	Cover	Made		1	\$200.00	\$200.00
3	Cover_Back	Made		1	\$200.00	\$200.00
4	Base_plate	Made	AL6061- 300x250x15	1	\$400.00	\$400.00
<b># Optical Lens Assembly</b>						
5	7734-E0W-lens/Prism-Support	Buy	KM100C	2	\$85.70	\$171.40
6	Plano-Convex Cylindrical Lens	Buy	5697-E0W-LJ1075L1-A - f = 25.00, H = 20.00, L = 22.0, N-BK7 Plano-Convex Cylindrical	2	\$71.80	\$143.60
7	Right Angle Prism Dielectric Mirror	Buy	13652-E0W-Right Angle Prism Dielectric Mirror, 400-750 nm, L = 25 mm/MRA25-E02	1	\$144.20	\$144.20
9	Adaptor-Joint-for Beam Displacer	Buy	20934-E0W-SM1 to M25.5 x 0.5	1	\$19.00	\$19.00
8	6564-E0W-Beam Displacers	Buy		1	\$588.60	\$588.60
10	Laser Diode Modoule	Buy	11837-E0W-Blue Laser Module, 405 nm, 4.0 mW// 20385-E0W-LDM670 -Deep Red Laser Module, 670 nm, 5.5 mW	1	\$912.90	\$912.90
11	Laser Diode Kinematic V-Clamp Mount	Buy	12135-E0W-Large Kinematic V-Clamp Mount, Metric	1	\$123.40	\$123.40
<b># Motor Support-Assembly</b>						
12	Servo Bracket	Made		1	\$350.00	\$350.00
13	Mirror Connection	Made		1	\$60.00	\$60.00
14	Stepping Motor with Planetary Gear with Controller drive	Buy	TIN40591-PK523PB-N10, Stepping Motor with Planetary Gear	1	\$900.00	\$900.00
<b># Mirror Assy</b>						
15	Mirror-Optical Mount	Buy	7664-E0W-FMP2_M - Fixed O2 inch Optical Mount	1	\$19.30	\$19.30
16	UV Enhanced Aluminium Mirror	Buy	3607-E0W-PF20-03-F01 - O2inch (50.8 mm) UV Enhanced Aluminum Mirror	1	\$94.90	\$94.90
<b># Articulated Joint</b>						
17	Manfrotto-486 498 Midi Ball Head	Buy		2	\$179.00	\$358.00
18	Adaptor-block-Joint-8020-2130	Made		2	\$50.00	\$100.00
<b># Heating System</b>						
19	Heater_E-TUB-150A	Made	HEATER, 150W, 120V	1	\$70.00	\$70.00
					<b>Total</b>	<b>\$4,905.30</b>

Figure A. 11: Laser Scanner Box Unit, Bill of Material with price (2011)

## ANNEX III

### CAMERA CALIBRATION PARAMETERS

Through the camera lens, images of the world are projected on a light-sensitive sensor and then stored in an image. This projection from world coordinates to image coordinates is defined by the intrinsic properties of the lens, also called “intrinsic camera properties”

The most common camera model is a simplified one, where the camera aperture is described as a point, the camera sensor size always encompasses the entire area of the image plane onto which the world is projected and the only types of distortion that arise are (approximately) radially symmetric or caused by alignment imperfections of the lens. This camera model, called the pinhole camera model, contains the following camera intrinsic:

**Focal length:** The distance from the center of the lens to the focal point of the lens.

**Principal point or Optical Center:** The point at the intersection of the optical axis and the image plane. If the light-sensitive sensor is not precisely aligned with the lens, the principal point does not coincide with the image center.

**Skew:** The skew of the two image axes.

**Radial distortion & Radial distortion parameters ( $K_1; K_2 ; \dots$ ):** The most common distortion that is radially symmetric due to the symmetry of the lens. It is usually classified as barrel distortion, pincushion distortion or a mixture of the two, known as moustache distortion.

**Tangential distortion & Tangential distortion parameters ( $P_1; P_2 ; \dots$ ):** The second-most common distortion that arises when the lens is not parallel to the imaging plane also called “decentering distortion”. The effect of the radial and tangential distortion parameters is illustrated by Figure A.13.

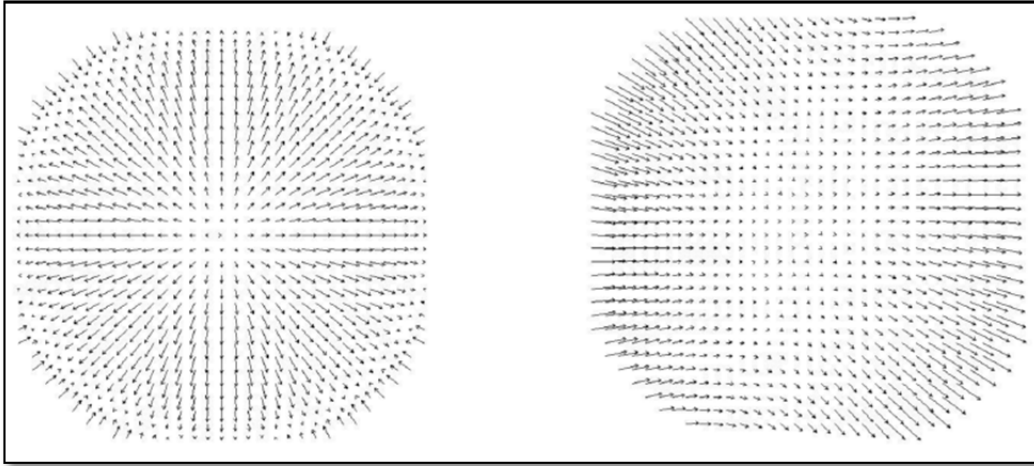


Figure A. 12: Left: Sample plot of radial distortion corrections at the intersections of a regular grid, Right: Sample plot of tangential distortion corrections at the intersections of a regular grid. Credit: U.S. Geological Survey, Department of the Interior/USGS

In the lens manufacturing process, lens aberrations may happen that affect the principal point and skew and cause radial and tangential distortions. When the camera intrinsic are known, a correction of the resulting image distortion can be performed.

The camera extrinsic properties consist of the camera rotation and translation, which describe the camera orientation and position in terms of some fixed world coordinate

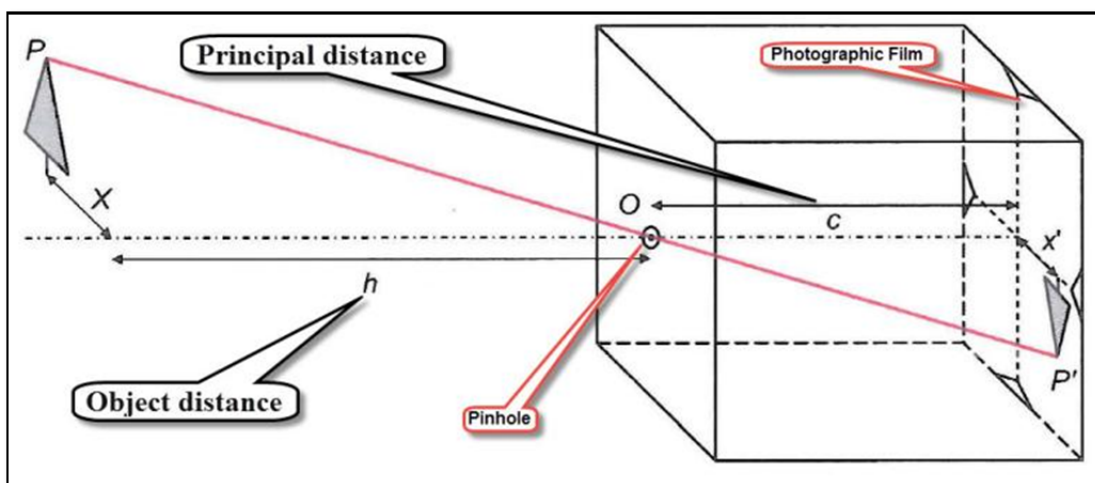


Figure A. 13: Illustration of a pinhole camera

The following is the calibration results generated with 3DF Lapyx software:

*--- Camera Information ---*

*Camera Make: Canon*

*Camera Model: Canon PowerShot SX10 IS*

*Image Resolution: 3648 x 2736 pixels*

*Focal Length (mm): 5.0 mm*

*--- Calibration Results ---*

*Focals (pixels) - Fx: 3078.41 Fy: 3078.07*

*Optical center - Cx: 1863.04 Cy: 1320.21*

*Radial distortion (Brown's Model)*

*K1: -0.17812 K2: 0.135732 K3: 0*

*P1: -0.000172835 P2: 0.00122447*

*Skew: 0*

*Mean Square Reprojection Error: 1.84289 pixels*



## ANNEX IV

### RETRO TARGETS

In many applications, locations to be measured on an object need to be signaled with artificial targets, for example:

- natural object points that cannot be identified sufficiently;
- providing uniquely defined points for comparable measurements;
- geodetic measurement of control points;
- automatic point identification and measurement;
- accuracy improvement.

The physical size and type of target to be used depends on the chosen imaging configuration (camera stations and viewing directions, image scale, resolution) and illumination (light source, lighting direction).

#### 1) **Circular targets**

Due to their radial-symmetric design, circular targets are well suited for photogrammetric use with the center of the target representing the actual 3D point to be measured. Determination of the target center is rotation-invariant and, over a wide range of image magnifications it is scale invariant. Circular targets are useful for not only manual, interactive measurements, but also for automated digital point detection and measurement.

#### 2) **Coded Target**

Targets, encoded with individual point identification numbers can be used to automate point identification. The point codes are arranged in lines, rings or regions around the central target point. Codes with more than several hundred point identification numbers can be designed (Niederost and Maas 1996, Schneider 1996, Ahn and Schultes 1997, Shortis et al. 2003).

Coded targets should meet the following requirements:

- invariance with respect to position, rotation and size;
- invariance with respect to perspective or affine distortion;
- robust decoding with error detection (even with partial occlusions);
- precise defined and identifiable center;
- sufficient number of different point identification numbers;
- perceptibility of the point pattern in arbitrary orientated images;
- fast processing times for pattern recognition;
- minimum pattern size;
- low production costs.

The point identification number is decoded by image analysis of the number and configuration of code patterns. The pattern displayed in Figure 24 is based on barcode-techniques where the code can be reconstructed from a series of black and white marks (bit series).

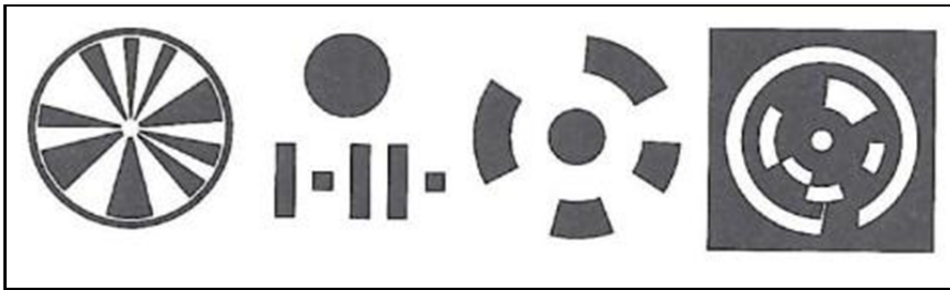


Figure A. 14: Selection of coded targets (bit series)

The number of bits of the barcode limits the number of coded targets characters. Due to their radial-symmetric design, circular targets are well suited for photogrammetric use with the center of the target representing the actual 3D point to be measured. Determination of the target center is rotation-invariant and, over a wide range of image magnifications, also scales invariant. Circular targets are useful not only for manual, interactive measurements, but also for digital point detection and for automatic measurement. Figure 25 shows the combination of coded retro targets and circular dot targets on Inspection of a Wind turbine Blade.

### 3) Retro-reflective targets

Retro-reflective targets (retro-targets) are widely used in practice, particularly in industrial applications. They consist of a retro-reflective material that either is covered by a black surround (mask) according to the target pattern, or is stamped in an equivalent form from the raw material. The retro-reflective material consists either of a dense arrangement of small reflective balls ( $\varnothing \cong 80 \mu\text{m}$ ), or an array of micro prisms (Clarke, 1994).

In order to achieve high contrast target images retro-reflective targets must be illuminated from the viewing direction of the camera (e.g. by a ring flash, see Figure 26).



Figure A. 15: Ring flash on DSLR camera helps to illuminate from viewing direction of camera, source: [www.capture3d.com](http://www.capture3d.com).

Further drawbacks of retro-targets include:

- relatively high costs per target, particularly for large or coded targets, due to the manufacturing process;
- limitations in target dimensions and therefore target density which can be adhered to the object surface;
- Self-adhesive targets can generally only be used once, requiring a new set of targets for each object to be measured.

The above-mentioned drawbacks of retro-reflective targets require alternative materials or targeting techniques for a number of applications.

Circular plastic targets with a centric target point are suitable for a long-term targeting of outdoor objects (e.g. buildings, bridges) that are also useful for geodetic measurements. They can be produced in almost any size. Self-adhesive paper marks can be used for temporary targeting of tie points where no long-term reproducibility is required. In this way, arbitrary patterns and additional information can be provided at minimal cost. Since paper prints are not retro-reflective, image contrast and target detect ability strongly depend on the acquisition of high quality photography and the abilities of the feature extraction algorithm selected for subsequent processing.

In order for accurate measurements to be made, the diameter of the circular target images needs to be suited to the target detection and measurement process to be used. For digital processing systems it is generally accepted that target images should be at least 5 pixels in diameter. Besides practical side conditions (e.g. maximum permitted size for pasting an object) the maximum usable target diameter is also a function of the maximum allowed eccentricity between the true position of the projected circle center and the center of the imaged elliptical target.

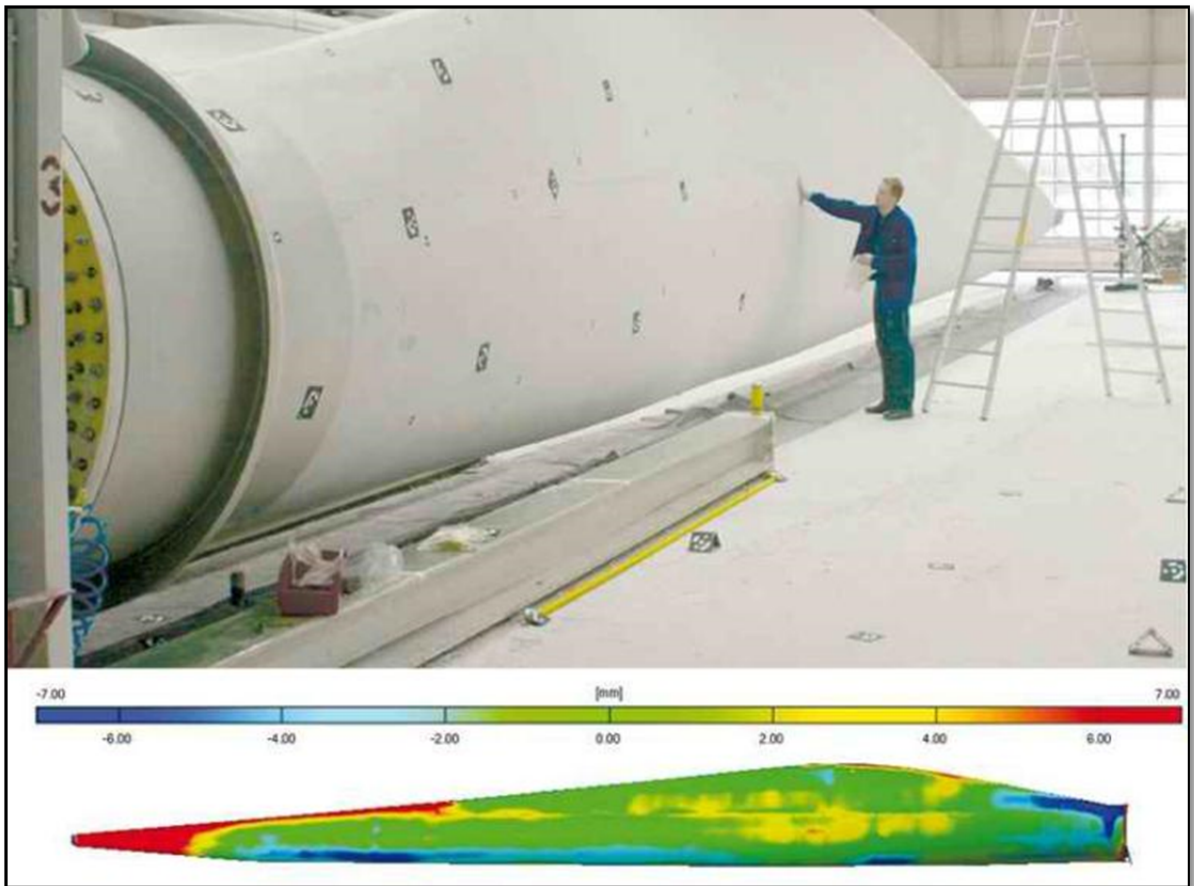


Figure A. 16: Inspection of a Wind turbine Blade (Retro coded targets and the scaling bar show in the photo, source [www.gom.com](http://www.gom.com))



## ANNEX V

### **SIFT/Bundler/PMVS2 Input Output**

#### **Sift (Scale-invariant feature transform)**

Scale-invariant feature transform (or SIFT) is an algorithm in computer vision to detect and describe local features in images. The algorithm was published by David Lowe in 1999 (Lowe, 1999). Applications include object recognition, robotic mapping and navigation, image stitching, 3D modeling, gesture recognition, video tracking, individual identification of wildlife and match moving.

The first version of the “Structure from Motion” pipeline was using the David Lowe’s Sift program. This is a good and accurate program to extract the key points of the image that it will be used to triangulate the positions and orientations of the cameras later. The main drawback of this program is the limitation of finding key points for images whose width or height are greater or equal 3200 pixels. Sift does not allow to extract the key points for those images and this is a patented algorithm in the US; the owner is the University of British Columbia. So as a free open source software in the VisualSfM GUI it uses the Andrea Vedaldi’s Sift++ (Vedaldi, 2009). The output of Andrea Vedaldi’s Sift++ is quite different from the David Lowe’s Sift. In addition, it can retrieve more key points than the David Lowe’s Sift.

#### **Bundler /PMVS2**

Bundler (Snavely, 2010; Snavely, Seitz et Szeliski, 2008) is an open source “Structure From Motion” system and its initial version was used for the Photo Tourism project (Snavely, Seitz et Szeliski, 2006). The main goal of the Photo Tourism project was the reconstruction of 3D models from large datasets of images, which could belong to private collections or extracted from Internet. Bundler does not have UI and all the processing is performed using a script

that uses the included applications. The output of bundler is a sparse geometry of the scene, and the relative orientation and position of the cameras.

Bundler takes a set of images, extracts the image features of each image, and matches as input, after it produces a 3D reconstruction of camera and sparse and basic scene geometry as output. Bundler reconstructs the scene incrementally, a few images at a time, using a modified version of the Sparse Bundle Adjustment (SBA) package as the underlying optimization engine.



Figure A. 17: Brief example of the use of Bundler: Structure from Motion (SfM) (Snavely, 2010)

The Bundler source distribution also contains potentially useful implementations of several computer vision algorithms, including:

- Fundamental matrix or F-matrix estimation;
- Calibrated 5-point relative pose;
- Triangulation of multiple rays.

As it was explained Bundler produces sparse point clouds and the information of the cameras which compose the scene. For denser points, it is strongly recommended to use Dr. Yasutaka Furukawa software package called PMVS2 for running dense multi-view stereo. A typical

pipeline is to run Bundler to get camera parameters, use the provided Bundle2PMVS program to convert the results into PMVS2 input, and then run PMVS2. Furthermore, the Bundler official webpage encourage us to use the Dr. Furukawa's CMVS view clustering software, which is a helpful and optional preprocess before running PMVS2.

### **Bundle Adjustment and Sparse Bundle Adjustment**

As it is mentioned previously, Bundler uses SBA algorithm in order to obtain the position and information of the cameras. We would not go in deep detail about this complex process but we explain the differences between the Bundle Adjustment and Sparse Bundle Adjustment in this section.

If it is assumed that we are given initial estimates of the 3D coordinates corresponding to a set of points seen in a series of images, as well as initial estimates for the viewing parameters pertaining to each image. The Bundle Adjustment (BA) is a large optimization problem involving the simultaneous refinement of the 3D structure and viewing parameters (i.e. camera pose and possibly intrinsic calibration and radial distortion), aiming to obtain a reconstruction which is optimal under certain assumptions regarding the noise pertaining to the observed image features: If the image error is zero-mean Gaussian, then BA is the Maximum Likelihood Estimator. Its name refers to the “bundles” of light rays originating from each 3D feature and converging on each camera's optical center, which are adjusted optimally with respect to both the structure and viewing parameters. SBA uses a custom implementation of the Levenberg-Marquardt nonlinear least squares algorithm to solve the sparse, large-scale optimization problem associated with BA (Lourakis et Argyros, 2009)

The meaning of sparse in SBA(Lourakis et Argyros, 2009) comes of the lack of interaction among parameters for different 3D points and cameras, the linear systems that have to be solved during BA contain lots of zeroes and are characterized by a sparse block structure. This structure can be exploited by avoiding storing and operating on zero elements, thus gaining considerable computational benefits.

## Running Bundler

The easiest way to start using Bundler is to launch the included bash shell script with the source code, `RunBundler.sh`. The provided script simply execute all the necessary steps in order to prepare the proper input to the Bundler binary program and after that, it launches Bundler. This script needs to be run in a directory with a set of images in JPEG format, and it automatically runs all the steps needed for recovering the reconstruction of the scene.

The Bundler executable is actually the last in a sequence of steps that need to be run to reconstruct a scene. The provided script `RunBundler.sh` takes care of all these steps for us, but it is useful to know what is going on. The main initial steps are to generate features and pairwise feature matches for the image set. Any type of image features can be used, but Bundler assumes the features are in the SIFT format, and so David Lowe's SIFT (**Scale-invariant feature transform**) (Lowe, 1999) detector is the easiest way to get working with Bundler (`RunBundler.sh` assumes that SIFT is used). A list of images containing estimating focal length information also must be created. The four steps to creating a reconstruction are therefore:

1. Create a list of images using the script '`extract_focal.pl`' (this extracts focal length information, when available, from each image, and stores it in an image list);
2. Generate features for each image using the SIFT program;
3. Match features between each pairs of images. The computed feature matches are stored in a file called '`matches.init.txt`';
4. Run '`bundler`' with a suitable options file.

Bundler itself is typically invoked as follows:

```
./bundler list.txt --options_file options.txt
```

## Output of Bundler

So far, we already know that Bundler has as input as set or collection of images which can be extracted from the Internet or any devices that can take photographs, and it's very important that those images contain the EXIF (Exchangeable image file format) information about the camera parameters (focal length, width of the sensor (CMOS Image Sensor Product Catalogue, 2012, model of the camera, etc.). In this section we focus on the output that Bundler generates.

Bundler produces files typically with the pattern 'bundle\_\*.out' (they are called "bundle files"). With the default commands, Bundler outputs a bundle file called 'bundle\_<n>.out' containing the current state of the scene after each set of images has been registered where n is the number of currently registered cameras). After all possible images have been registered, Bundler outputs a final file named 'bundle.out'. In addition, a "ply" file containing the reconstructed cameras and points is written after each round. The bundle files, which contain the estimated scene and camera geometry, have the following format:

```
# Bundle file v0.3
<num_cameras> <num_points> [two integers]
<camera1>
<camera2>
...
<cameraN>
<point1>
<point2>
...
<pointM>
```

Figure A. 18: Bundler file format (source Bundler help)

### Bundler Camera entry

Each camera entry contains the estimated camera intrinsic and extrinsic , and has the following form:

<camera N>	<f><k1><k2>	The focal length, followed by two radial distortion coefficients.
	<R>	The 3x3 matrix representing the camera rotation.
	<t>	The 3-vector describing the camera translation.

Figure A. 19: Bundler Camera entry

The cameras are specified in the order they appear in the list of images.

### Point entry

Each point entry has the form:

<pointN>	<position>	The 3-vector describing the 3D position of the point.
	<color>	The 3-vector describing the RGB colour of the point.
	<view list>	The list of views the point is visible in.

Figure A. 20: Bundler point entry

The view list begins with the length of the list (i.e., the number of cameras the point is visible in). The list is then given as a list of quadruplets <camera> <key> <x> <y>, where:

<code>&lt;view list&gt;</code>	<code>&lt;num&gt;&lt;camera&gt;&lt;key&gt;&lt;x&gt;&lt;y&gt;</code>	<code>&lt;num&gt;</code>	Total of quadruplets for this view list.
		<code>&lt;camera&gt;</code>	It's the camera index.
		<code>&lt;key&gt;</code>	the index of the SIFT keypoint where the point was detected in that camera.
		<code>&lt;x&gt;&lt;y&gt;</code>	They are the detected positions of that keypoint!

Figure A. 21: Bundler view list

Both indices are 0-based (e.g., if camera 0 appears in the list, this corresponds to the first camera in the scene file and the first image in "list.txt").

The pixel positions are floating point numbers in a coordinate system where the origin is the center of the image, the x-axis increases to the right, and the y-axis increases towards the top of the image. Thus,  $(-w/2, -h/2)$  is the lower-left corner of the image, and  $(w/2, h/2)$  is the top-right corner, where  $w$  and  $h$  are the width and height of the image.

Example of a bundler file:

```
# Bundle file v0.3
63 30381 <num_cameras> <num_points>
2.4644506065e+03  1.3013589394e-01  -3.8686423271e-01
<f><k1><k2>
3.3909195592e-02  -3.6195609456e-01  -9.3157820502e-01
<R>
3.4414460143e-01  8.7933868688e-01  -3.2913214226e-01
9.3830414033e-01  -3.0943700388e-01  1.5438290342e-01
-2.0941057341e+01  -2.1778910442e+01  -3.0263678751e+01
<t>
... end cameras
3.1611474412e+01  4.0250791002e+00  -2.2884623441e+01
<position>
106 113 116 <color>
2 31 11300 -58.9200 67.3700 28 5465 -16.6400 82.9200
<view list> ... end points
```

Figure A. 22: Example of a bundler file

### How Bundler software project a 3D point into a camera

Bundler uses a pinhole camera model. The parameters Bundler estimates for each camera are a focal length ( $f$ ), two radial distortion parameters ( $k_1$  and  $k_2$ ), a rotation ( $R$ ), and translation ( $t$ ), as described in the file specification above. The formula for projecting a 3D point  $X$  into a camera ( $R, t, f$ ) is:

$$P = R \times X + t$$

Conversion from world to camera coordinates

$$p = \frac{-P}{P.z}$$

Perspective division. Where  $P.z$  is the third ( $z$ ) coordinate of  $P$ .

$$\hat{p} = f \times r(p) \times p$$

Conversion to pixel coordinates

In the last equation,  $r(p)$  is a function that computes a scaling factor to undo the radial distortion:

$$r(p) = 1.0 + k_1 \times \|p\|^2 + k_2 \times \|p\|^4$$

This gives a projection in pixels, where the origin of the image is the center of the image, the positive x-axis points right, and the positive y-axis points up (in addition, in the camera coordinate system, the positive z-axis points backwards, so the camera is looking down the negative z-axis, as in OpenGL<sup>1</sup> (Ho AHN, 2012)).

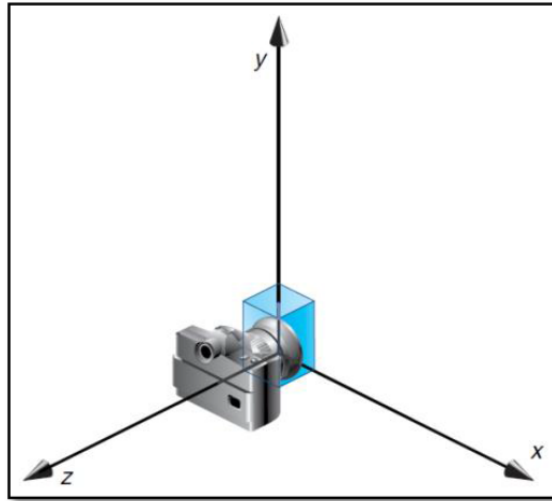


Figure A. 23:Coordinates axis of the camera

Finally, the equations above imply that the camera viewing direction is:

$$\hat{R} \times [0 \quad 0 \quad -1]'$$

(i.e., the third row of  $-R$  or third column of  $-R'$ )

Where ' indicates the transpose of a matrix or vector.

In addition, the 3D position of a camera is:

$$C = -R' \times t$$

The presented formulas above will be used in order to clean the final point set after the Bundler and PMVS2 have been executed

### Output of PMVS2

Reconstruction results will be saved under models in 3 different files. Let  $S$  denote the name of the option file used in the reconstruction. Then, we would obtain  $/root/models/S.ply$ ,  $/root/models/S.patch$  and  $/root/models/S.pset$ .

S.ply, it contains 3D colored points with the normal for visualization purposes.

S.patch, it contains full reconstruction information. The file starts with a header "PATCHES" followed by the number N of reconstructed 3D oriented points. The file then contains information for N points in the following format. For each point, there should be a line "PATCHS". The next two lines contain the 3D location and the estimated surface normal, respectively. Note that the 3D location and the normal are given in 3D homogeneous coordinates. The following line contains three numbers. The first number is the photometric consistency score associated with the point, which is the average of the normalized cross correlation score ranging from -1.0 (worse) to 1.0 (good), while the remaining two numbers are for debugging purposes. The next line contains the number of images in which the point is visible and textures agree well, followed by actual image indexes. The next line contains the number of images in which textures may not agree well but the point should be visible from visibility analysis, followed by the actual image indexes. Refer to our papers for more detailed explanations of these two different types of visible images.

S.pset, it is simply a list of the 3D locations and estimated surface normal for all the reconstructed points, which can be used as an input to surface reconstruction software.

'PLY' is a computer file format known as the "Polygon File Format" or the "Stanford Triangle Format".

The format was principally designed to store three-dimensional data from 3D scanners. It supports a relatively simple description of a single object as a list of nominally flat polygons. A variety of properties can be stored including: color and transparency, surface normal, texture coordinates and data confidence values. The format permits one to have different properties for the front and back of a polygon. (source Wikipedia)

The ply format as a standard polygonal format, are common output of most cloud point inspection software such as Polyworks.

## LIST OF BIBLIOGRAPHICAL REFERENCES

- Abdel-Wahab, Mohammed, Konrad Wenzel et Dieter Fritsch. 2012. « Automated and Accurate Orientation of Large Unordered Image Datasets for Close-Range Cultural Heritage Data Recording ». *Photogrammetrie-Fernerkundung-Geoinformation*, vol. 2012, n° 6, p. 679-689.
- Ackermann, M, J Ahrens, X Bai, M Bartelt, SW Barwick, RC Bay, T Becka, JK Becker, K-H Becker et P Berghaus. 2006. « Optical properties of deep glacial ice at the South Pole ». *Journal of Geophysical Research: Atmospheres (1984–2012)*, vol. 111, n° D13.
- Andersen, Elin, Elin Börjesson, Päivi Vainionpää et Linn Silje Udem. 2011. « Wind Power in cold climate ».
- Antikainen, Petteri, et Sami Peuranen. 2000. « Ice loads, case study ». In *BOREAS V, Wind power production in cold climates, Proceedings of an International conference*, Levi, Finland.
- Bay, Herbert, Andreas Ess, Tinne Tuytelaars et Luc Van Gool. 2008. « Speeded-up robust features (SURF) ». *Computer vision and image understanding*, vol. 110, n° 3, p. 346-359.
- Botta, G, M Cavaliere et H Holttinen. 1998. « Ice accretion at Acqua Spruzza and its effects on wind turbine operation and loss of energy production ». *BOREAS IV*. FMI, Hetta, Finland, p. 77-86.
- Burton, Tony, Nick Jenkins, David Sharpe et Ervin Bossanyi. 2011. *Wind energy handbook*. John Wiley & Sons.
- Canice, Ice Accretion Simulation Code. 2015. « IOPARA Inc. - Our Softwares- Code CANICE-2D & -3D ». < <http://www.iopara.ca/software.shtml> >.
- canwea.ca. 2013. « La poursuite du développement éolien : une stratégie gagnante pour le Québec et ses régions ». < <http://canwea.ca/wind-energy/quebec/> >. Consulté le 15 MAY.
- Cattin, René. 2015. « Alpine Test Site Gütsch - Cost Action 727 ». < <http://www.meteotest.ch/cost727/index.html> >.
- Chauve, A-L, Patrick Labatut et J-P Pons. 2010. « Robust piecewise-planar 3D reconstruction and completion from large-scale unstructured point data ». In

- Computer Vision and Pattern Recognition (CVPR), 2010 IEEE Conference on. p. 1261-1268. IEEE.
- eolien.qc.ca, TechnoCentre éolien. 2015. « Site nordique expérimental en éolien CORUS (SNEEC) ». < <https://www.eolien.qc.ca/fr/infrastructures/site-nordique-experimental-en-eolien-sneec.html> >.
- Falkingham, Peter L. 2013. Generating a photogrammetric model using VisualSfM, and post-processing with meshlab. Brown University, Tech. Rep.
- Fikke, S, G Ronsten, A Heimo, S Kunz, M Ostrozlik, PE Persson, J Sabata, B Wareing, B Wichure et J Chum. 2006. « COST 727: Atmospheric Icing on structures ». Measurements and data collection on icing: State of the Art, Publication of MeteoSwiss, vol. 75, n° 110, p. 1422-1381.
- Frohboese, Peter, Michael Steiniger et Andreas Anders. 2007. « Ice loads on wind turbines ». In Eur. Wind Energy Conf. & Exhibition EWEC.
- Furukawa, Yasutaka, Brian Curless, Steven M Seitz et Richard Szeliski. 2009. « Manhattan-world stereo ». In Computer Vision and Pattern Recognition, 2009. CVPR 2009. IEEE Conference on. p. 1422-1429. IEEE.
- Furukawa, Yasutaka, et Jean Ponce. 2010. « Patch-based multi-view stereo software ». Online URL < <http://grail.cs.washington.edu/software/pmvs>.
- Ganander, H, et G Ronsten. 2003. « Design load aspects due to ice loading on wind turbine blades ». In Boreas VI, proceedings of the international conference, Pyhäntunturi, Finland.
- Haala, Norbert, et Martin Kada. 2010. « An update on automatic 3D building reconstruction ». ISPRS Journal of Photogrammetry and Remote Sensing, vol. 65, n° 6, p. 570-580.
- Homola, Matthew C, Per J Nicklasson et Per A Sundsbø. 2006. « Ice sensors for wind turbines ». Cold regions science and technology, vol. 46, n° 2, p. 125-131.
- Hugemann, Wolfgang. 2010. « Correcting lens distortions in digital photographs ». Ingenieurbüro Morawski+ Hugemann: Leverkusen, Germany.
- Jasinski, William J, Shawn C Noe, Michael S Selig et Michael B Bragg. 1998. « Wind turbine performance under icing conditions ». Journal of Solar Energy Engineering, vol. 120, n° 1, p. 60-65.
- Joshi, Ravisha. 2014. « Automated 3D feature extraction for simple geometry buildings using images for GIS data collection ».

- kaupunki, Rauman. 2011. KOILLINEN TEOLLI-SUUSALUE, RAUMA JÄÄVAARASELVITYS 82138782. <  
[http://www.rauma.fi/tevi/kaavoitus/Materiaalit/voimassa/asemakaavat/AK13-009Lakari/tuulivoimaselvitykset/82138782\\_Rauma\\_J%C3%A4%C3%A4vaararaportti\\_2011-12-20.pdf](http://www.rauma.fi/tevi/kaavoitus/Materiaalit/voimassa/asemakaavat/AK13-009Lakari/tuulivoimaselvitykset/82138782_Rauma_J%C3%A4%C3%A4vaararaportti_2011-12-20.pdf)>.
- Kazhdan, Michael, Matthew Bolitho et Hugues Hoppe. 2006. « Poisson surface reconstruction ». In Proceedings of the fourth Eurographics symposium on Geometry processing.
- Kersten, Thomas P, et Maren Lindstaedt. 2012. « Automatic 3D object reconstruction from multiple images for architectural, cultural heritage and archaeological applications using open-source software and web services ». Photogrammetrie-Fernerkundung-Geoinformation, vol. 2012, n° 6, p. 727-740.
- Google Patents. 1990. Optical sensor for the detection of ice formation and other chemical species.
- Krogh-Jepesen, Katrine. 2014. « Problematic-ice-on-wings ». <  
[www.dtu.dk/english/News/2014/01/Problematic-ice-on-wings](http://www.dtu.dk/english/News/2014/01/Problematic-ice-on-wings)>.
- Lourakis, Manolis IA, et Antonis A Argyros. 2009. « SBA: A software package for generic sparse bundle adjustment ». ACM Transactions on Mathematical Software (TOMS), vol. 36, n° 1, p. 2.
- Lowe, David G. 1999. « Object recognition from local scale-invariant features ». In Computer vision, 1999. The proceedings of the seventh IEEE international conference on. Vol. 2, p. 1150-1157. Ieee.
- Lowe, David G. 2004. « Distinctive image features from scale-invariant keypoints ». International journal of computer vision, vol. 60, n° 2, p. 91-110.
- Luhmann, Thomas. 2010. « Close range photogrammetry for industrial applications ». ISPRS Journal of Photogrammetry and Remote Sensing, vol. 65, n° 6, p. 558-569.
- Luhmann, Thomas, Stuart Robson, Stephen Kyle et Ian Harley. 2006. Close range photogrammetry: Principles, methods and applications. Whittles.
- Google Patents. 1977. Microwave ice detector.
- Makkonen, L. 1994. « Ice and Construction—Rilem Report 13 ». Chapman & Hall, London, England, p. 53.
- Mason, Basil John. 2010. Physics of clouds. Clarendon Press.

- Mauro, Massimo, Hayko Riemenschneider, Luc Van Gool, Riccardo Leonardi et Italia Brescia. 2013. « Overlapping camera clustering through dominant sets for scalable 3D reconstruction ». In Proc. British Machine Vision Conference (BMVC).
- Montgomerie, Björn. 2014. « Ice ejection from rotating wind turbine blades ».
- Musialski, Przemyslaw, Peter Wonka, Daniel G Aliaga, Michael Wimmer, L Gool et Werner Purgathofer. 2013. « A survey of urban reconstruction ». In Computer Graphics Forum. Vol. 32, p. 146-177. Wiley Online Library.
- Patel, Mukund R. 2012. Wind and solar power systems: design, analysis, and operation. CRC press.
- Persson, Per-Erik. 2009. Mätningar av nedisning i en hög mast. 09:24: Elforsk, 18 p.
- Remondino, Fabio, et Sabry El-Hakim. 2006. « Image-based 3D modelling: A review ». The Photogrammetric Record, vol. 21, n° 115, p. 269-291.
- Schindler, Falko, W Worstner et J-M Frahm. 2011. « Classification and reconstruction of surfaces from point clouds of man-made objects ». In Computer Vision Workshops (ICCV Workshops), 2011 IEEE International Conference on. p. 257-263. IEEE.
- Schnabel, Ruwen, Roland Wahl et Reinhard Klein. 2007. « Efficient RANSAC for Point-Cloud Shape Detection ». In Computer graphics forum. Vol. 26, p. 214-226. Wiley Online Library.
- Seifert, Henry, Annette Westerhellweg et Jürgen Kröning. 2003. « Risk analysis of ice throw from wind turbines ». Boreas, vol. 6, n° 9, p. 2006-01.
- Shortis, MR, S Robson et HA Beyer. 1998. « Principal point behaviour and calibration parameter models for Kodak DCS cameras ». The Photogrammetric Record, vol. 16, n° 92, p. 165-186.
- Snavely, Noah. 2010. « Bundler: Structure from motion (SFM) for unordered image collections ». Available online: [phototour.cs.washington.edu/bundler/](http://phototour.cs.washington.edu/bundler/) (accessed on 11 October 2013).
- Snavely, Noah, Steven M Seitz et Richard Szeliski. 2006. « Photo tourism: exploring photo collections in 3D ». In ACM transactions on graphics (TOG). Vol. 25, p. 835-846. ACM.
- Snavely, Noah, Steven M Seitz et Richard Szeliski. 2008. « Modeling the world from internet photo collections ». International Journal of Computer Vision, vol. 80, n° 2, p. 189-210.

- Warren, Stephen G. 1984. « Optical constants of ice from the ultraviolet to the microwave ». Applied optics, vol. 23, n° 8, p. 1206-1225.
- Westerlund, Rolf. 2004. Utveckling av en RetroOptisk isindikator. 100/1023/14/sv. < [http://www.elforsk.se/Global/Vindforsk/Rapporter\\_fran\\_aldre\\_program/retroice.pdf](http://www.elforsk.se/Global/Vindforsk/Rapporter_fran_aldre_program/retroice.pdf) >.
- Westoby, MJ, J Brasington, NF Glasser, MJ Hambrey et JM Reynolds. 2012. « ‘Structure-from-Motion’ photogrammetry: A low-cost, effective tool for geoscience applications ». Geomorphology, vol. 179, p. 300-314.
- Wikipedia, The Free Encyclopedia. 2014. « Exchangeable image file format - Wikipedia, the free encyclopedia ». < [http://en.wikipedia.org/wiki/Exchangeable\\_image\\_file\\_format](http://en.wikipedia.org/wiki/Exchangeable_image_file_format) >. Consulté le 27 Feb. 2015.
- Wikipedia, the free encyclopedia. 2015. « Photogrammetry ». < <http://en.wikipedia.org/wiki/Photogrammetry> >.
- Wu, Changchang. 2011a. « SiftGPU: A GPU implementation of scale invariant feature transform (SIFT)(2007) ». URL <http://cs.unc.edu/~ccwu/siftgpu>.
- Wu, Changchang. 2011b. « VisualSfM: A visual structure from motion system ». URL: <http://homes.cs.washington.edu/~ccwu/vSfM>, vol. 9.
- Wu, Changchang. 2013. « Towards linear-time incremental structure from motion ». In 3D Vision-3DV 2013, 2013 International Conference on. p. 127-134. IEEE.
- Wu, Changchang, Sameer Agarwal, Brian Curless et Steven M Seitz. 2011. « Multicore bundle adjustment ». In Computer Vision and Pattern Recognition (CVPR), 2011 IEEE Conference on. p. 3057-3064. IEEE.



